Synthesis and Characterization of Microporous Inorganic Membranes for Propylene/Propane Separation

by

Xiaoli Ma

A Dissertation Presented in Partial Fulfillment
of the Requirements for the Degree
Doctor of Philosophy

Approved January 2015 by the
Graduate Supervisory Committee:

Jerry Lin, Chair
Candace Chan
Terry Alford

ARIZONA STATE UNIVERSITY

May 2015

ABSTRACT

Membrane-based gas separation is promising for efficient propylene/propane (C_3H_6/C_3H_8) separation with low energy consumption and minimum environment impact. Two microporous inorganic membrane candidates, MFI-type zeolite membrane and carbon molecular sieve membrane (CMS) have demonstrated excellent thermal and chemical stability. Application of these membranes into C_3H_6/C_3H_8 separation has not been well investigated. This dissertation presents fundamental studies on membrane synthesis, characterization and C_3H_6/C_3H_8 separation properties of MFI zeolite membrane and CMS membrane.

MFI zeolite membranes were synthesized on α-alumina supports by secondary growth method. Novel positron annihilation spectroscopy (PAS) techniques were used to non-destructively characterize the pore structure of these membranes. PAS reveals a bimodal pore structure consisting of intracrystalline zeolitic micropores of ~0.6 nm in diameter and irregular intercrystalline micropores of 1.4 to 1.8 nm in size for the membranes. The template-free synthesized membrane exhibited a high permeance but a low selectivity in C_3H_6/C_3H_8 mixture separation.

CMS membranes were synthesized by coating/pyrolysis method on mesoporous γ-alumina support. Such supports allow coating of thin, high-quality polymer films and subsequent CMS membranes with no infiltration into support pores. The CMS

membranes show strong molecular sieving effect, offering a high C_3H_6/C_3H_8 mixture selectivity of ~30. Reduction in membrane thickness from 500 nm to 300 nm causes an increase in C_3H_8 permeance and He/N_2 selectivity, but a decrease in the permeance of He, N_2 and C_3H_6 and C_3H_6/C_3H_8 selectivity. This can be explained by the thickness dependent chain mobility of the polymer film resulting in final carbon membrane of reduced pore size with different effects on transport of gas of different sizes, including possible closure of C_3H_6-accessible micropores.

CMS membranes demonstrate excellent C_3H_6/C_3H_8 separation performance over a wide range of feed pressure, composition and operation temperature. No plasticization was observed at a feed pressure up to 100 psi. The permeation and separation is mainly controlled by diffusion instead of adsorption. CMS membrane experienced a decline in permeance, and an increase in selectivity over time under on-stream C_3H_6/C_3H_8 separation. This aging behavior is due to the reduction in effective pore size and porosity caused by oxygen chemisorption and physical aging of the membrane structure.

DEDICATION

To my parents and wife

ACKNOWLEDGMENTS

First and foremost, I would like to express my deepest appreciation to my advisor, Dr. Jerry Lin. It has been an honor for me to be his first Ph.D. student from the program of Materials Science and Engineering. He gave me the opportunity to do exciting and interesting research in several different projects. I want to thank him for all his continuous support, guidance, assistance and encouragement during my pursuit of Ph.D. I have been motivated by the joy, curiosity and enthusiasm he has for his research. Dr. Lin is committed to helping his students find success and gratification in their future chosen profession. I am very grateful to his insightful advices on a lot of other aspects besides research. Everything I learnt from him is extremely beneficial to both my future career and life.

I would like to thank Dr. Alford and Dr. Chan for their willingness to serve on my committee. I really appreciate them for taking the time and efforts to make invaluable inputs and suggestions to my research and dissertation. I would also like to thank Fred Pena for his assistance in building set up, equipment repair and maintenance in the lab. I want to thank Yolanda Murphy for her help and support to both me and my wife during our PhD studies. I am also very thankful to Dr. Xiaotong Wei and Dr. Jay Kniep, whom I have closely worked with in project.

Finally, I would like to thank all the current and former group members in Dr. Lin's group that I have had the pleasure to work with: Dr. Matthew Anderson, Dr. Haibing Wang, Dr. Jose Ortiz-Landeros, Dr. Shriya Seshadri, Dr. Carrie Eggen, Dr. Ding Wang, Teresa Rosa, Dr. Tyler Norton, Dr. Xiaoping Liang, Huifeng Zhang, Dr. Yang Liu, Dr. Xueliang Dong, Dr. Xiaojuan Hu, Dr. Defei Liu, Dr. Wanliang Mi, Dr. Bo Lv, Dr. Nick Linneen, Stewart Mann, Suzanne Williams, Alex Kasik, Joshua James, and Dr. Hong Meng, Ben Wu, Amr Ibrahim, Gaurav Sharma and Dr. Xuefei Sun.

I highly appreciate the National Science Foundation and Membrane Research and Technology Inc. for the financial support of this work.

TABLE OF CONTENTS

Page

CHAPTER Page

CHAPTER Page

CHAPTER Page

CHAPTER Page

CHAPTER Page

LIST OF TABLES

Table Page

LIST OF FIGURES

Figure Page

Figure Page

Figure Page

Figure Page

Figure Page

Figure Page

CHAPTER 1

GENERAL INTRODUCTION

1.1 Introduction

Gas separation or purification in industry is realized through two major processes: (1) adsorption and (2) fractional/cryogenic distillation, both of which are generally not cost or energy effective (Yang et al., 2010). Membrane separation is a new technology with the potential of solving challenging gas separation problems at lower energy consumption and minimum environmental impact. Since the launch of the first industrial membrane in 1980 by Permea (now a division of Air Products) for hydrogen separation, membrane-based gas separation technology has rapidly developed during the past 30 years (Ockwig & Nenoff, 2007; Merkel et al., 2010). The market of membrane gas separation equipment was $150 million/year in 2000, and was predicted to grow into $760 million/year by 2020 (Baker, 2002).

Membrane used for gas separation is a thin film with molecule-scale sieving or filtering capability, which allows the preferential permeation of the selective gas through the membrane, while excluding or restricting the permeation of the other gases, as shown in Figure 1.1. The driving force for the transport through membranes is the transmembrane pressure drop for each species. Gas transport/permeation through membranes is a complex process involving diffusion and adsorption. Membrane-based separation process essentially depends on the different diffusivity and/or solubility of the permeating gases in the membrane. The fundamental parameters describing the separation performance of membranes are permeability, permeance, and selectivity (Freeman, 1999). The permeability is defined as the product of permeation flux and

membrane thickness divided by the transmembrane pressure drop. Permeance is permeability divided by the membrane thickness. The selectivity is the ratio of permeability or permeances of two gases. In addition, stability including the mechanical, chemical and thermal stability are other important factors evaluating the membrane performances. All of these characteristics are determined by the pore structure, pore surface chemistry and bulk material properties of the membranes, as well as the specific separation conditions.

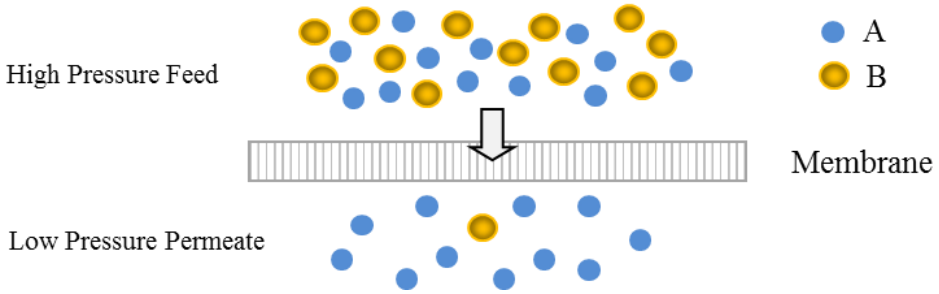

Figure 1.1 Membrane-based gas separation process

Based on the type of membrane material, gas separation membranes can be mainly categorized into polymer, microporous inorganic, dense metal and facilitated membranes. Among them, polymers remain the most studied membrane materials because of its advantages of low cost and ease of manufacture (Faiz & Li, 2012; Iinitch et al., 1992). Several polymer membranes including polysulfone, polyimide, polycarbonate, cellulose acetate have been successfully commercialized in industry for air separation, removal of carbon dioxide from natural gas, and separation of hydrogen (Baker, 2002). However, many polymer membranes suffer stability issues at high temperatures and under aggressive chemical environments. On the other hand, polymer membranes lose their selectivity dramatically upon exposure to high pressure hydrocarbon gases or carbon dioxide, due to the strong plasticization effect. Furthermore, polymer membranes appear

to have reached a general upper bound limit in the trade-off between permeability and selectivity: membranes that are more permeable are usually less selective and vice versa (Freeman, 1999). Figure 1.2 shows the upper bound correlation for O_2/N_2 separation (Robeson, 2008). Metal and facilitated membranes also suffer severe membrane fouling and stabilities issues, which restrict their industrial applications (Ockwig and Nenoff, 2007).

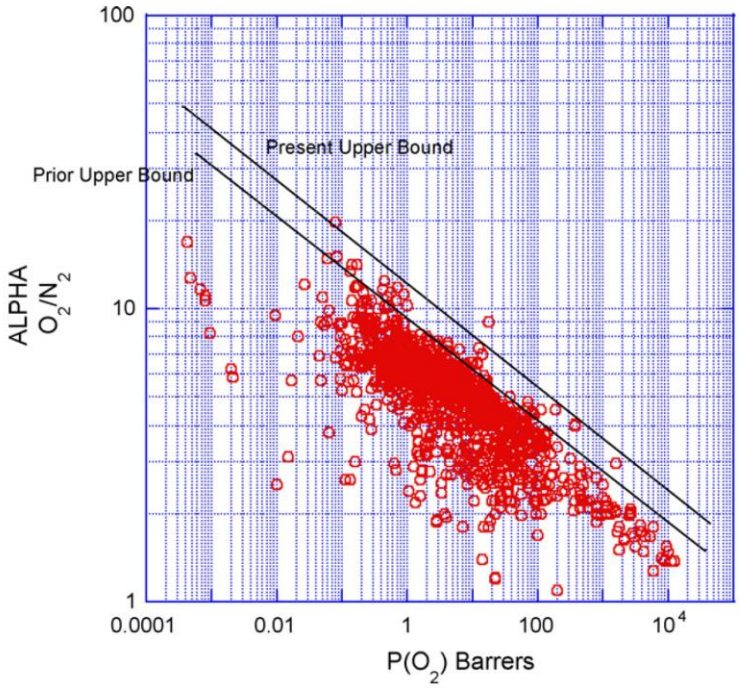

Figure 1.2 Upper bound correlation for O_2/N_2 separation (Robeson, 2008)

Microporous inorganic membranes possess excellent chemical and thermal stability, and are capable of exceeding the separation performance trade-off observed for polymer membranes (Lin et al., 2002; Lin & Duke, 2013; Caro & Noack, 2008). These attributes make them very promising for industrial gas separations, particularly the separations under harsh conditions or/and at high temperatures. According to the definition of International Union of Pure and Applied Chemistry, the pore size of

microporous inorganic membranes is smaller than 2 nm. Based on the structure of membrane materials, microporous inorganic membranes can be divided into two categories: (1) amorphous microporous inorganic membranes including silica and carbon molecular sieve (CMS) membranes; (2) crystalline microporous inorganic membranes which include zeolite, metal organic framework (MOF) and zeolitic-imidazolate framework (ZIF) membranes.

Over the last two decades, extensive research have been conducted on membrane synthesis, post-synthesis modification, characterization, gas permeation and separation properties of microporous inorganic membranes (Tavolaro & Drioli, 1999; Yao & Wang, 2014; Qiu et al., 2014). It is difficult to comprehensively review all the work accomplished in these areas. Therefore, this chapter focused on the recent developments on membrane synthesis, structure, stability, and propylene/propane separation properties of microporous inorganic membranes. Special attention has been paid to the microporous inorganic membranes with relatively small pore size (0.3-0.7 nm), because this pore size range is on the order of the kinetic diameters of several industrially important gas molecules.

1.2 Amorphous microporous inorganic membrane

Silica and carbon molecular sieve membranes (CMS) are representatives of amorphous microporous inorganic membranes. Although not well defined, the micropores of these two membranes are still narrowly distributed with the pores size typically in the range between 0.3 to 0.5 nm. Besides, silica and CMS membranes also share a lot of similarities in membrane synthesis. For example, chemical vapor deposition method can be used to prepare both membranes (Ockwig and Nenoff, 2007). Another

method, named sol gel method for synthesizing silica membrane, is also similar to the coating/pyrolysis method used for preparing CMS membranes. Both of these two methods involve three steps including the selection/synthesis of precursors, formation of precursor films on support and a final high temperature treatment to consolidate and form the final inorganic membrane structure.

1.2.1 Microporous silica membranes

Microporous silica membrane generally consists of three layers: (1) a bottom macroporous substrate with pore size usually larger than 200 nm providing the mechanical strength and low gas diffusion resistance; (2) a mesoporous intermediate layer which allows coating of thin and high quality silica membrane on the surface; and (3) a thin selective silica membrane layer on top. Silica membranes derived from the widely used tetraethyl orthosilicate (TEOS) precursor usually possess micropores of approximately 0.3 nm in size, which is only desirable for hydrogen separation. Although excellent permeance and selectivity can be achieved, silica membranes suffer severe hydrothermal stability issues due to the nature of the membrane materials. Therefore, the latest research on silica membranes over the past several years has been focusing on the two critical issues that remain to be solved: the control of pore size and the hydrothermal stability.

Researchers proposed to replace the siloxane bonds by Si-C bonds in the silica network by using new precursors like bis(triethoxysilyl)methane (BTESM) and bis(triethoxysilyl)ethane (BTESE), which contain methylene and ethylene groups respectively (Castricum et al., 2008;, Kanezashi et al., 2011). These groups, which can not be hydrolyzed, remains in the pore network and act as a spacer to enlarge the pore

size (as shown in Figure 1.3). A BTESE-derived silica membrane showed a H_2 permeance about 1 order of magnitude higher than previously reported TEOS-derived silica membranes. The BTESM-derived membrane with the pore size between those of TEOS and BTESE-derived membranes was found to be suitable for separation of the relatively large C_3H_6 and C_3H_8 molecules (Kanezashi et al., 2012; Kanezashi et al., 2014). In addition to these pore size control effect, the incorporation of the Si-C-Si and Si-C-C-Si units into the silica networks significantly improved the hydrothermal stability of the membranes. The BTESE derived hybrid silica membrane prepared by Castricum et al. (2008) exhibited excellent stability in the dehydration of *n*-butanol at 150 ℃ for almost two years.

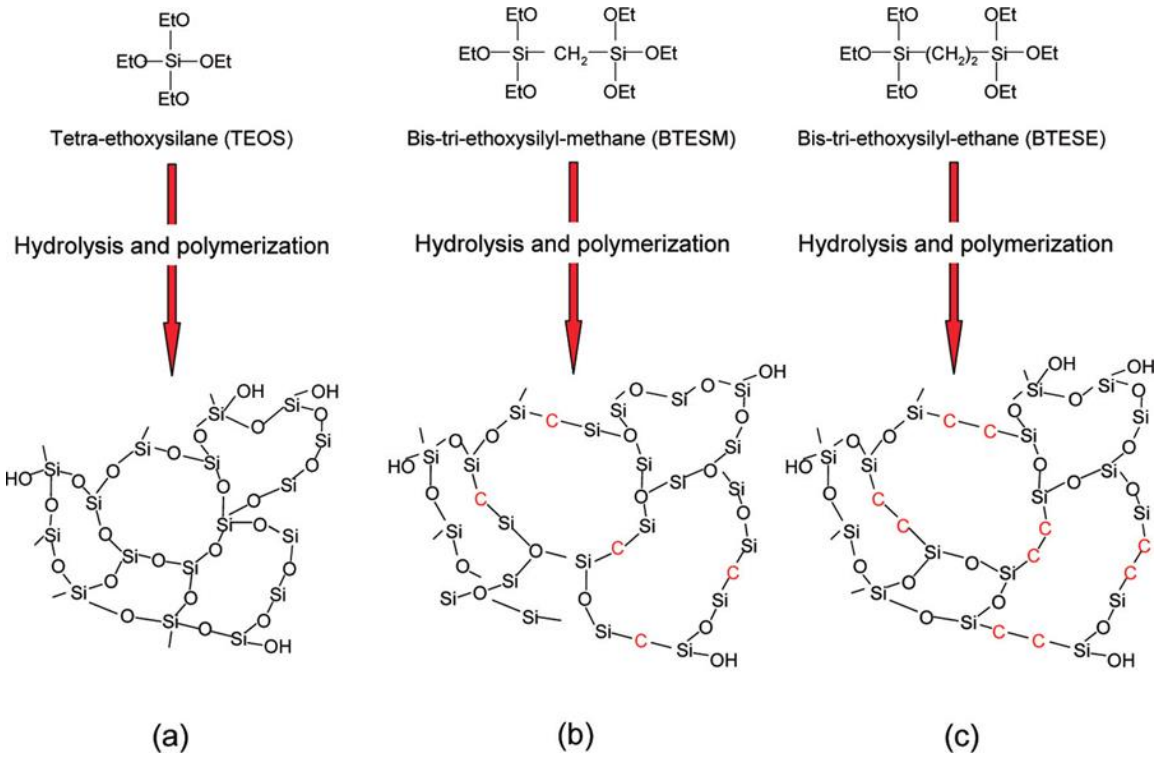

Figure 1.3 Schematic micropore network of amorphous silica membranes derived from (a) TEOS, (b) BTESM, and (c) BTESE (Kanezashi et al., 2011)

1.2.2 Carbon molecular sieve membrane

Carbon molecular sieve (CMS) membranes are generally prepared by the pyrolysis or carbonization of appropriate polymer precursor membranes under vacuum or inert atmosphere. The chemical composition of CMS membrane usually contains >80% carbon elements and a small amount of other elements, such as H, O, N, etc (Salleh et al., 2011). Due to their inorganic nature and high rigidity, CMS membranes possess excellent thermal and chemical stability.

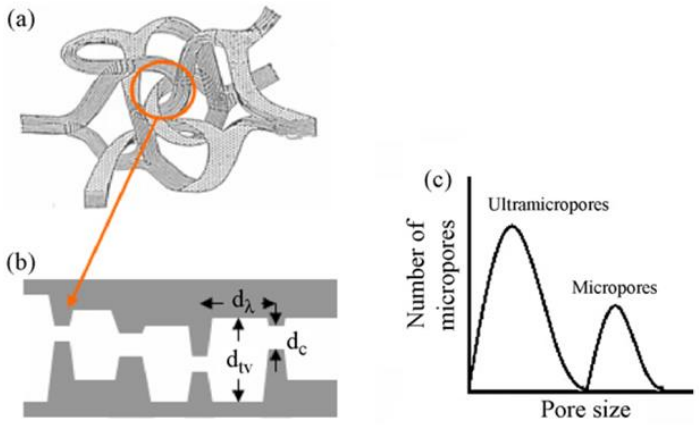

Figure 1.4 Structure of carbon materials (a), pore structure of carbon membrane (b), and bimodal pore distribution (c) (Kiyono et al., 2010)

The pore structure of carbon membrane is formed by the irregular/imperfect packing of aromatic domains and graphene sheets. The structure of CMS membrane is still considered to be amorphous due to the lack of long range orders. The micropore structure of CMS membrane is idealized to be slit-like, as schematically shown in Figure 1.4 (Kiyono et al., 2010). The pore constriction, with the critical dimension d_c approaching the kinetic diameter of the diffusing molecules, is responsible for the strong molecular sieving effect. The larger micropores d_{tv}, allows the transport of gases with low

resistance. Such a slit-like bimodal micropore structure provides CMS membranes with separation performance above the upper bound trade-off curve of polymer membranes.

In general, the fabrication of CMS membranes involves several steps shown in Figure 1.5. Each step needs to be well controlled to ensure a final high quality membrane with desirable pore structure for the targeted gas separation. The synthesis/selection of precursor materials is the first step in making CMS membranes. The basic requirement for polymer precursor is that it should have good thermal stability, without liquefying or softening during the high temperature pyrolysis process. The glass transition temperature and the free volume are the most important factors in determining the pore structure of the final membrane. The second step is the preparation of a thin film of the precursor materials on porous supports or a self standing polymer precursor membrane with a hollow fiber configuration. This step needs to be carefully controlled to avoid the formation of defects in the film, which might be transferred into the final CMS membrane. Pyrolysis is another critical step in which the polymer precursor decompose and form the amorphous carbon structure under the high temperature treatment in an almost oxygen-free atmosphere. Post-treatment provides an option to further modify the pore size and structure, or chemistry properties of the CMS membranes.

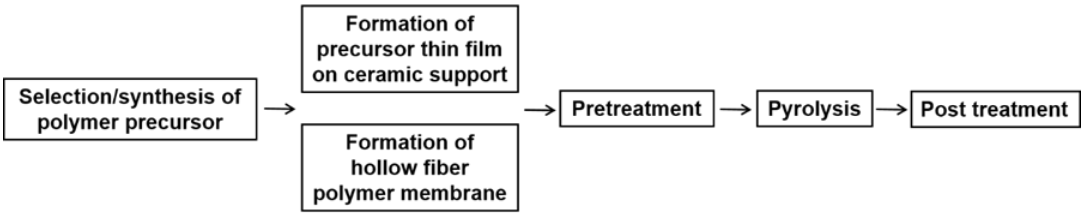

Figure 1.5 Typical process for CMS membrane fabrication

CMS membranes typically have two configurations: supported membrane and unsupported hollow fiber membrane. High mechanical strength is achieved through

fabricating CMS membranes on ceramic or stainless steel supports. The pore size of the support is usually larger than 200 nm, providing low resistance for gas transport. The supported CMS membrane usually has a membrane thickness above 1 μm, because a substantial membrane layer is required to cover the macropores of support. Hollow fiber CMS membrane has the advantage of high packing density. It can be prepared by direct pyrolysis of hollow fiber polymer membrane. However, CMS membrane with hollow fiber structure is brittle and requires careful handling during operation.

For both supported and hollow fiber CMS membranes, the microporous structure is directly related to the properties of polymer precursors. A wide range of polymer precursors including polyimides, phenolic resin, polyetherimide and polyfurfuryl alcohol have been used to produce CMS membranes (Salleh et al., 2011). Different precursors with different free volume and glass transition temperature usually require different pyrolysis conditions to ensure a good quality CMS membrane. The application of most CMS membranes is mainly in the area for the separation of gas mixtures with relatively small kinetic diameters, such as H_2/N_2, H_2/CO_2, CO_2/N_2, O_2/N_2. Recently, researchers have synthesized several types of novel 6FDA-based polyimides that are not commercially available as the polymer precursor for CMS membranes. Although these polyimide polymers are more expensive than the others, CMS membranes derived from them have appropriate pore size for the separation of larger molecules, like ethylene/ethane and propylene/propane separation.

Regarding to the pyrolysis, extensive work has been conducted to study the effects of various important parameters including pyrolysis atmosphere, final pyrolysis temperature, thermal soak time and ramping rate on the formation of CMS membrane. In

general, CMS membranes pyrolyzed in vacuum are more selective but less permeable than those prepared in an inert atmosphere (Geiszler & Koros, 1996). Higher pyrolysis temperature and longer thermal soak time tend to narrow the pore constrictions by sintering effect, resulting in a membrane with higher selectivity and lower permeability. It should be noted that the pyrolysis parameters are closely related to the type and properties of the selected polymer precursor, thus require a delicate optimization to ensure a final membrane with desirable properties.

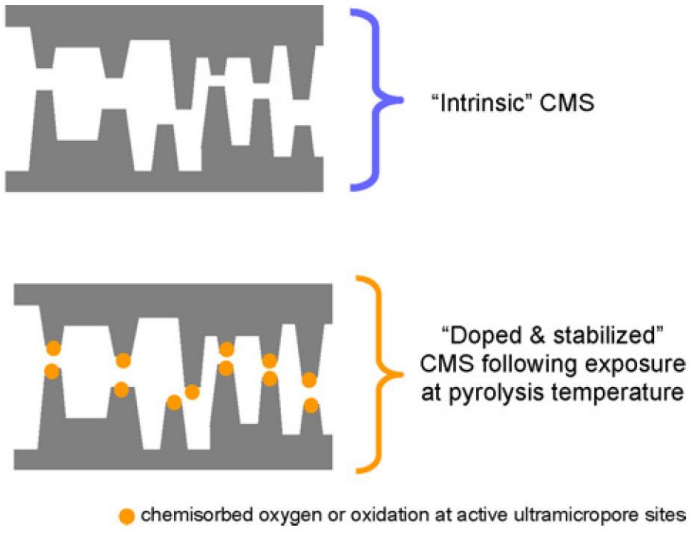

Figure 1.6 A schematic of oxygen doping process during pyrolysis (Kiyono et al., 2010)

A novel method called oxygen doping method was recently developed by Koros' group (2010) to tune the pore size. This approach introduces a controlled amount of oxygen into the pyrolysis atmosphere. The chemisorption of oxygen on the active sites in membrane occurred during the pyrolysis process, forming oxygen containing groups on the pore windows, as schematically shown in Figure 1.6. Improved CO_2/CH_4 selectivity was realized as a consequence of the narrowed effective pore size. It should be noted that

the concentration of oxygen needs to be carefully controlled to avoid overdoping, forming micropores with undesirable pore size.

1.3 Crystalline microporous inorganic membrane

Crystalline microporous inorganic membrane including zeolites, metal organic framework (MOF) and zeolitic-imidazolate framework (ZIF) membranes possess highly defined intracrystalline micropores with unique molecular sieving and preferential adsorption properties. Zeolite membranes research took off rapidly in the 1990s and has received continuing interests until now. Extensive studies in this area have established two effective membrane synthesis methods: in-situ crystallization and secondary growth hydrothermal synthesis. Because of the similarities between zeolites and MOF/ZIFs, these two methods were successfully adopted to preparing MOF and ZIF membranes shortly after the discoveries of MOF and ZIF materials. Despite great effort over the past three decades, synthesis of high quality crystalline microporous inorganic membrane in a low-cost, efficient, and reproducible way still remains a major challenge.

1.3.1 Zeolite membranes

Zeolites are crystalline aluminosilicates with pore framework structures built up by SiO_4 and AlO_4 tetrahedras. More than 200 different zeolite framework types have been discovered or synthesized. The majority of the zeolite membranes reported includes FAU, MFI, LTA, DDR and CHA type zeolite membranes (Lin et al., 2002), because their pore sizes lie in the kinetic diameter ranges of import gas molecules (shown in Figure 1.7). The pore size of theses zeolite framework decreases in the order: FAU (0.7 nm) > MFI (0.55 nm) > LTA (~0.4 nm), DDR (0.4 nm), SAPO-34 (0.38 nm). Among them, MFI type zeolites (ZSM-5 and silicalite) membranes are the most studied membranes,

because of its excellent performance, chemical and thermal stability for the separation of several important gas mixture systems, including hydrogen separation, carbon dioxide capture, and xylene isomers separation (Lin & Duke, 2013; Caro & Noack, 2008).

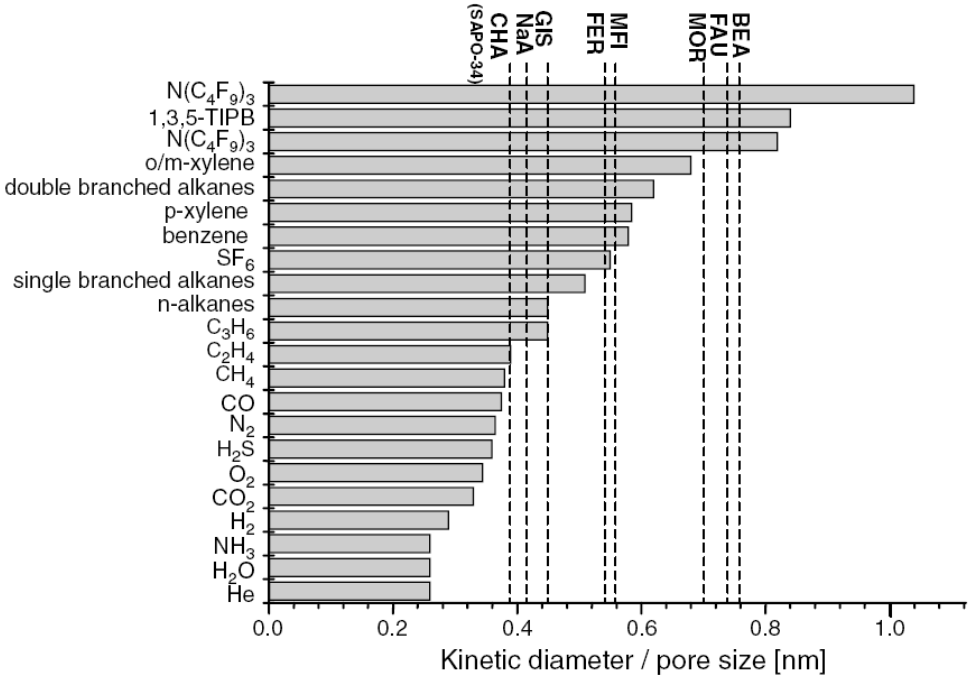

Figure 1.7 Comparison between the effective pore sizes of different zeolites and the kinetic diameters of gas molecules (McLeary et al., 2006)

To provide strong mechanical strength, zeolite membranes are usually prepared on macroporous stainless steel or ceramic supports to form a composite membrane structure. Figure 1.8 shows the typical steps for fabricating macroporous ceramic supports and then synthesizing zeolite membranes on the support surface by secondary growth method. The ceramic supports in the geometry of disk, tubular or hollow fiber are fabricated by traditional ceramic processing method, such as pressing and extrusion, followed by a high temperature sintering treatment. The fabricated ceramic supports are usually coated with an additional ceramic layer to repair the surface flaws. The zeolite

membrane is synthesized on the support by either in-situ or secondary growth method. As compared to the in situ method which usually requires several cycles of synthesis, secondary growth method gives a better control of the zeolite membrane quality by decoupling the nucleation and crystal growth step. The as-synthesized zeolite membrane needs to be heat treated at medium to high temperature to remove any adsorbed impurities or the organic templates used during the membrane synthesis step.

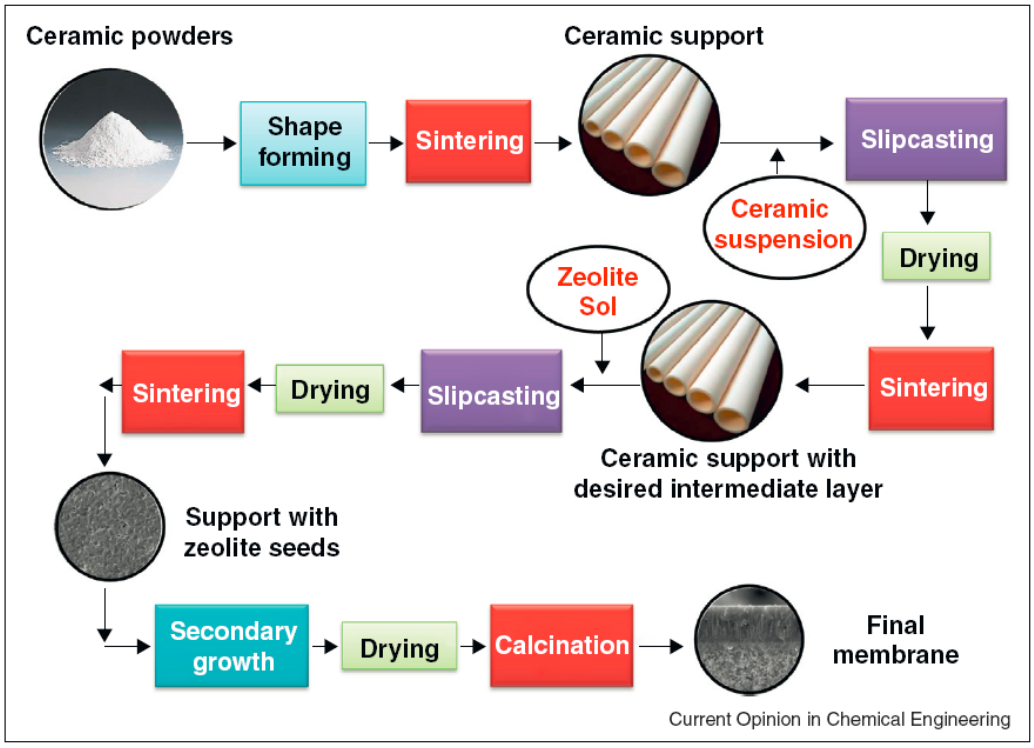

Figure 1.8 Steps for preparing ceramic supported polycrystalline zeolite membranes by secondary growth method. (Lin & Duke, 2013)

The interesting gas separation properties of zeolite membranes arise from their unique molecular sieving effect and adsorption characteristics of the highly defined molecular-scale intracrystalline micropores. However, zeolite membranes contain inter-crystalline gaps usually unavoidably formed during membrane synthesis, and/or during

the post-synthesis template removal by high temperature calcination. These gaps, with sizes larger than the zeolitic pores, provide non-selective transport of gas or liquid molecules, degrading the overall membrane performance. Recently, several new approaches including the manipulation of crystal orientation (Lai et al., 2004; Lai et al., 2003; Pham et al., 2011), template-free synthesis (Pan & Lin, 2001; Lai & Gavalas, 2000; Kanezashi et al., 2006) and rapid calcination process (Choi et al., 2009, Yoo et al., 2010) have been proposed and studied by researchers to minimize or eliminate these inter-crystalline defects.

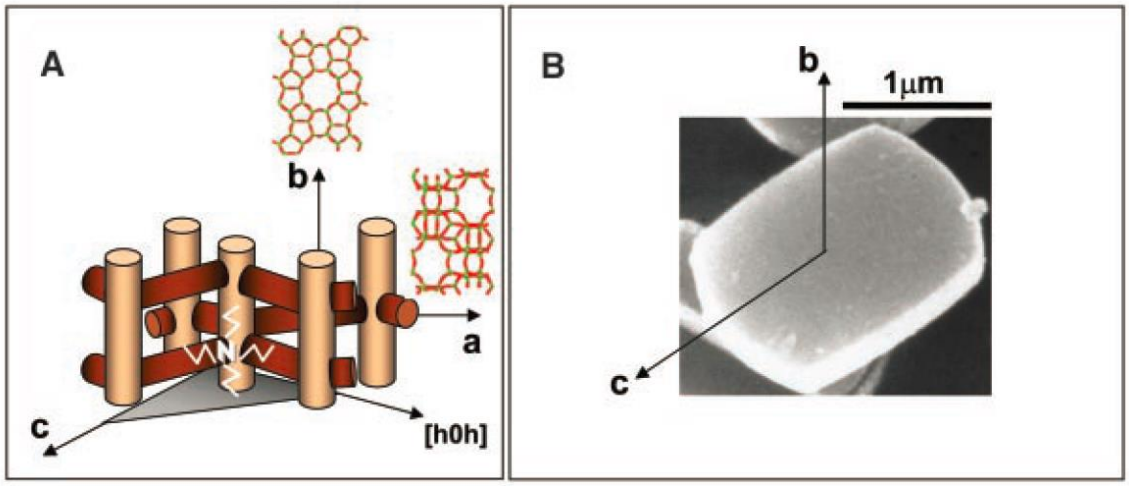

Figure 1.9 (A) A schematic representation of MFI zeolite framework structure. (B) SEM images of the characteristic shape of a MFI zeolite crystal (Lai et al., 2003)

The orientation of the crystallites that consists of the membrane layer plays an important role in controlling the amounts of intercrystalline gaps formed during the membrane synthesis step. For example, it is well know that columnar *c*-oriented MFI zeolite membrane contains more intercrystalline pores than the random, *h0h* or *b*-oriented MFI membranes. On the other hand, manipulating the crystal orientation is of particular interest for zeolite membranes with asymmetric intracrystalline micropore structure. For

example, the MFI zeolites pore structure, as shown in Figure 1.9, consists of a straight channel along the *b*-axis with circular openings of 0.54×0.56 nm and a sinusoidal channel along the *a*-axis with elliptical openings of 0.51×0.55 nm. Along *c*-direction, which is the channel intersections, the transport of molecules will take a tortuous path either through the straight channel and/or the sinusoidal channel. Apparently, membrane with a preferential *b* orientation allows the transport of molecules through the straight channels with the lowest resistance, offering the optimum performances.

The first high quality *b*-oriented MFI zeolite membranes were synthesized by Tsapatsis group (2003). Secondary growth method was used for the membrane synthesis, in which a *b*-oriented zeolite seeds layer was first prepared on substrate, followed with a controlled secondary growth to seal the gaps between seeds and form a well-intergrown *b*-oriented membrane. Trimer-TPA was used as structure direction agent to enhance relative growth rates along the desirable out-of-plane direction, avoiding twin overgrowths and random nucleation. The resultant membranes exhibited a *p*-/*o*-xylene separation factor as high as 500, as well as a superior *p*-xylene permeance approaching that through alumina support. Several research groups followed this direction, but highly uniform *b*-oriented MFI membrane has not been achieved. More recently, Yoon et al (2011) reported facile methods to grow highly uniform *b*-oriented silicalite-1 membranes on porous substrate through precise control on gel compositions and processing temperatures. Their membranes exhibited a *p*-/o-xylene separation factor above 1000, which is the highest value reported in literature.

Intercrystalline defects formed during the post-synthesis treatments are mainly from the template removal process. Organic templates, such as tetrapropylammonium

hydroxide (TPAOH), or tetrapropylammonium bromide (TPABr) are generally used as structure direction agents during the synthesis of MFI zeolite membrane to facilitate the membrane growth. These templates trapped inside the zeolitic pores need to be removed by high temperature calcination (> 400 ℃) to open up the zeolite channels, which will cause a shrinkage of the zeolite framework. Substantial stresses developed during this template removal process create/enlarge intercrystalline gaps between zeolite crystallites, and sometimes even cause cracks in the membrane layer. On the other hand, the thermal expansion mismatch between the zeolite membrane layer and the support also results in stresses in the membrane, increasing the amount of intercrystalline defects.

In order to overcome these drawbacks brought by using organic templates, template-free synthesis approach was proposed by researchers, and has attracted attention over the past several years (Pan & Lin, 2001). This novel method, which avoids the high temperature calcination step, not only leads to a membrane with fewer intercrystalline defects, but also reduces the cost of membrane synthesis. Hedlund et al (1999) reported the synthesis of ZSM-5 membrane on α-alumina disk support by template-free method. Their membrane showed higher H_2/*i*-butane mixture separation factors than previously reported results. Lai and Gavalas (2000) prepared ZSM-5 membrane on asymmetric α-alumina tubes by template-free secondary growth, and achieved a membrane with a H_2/*n*-butane ideal selectivity above 104 and an O_2/N_2 selectivity of ~9. Kanezashi et al. (2006) found that template-free secondary growth could also be applied to synthesizing good quality MFI zeolite membrane on zirconia coated alumina support. The resultant membrane showed a He permeance above 10^{-7} mol/(m^2·s·Pa) with a He/SF_6 perm-selectivity of around 50 at 25 ℃.

Another approach to minimize the intercrystalline defects in columnar *c*-oriented MFI zeolite membranes is a rapid thermal process (RTP) methodology proposed by Tsapatsis (2009). Different from the conventional calcination using a slow ramping rate usually smaller than 1 ℃/min, the rapid thermal process heats the membrane up to 700 ℃ within one minute using an infrared lamp-based furnace followed by soaking the membrane at 700 ℃ for 30 s to 2 min. It was hypothesized that this new method results in condensation of Si-OH groups between adjacent crystallites, thus strengthening the grain bonding before the removal of templates. The membrane treated by a rapid thermal process followed with a conventional calcination exhibited a superior *p*-/*o*-xylene mixture separation factor up to 128 as compared to the conventionally calcined membrane with a separation factor less than 4. Yoo et al. (2010) then reported the use of only one RTP step to remove the templates from thin (400-500 nm) randomly oriented zeolite membranes. The resultant membrane showed very attractive performances with the highest *p*-/*o*-xylene separation factor up to 335, which is already comparable to that of *b*-oriented membranes synthesized by using specially designed structure-directing agents (Lai et al., 2003).

These progresses in minimizing the intercystalline defects have successfully synthesized MFI zeolite membranes with excellent xylene isomers separation. However, even for a high quality MFI zeolite membrane with minimum defects, good separation to gases with small kinetic diameters is difficult to achieve due to the relatively large zeolitic pore size (~0.6 nm).In order to realize other interesting separation properties that are not expected from normal zeolite membranes, researchers have developed a catalytic cracking deposition method (CCD) to modify the intracrystalline zeolitic pores. In this

method, which was first proposed by Masuda et al. (2001), silane compounds are adsorbed and then catalytically cracked on the active site inside the zeolitic channels, thus reducing the effective pore size and enhancing the molecular sieving characteristic of zeolite membrane. The modified membrane showed a remarkably enhanced H_2 selectivity of ~100 over N_2 or O_2, as compared to the Knudsen-like selectivity for the non-treatment membrane.

In the past decade, several groups have synthesized CCD modified MFI zeolite membrane for high temperature H_2/CO_2 separation in water gas shift reaction. Falconer and co-workers (2005) reported a high H_2/CO_2 selectivity of 47 for a CCD modified boron-substituted ZSM-5 membrane. However, the improvement in hydrogen selectivity was compromised with the permeance decreased more than one order of magnitude after the modification. Dong and co-workers (2009) used in-situ synthesis method to synthesize MFI membrane on alumina support. The membrane prepared at such condition allowed a controlled partial modification of the zeolitic channels, achieving a high H_2/CO_2 mixture selectivity of 108 with a moderate ~40% reduction in H_2 permeance. Recently, a ZSM-5/silicalite bilayer membrane was designed and synthesized by Lin and co-workers (2012) for CCD modification. The deposition occurred only in the thin ZMS-5 top layer which contains active sites, ensuring a minimal reduction of only about 31% in H_2 permeance from the fresh membrane.

1.3.2 MOF membranes

Metal organic frameworks (MOF) are new porous materials consisting of metal ions and organic linkers. Due to their uniform but tunable pore sizes and high porosity, MOFs have received widespread attention over the last 15 years for a variety of

applications including separation, sensors, energy storage, etc (Li et al., 1999; Eddaoudi et al., 2002; Yaghi et al., 2003). MOF-5 (shown in Figure 1.10) and HKUST-1($Cu_3(BTC)_2$) are two typical MOF materials have been fabricated into thin films on support to be used as a membrane for separation (Qiu et al., 2014). However, the performances for gas separations of these two and other MOF membranes are generally not impressive due to their relatively large pore size. For example, the permeances of several gases were found to decrease with increasing molecular weight of the molecules in the order of H_2 > He > CO ~ N_2 > CO_2 > SF_6 for a high quality MOF-5 membrane (Zhao et al., 2011). The single gas selectivity is close to the value expected from Knudsen diffusion. On the other hand, it has been reported that a lot of MOFs are not very stable, and are especially sensitive to water.

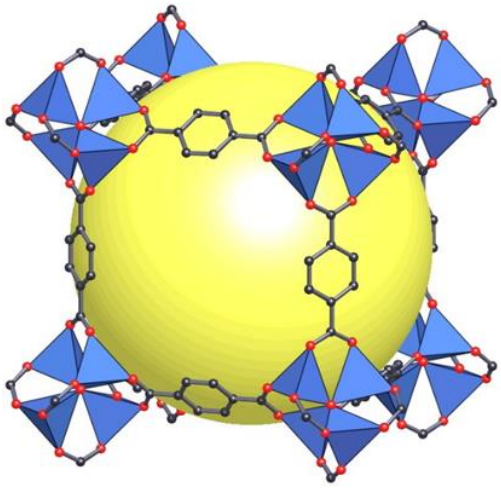

Figure 1.10 Structure of a MOF-5 metal organic framework (Li et al., 1999)

1.3.3 ZIF membranes

Zeolitic imidazolate frameworks (ZIFs) are a class of metal-organic frameworks with three-dimensional structures composed of tetrahedrally-coordinated metal ions (e.g., Zn, Co) bridged by imidazolate (Im). ZIFs are topologically isomorphic with zeolites,

with Metal-Im-Metal angle similar to the Si-O-Si angle in zeolites. Figure 1.11 shows the structure of ZIF-8. In comparison to the other MOFs, ZIFs possess permeant porosity, excellent thermal and chemical stability, and ZIF membranes have been extensively studied for gas separation since 2010 (Yao & Wang, 2014; Betard & Fischer, 2011; Li et al., 2011).

The traditional methods used for zeolite membrane synthesis, such as in-situ growth and secondary growth are also very effective in synthesizing high quality ZIF membranes. Langmuir-Blodgett and layer-by-layer thin-film preparation techniques can also be used to prepared ZIF films and membranes (Yao & Wang, 2014). As compared to the synthesis of zeolite membranes, ZIF membrane synthesis does not have any problems associated with templates removal, because organic template is not required for the crystal nucleation/growth. However, synthesis of ZIF membranes has experienced other issues, like the weak bonding strength between the seed/membrane layer and support due to the surface chemistry incompatibility. In order to further improve the membrane quality and synthesis reproducibility, several modified membrane synthesis strategies including support surface modification, reactive seeding and counter diffusion synthesis have been developed by researchers recently.

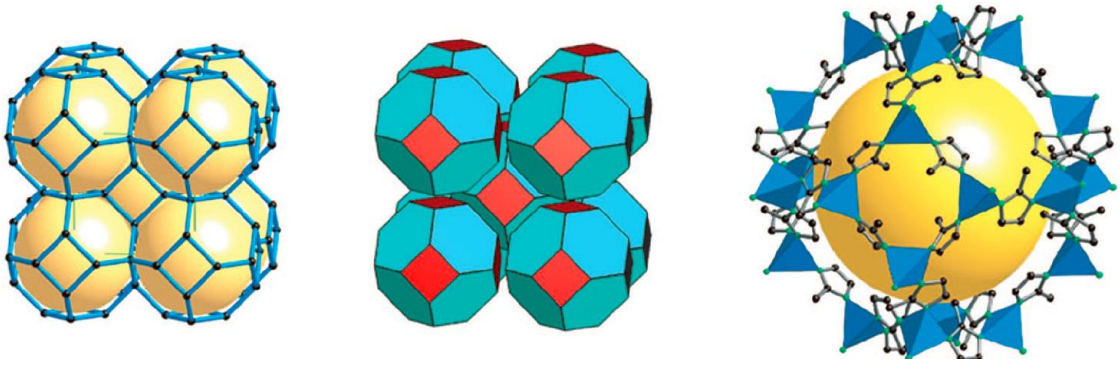

Figure 1.11 Structure of ZIF-8 (Park et al., 2006)

The surface chemistry incompatibility between ZIFs and alumina supports is caused by the fact that no direct chemical bonds can be formed between the organic linkers of ZIFs and the OH groups on the support surface. To address this issue, Caro and co-workers (2010) developed a novel covalent functionalization method using 3-aminopropyltriethoxysilane (APTES) as covalent linkers between the ZIF layer and alumina support. As shown in Figure 1.12, APTES was first coated on the support with strong bonding formed between the ethoxy groups of APTES and the surface hydroxyl groups of the Al_2O_3 support. Then the amino groups of APTES react with the aldehyde groups of the organic linker imidazolate-2-carboxyaldehyde (ICA) via imines condensation. Nucleation and growth of ZIF-90 was facilitated on the modified support surface, eventually forming a continuous molecular sieve membrane layer. Additionally, this novel approach avoided the seeding step for membrane synthesis. This method was then widely used by other researchers to synthesize different ZIF membranes on different type supports.

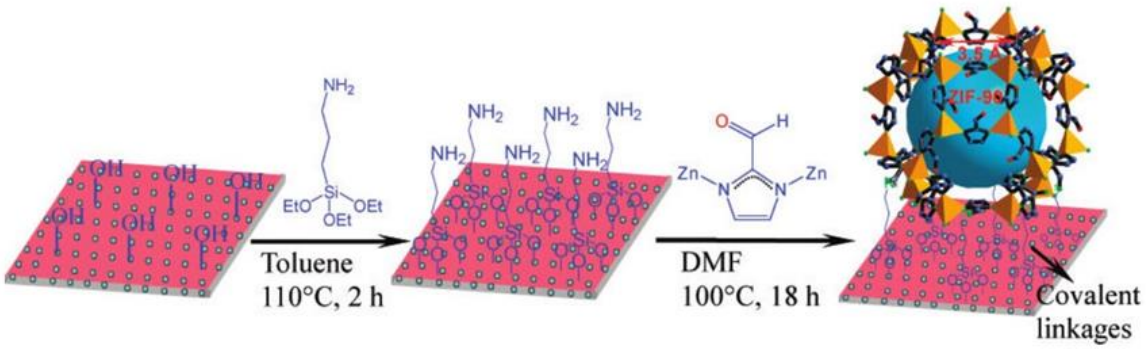

Figure 1.12 Surface modification of support and subsequent synthesis of ZIF membrane (Huang et al., 2010)

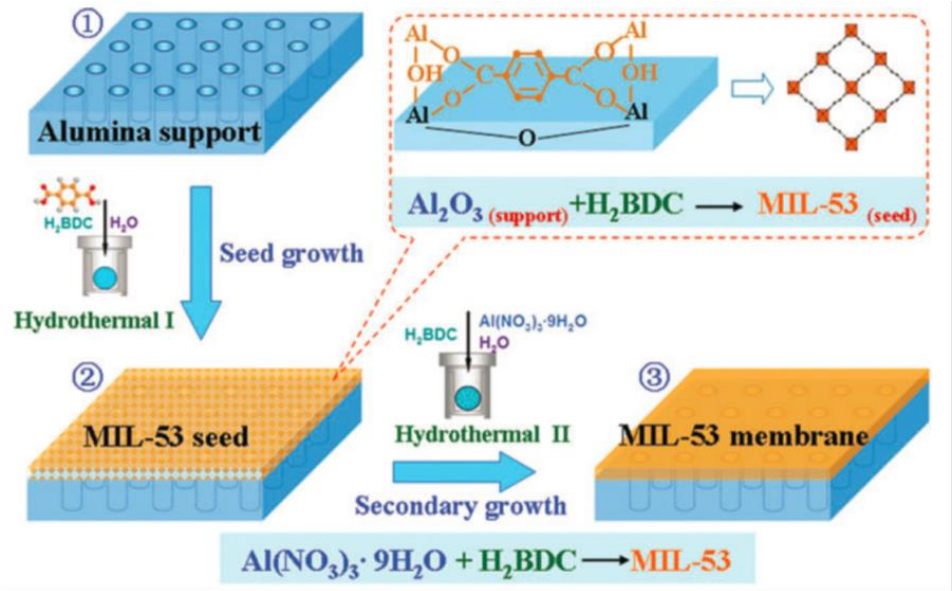

Figure 1.13 Reactive seeding synthesis of MIL-53 membrane (Hu et al., 2010)

The reactive seeding method developed by Jin and co-workers (2010) is another new strategy to address the bonding issue in MOF/ZIF membrane synthesis. The concept behind this method is using the support itself to provide inorganic sources reacting with the organic precursor to directly form a seeds layer on the support surface. The uniform seeds layer formed in such manner is strongly chemically bonded with the substrate, and greatly aid in the following membrane growth step. This method was first designed and used in the synthesis of MIL-53 membrane with the synthesis steps shown in Figure 1.13. In the cases for ZIF membranes containing zinc as metal coordinators in the frameworks, porous zinc oxide support was used as substrate to provide the zinc source for the formation of seeds layer, followed with a normal secondary growth step using both zinc and organic sources. Using this approach, Zn-BLD, ZIF-78, ZIF-71 and ZIF-68 membranes have been successfully prepared (Wang et al., 2012; Dong et al., 2012; Dong & Lin, 2013; Kasik et al., 2015). Although effective for ZIF membrane synthesis, the

zinc oxide support is not as robust as alumina support. The mechanical strength of zinc oxide supported composite membrane needs to be improved in the future.

The concept for counter-diffusion synthesis was originally developed for the synthesis of silica and zeolite membrane, and was recently introduced to ZIF membrane synthesis. In this method, ZIF nucleation and crystallization occurs on the substrate when the metal ion solution and the organic linker solution, which counter-diffuse through the porous the substrate, meet with each other. Yao et al. (2011) for the first time prepared ZIF-8 membrane on a Nylon membrane using counter-diffusion method. The two precursors solutions zinc nitrate methanol solution and 2-methylimidazole methanol solution separated by the Nylon membrane diffuse through the porous Nylon membrane and crystallize at the interface. After 72 h of synthesis, a continuous ZIF-8 membrane with a H_2/N_2 ideal selectivity of 4.3 was formed on the zinc nitrate solution side. Several other groups have also successfully made high quality ZIF membranes on other substrates including coarse alumina macroporous support and alumina hollow fibers.

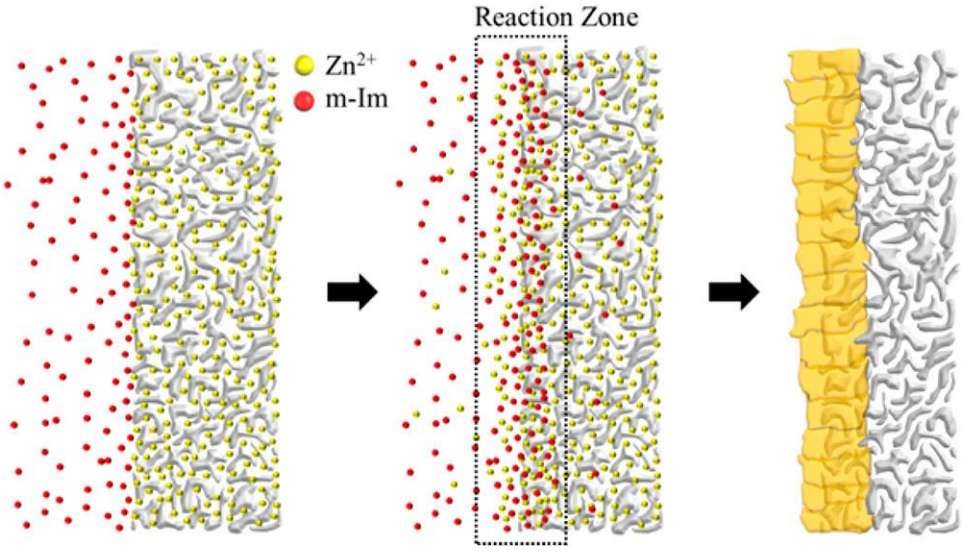

Figure 1.14 In situ counter-diffusion synthesis of ZIF-8 membrane (Kwon & Jeong, 2013)

More recently, Kwon & Jeong (2013) developed this method into an in situ counter-diffusion approach to synthesize ZIF-8 and ZIF-7 membranes. As schematically shown in Figure 1.14, a support with support pores pre-infiltrated with zinc nitrate was immersed in a ligand solution containing sodium formate. Then the zinc nitrate diffused out from the support and meet with 2-methylimidazole solution at the solution/support interface to form a reaction zone. Rapid nucleation and crystal growth took place in the reaction zone to eventually form a continuous membrane layer. Excellent propylene/propane mixture separation performance with a selectivity of around 50 was observed for this membrane.

1.4 Membrane stability

Besides the permeability/permeance and selectivity, the stability of membranes, including mechanical stability, thermal and chemical stability is critical to industrial application. Good mechanical stability has been achieved by preparing the membranes on inorganic supports (e.g. alumina, zirconia and stainless steel) to form a composite membrane structure. Although generally more stable than their polymer membranes counterparts, microporous inorganic membranes have been experiencing some thermal and chemical stability problems associated with the specific membrane type, membrane composition and operation condition.

1.4.1 Stability of amorphous microporous inorganic membrane

Silica membrane is known to be not very stable under humid conditions. It was reported that water could significantly hinder the permeation of the other gases, reducing their permeances (Anderson et al., 2012). At high temperature conditions with the presence of water vapor, the silica membrane structure suffers densification and defect

formation issues. Several approaches as discussed earlier in this chapter have been developed by researchers to improve the hydrothermal stability.

CMS membrane is much more stable than silica membrane in terms of membrane structure, due to the excellent chemical and thermal stability of activated carbon materials. However, CMS membrane was reported to experience stability problems associated with the adsorption of organics, water and oxygen. Figure 1.15 schematically showed the aging mechanism due to the adsorption (Xu et al., 2014). Because of the organophilic nature of carbon surface, CMS membranes are vulnerable to the adsorption of organic contaminants. Severe losses in membrane performance were found for a feed stream containing organics with a concentration as low as 0.1 ppm (Jones & Koros, 1994). Although the surface of CMS membrane is hydrophobic, adsorption of water vapors could take place on the oxygen containing groups on micropore walls, blocking the permeation of other gas molecules through the membrane. Jones and Koros (1995) found that both the O_2 and N_2 permeace and O_2/N_2 selectivity of CMS membrane decreased as the relative humidity in the gas mixtures increased from 23% to 85%. In their following study to improve the stability of CMS membrane under humid conditions, a hydrophobic polymer layer was coated on the membrane surface to protect the membrane from the attack of water vapor (Jones & Koros, 1995).

Oxygen chemisorption onto activated carbon materials is a known phenomenon. This could also occur to CMS membrane, because the materials of CMS membrane are essentially activated carbon. The chemisorption involves a reaction between oxygen and the active sites, which are usually the defects in graphene structure, to form carbonyl or other oxygen containing species on the pore walls, reducing the effective pore size and

porosity (Menendez & Fuertes, 2001; Lagorsse et al., 2008). Different from the physical adsorption of water vapor, the adsorption of oxygen is chemical adsorption and irreversible.

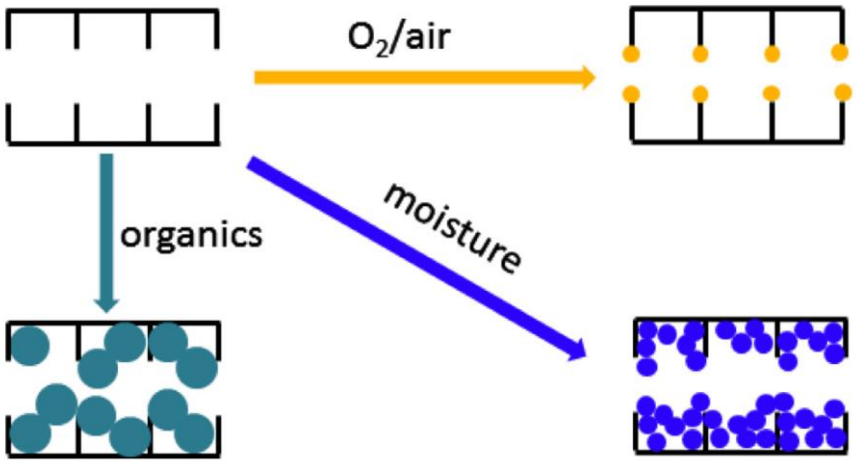

Figure 1.15 Cartoon representation of mechanisms of aging in CMS membranes caused by adsorption (Xu et al., 2014)

1.4.2 Stability of crystalline microporous inorganic membrane

In general, the stability of the three crystalline microporous inorganic membranes increases in the order of MOF < ZIF < zeolite. MOF are known to be not very stable under a lot of conditions, because the carboxylates ligands could be displaced by water or other nucleophiles, resulting in the collapse of framework. In contrast, ZIFs with frameworks that mimic zeolite topology are more chemical and thermal stable. ZIF membranes have been reported to stable for the separation of H_2/CO_2 and C_3H_6/C_3H_8 mixtures (Peng et al, 2014; Liu et al., 2014). However, it was recently found that ZIF-8, one of the most stable ZIF materials, will undergo hydrolysis under hydrothermal conditions (Yang et al., 2013). Therefore, the overall research on the stability of ZIF

membrane is rather limited and more research will be required to study their stability under different separation conditions.

Zeolite membranes usually exhibited much better thermal and chemical stability than all the other micropores membrane candidates. For a given zeolite membrane type, the chemical and thermal stability depends on the silicon to aluminum ratio in the zeolite framework. High or all-silica zeolite membranes are considered to be the most stable microporous membranes, due to the excellent stability of high silica zeolite materials. Moreover, high silica zeolite membrane is hydrophobic, making them less vulnerable to the effect of water vapor. However, it was reported that under long time high temperature operations, aluminum atoms could diffuse from alumina supports into the zeolite membrane framework, degrading the membrane stability. Lin and co-workers (2006) proposed the usage of a highly thermal stable zirconia intermediate layer between the alumina support and the zeolite layer to avoid the incorporation of aluminum. The MFI zeolite membrane with such multilayered structure demonstrated excellent long term stability (stable at least for a month) for hydrogen separation with simulated syngas feed (equal molar of H_2, CO_2, CO, and H_2O) with 500 ppm H_2S at 500 ℃ (Wang et al., 2014). This is the only hydrogen selective membrane candidate which is stable under such conditions.

Despite all these efforts, research on membrane stability under off-stream storage and on-stream separation operation conditions is relatively rare, as compared to the extensive studies on membrane synthesis and gas permeation/separation properties. More work are required to study and address the stability issues before scale up or/and eventual industrial commercialization of these promising membranes can be realized.

1.5 Membrane for propylene/propane separation

Propylene is the second most important starting material in petrochemical industry, making propylene/propane (C_3H_6/C_3H_8) separation one of the most important processes in the petrochemical industries (Eldridge, 1993; Motelica et al., 2012). It is traditionally performed by distillation, which is highly energy and capital intensive, because of the similar physicochemical properties of those compounds as shown in Table 1.1. As a more energy-saving and environmental friendly separation technology, membrane-based separation has been attracting great interest in recent years for the separation of C_3H_6/C_3H_8 mixtures.

Enormous amounts of effort have been expended in searching for and studying appropriate membrane materials for C_3H_6/C_3H_8 separation (Faiz & Li, 2012). Most studies have focused on processable polymers, including poly (p-phenylene oxide) (PPO), cellulosic and polyimide polymers (Iinitch et al., 1992; Ito & Hwang, 1989; Sridhar & Khan, 1999; Tanaka et al., 1996). However, polymer membranes appear to have reached an upper limit in the tradeoff between permeability and selectivity (Robeson, 2008; Burns & Koros, 2003). The separation performance of current polymer membranes is inadequate to meet the economical requirements for commercial applications. Furthermore, polymer membranes lose their selectivity upon exposure to high pressure hydrocarbon gases (due to the strong plasticization effect), which also makes them less attractive for large-scale application. Facilitated membrane is another membrane candidate for C_3H_6/C_3H_8 separation. The transition metal ions in the membrane can form reversible chemical bonds with olefin to offer high selectivity to olefins. However, the commercialization of facilitated transport membranes for C_3H_6/C_3H_8 separation has not

been realized due to the problems of carrier poisoning and short life span of the membranes. Therefore, special attention has been paid to the area of microporous inorganic membranes.

Table 1.1

Summary of properties of propylene and propane

Property	Unit	C_3H_6	C_3H_8
MW		42.08	44.10
Density	kg/m^3	1.77	1.85
bp, at 1 bar	℃	-47.6	-42.2
Mp	℃	-185.2	-187.7

1.5.1 Silica membrane

Most silica membranes are not suitable for C_3H_6/C_3H_8 separation, because their effective micropore size is smaller than the kinetic diameters of both propylene and propane molecules. An organic-inorganic hybrid silica membrane derived from bis(triethoxysilyl) methane (BTESM) was synthesized by Kanezashi and co-workers (2012) for the separation of propylene/propane. The silica network size of the membrane was precisely enlarged via a "spacer" using the Si-C-Si unit. Different calcination temperatures were used to fine tune the average pore size of the membranes. The resultant BTESM derived silica membrane contains a high concentration of silanol groups, which can interact with the C=C double bond of C_3H_6 molecules. Promising separation performances with a C_3H_6 permeance in the range of 1.0~3.0 $mol/(m^2 \cdot s \cdot Pa)$, and a mixture selectivity of around 30 were observed for the membrane calcined at 350 ℃. The stability of these membranes needs to be further examined, because the silanol groups are also potential active sites for the adsorption of water vapors.

1.5.2 Carbon membrane

Carbon molecular sieve (CMS) membranes, pyrolyzed from appropriate polymer precursors (Anderson et al., 2012; Yamamoto et al., 1997; Chng et al., 2009; Suda & Haraya, 1997), are other candidates for C_3H_6/C_3H_8 separation. As discussed earlier, due to their high rigidity and slit-like pore structure, CMS membranes possess exceptional thermal and chemical stability. Additionally, the separation performance can potentially surpass conventional polymer membranes, especially when separating gas pairs with similar physical properties like ethylene/ethane (C_2H_4/C_2H_6) or propylene/propane (C_3H_6/C_3H_8).

So far, much of the effort has focused on identifying appropriate polymer precursors and pyrolysis conditions to develop CMS membranes with desirable structures. For instance, Suda and Haraya (1997) synthesized CMS membranes by vacuum pyrolysis of Kapton polyimide film at 1000 ℃, and then activated the membranes in water vapor to slightly enlarge the pore dimension. The resultant CMS membrane displayed a pure-gas C_2H_4/C_2H_6 selectivity of 6 and a C_3H_6/C_3H_8 selectivity of 20. Steel and Koros (2005) investigated the effects of polymer precursors and pyrolysis parameters on the gas separation properties of dense, flat CMS membranes. A number of high-performance CMS membranes were developed in their work. For instance, the CMS membrane pyrolyzed at 550 ℃ using 6FDA/BPDA-DAM as precursor (with the structure shown in Figure 1.16) showed a C_3H_6 permeance of $1.1\sim1.9\times10^{-9}$ mol m^{-2} s^{-1} Pa^{-1} (3.3~5.7 gpu), calculated from the reported permeability of 200 Barrers and membrane thickness of 35~60 μm, and a pure-gas C_3H_6/C_3H_8 selectivity of 100.

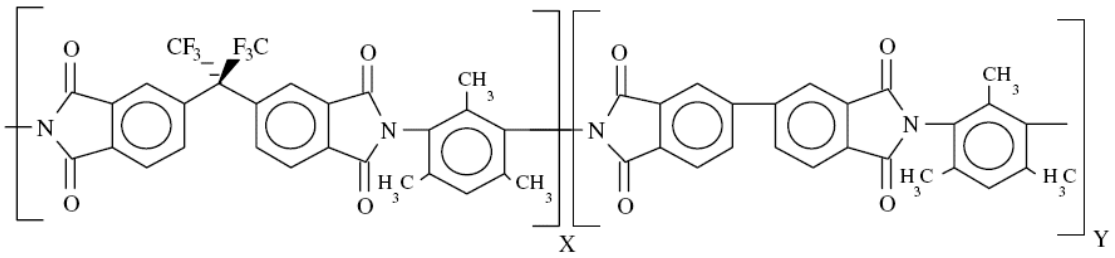

Figure 1.16 Structure of 6FDA/BPDA-DAM polymer precursor (Steel & Koros, 2005)

Asymmetric or composite membranes in the form of hollow fibers or flat sheets are often used in industrial membrane systems. Asymmetric hollow fiber CMS membranes can offer high packing density and reasonably high permeance. For instance, Okamoto et al. (1999) prepared hollow fiber CMS membranes by pyrolyzing an asymmetric hollow fiber polymer membrane of 3, 3', 4, 4'-biphenyltetracarboxylic dianhydride and aromatic diamines. The membrane had an asymmetric wall structure with a thin selective layer of approximately 200 nm and exhibited a high permeance of 8.7×10^{-9} mol·m^{-2}·s^{-1}·Pa^{-1} (26 gpu) for C_3H_6 at 35 ℃. However, a relatively low selectivity of 11 for a C_3H_6/C_3H_8 mixture separation was observed. Recently, Matrimid® derived CMS hollow fiber membranes were fabricated by Koros's group for C_2H_4/C_2H_6 separation (Xu et al., 2011). Their membranes showed a high selectivity of 12 and a C_2H_4 permeance below 3.35×10^{-10} mol·m^{-2}·s^{-1}·Pa^{-1} (1gpu). The relatively low permeance was caused by collapse of the porous substructure into a dense separation layer during pyrolysis. Another advantage of asymmetric CMS hollow fibers is that they do not require the use of high-temperature substrates, which can potentially reduce the cost for membrane production.

1.5.3 Zeolite membranes

Two types of zeolite membranes, faujasite-type (FAU) and titanosilicate ETS-10 membranes were studied for propylene/propane separation. A FAU membrane synthesized by secondary growth method showed a maximum propylene/propane ideal selectivity of approximately 28 (Giannakopoulos & Nikolakis, 2005). However, the maximum mixture separation factor was only about 13.7, indicating that the permeation of propane through membrane was enhanced by the presence of propylene gas. ETS-10 membranes prepared by Tiscornia et al. (2008) under the optimum synthesis conditions showed an average high propylene permeance of 7.9×10^{-8} mol/(m^2·s·Pa) and a low selectivity of 5.5. After 15 days of on-stream mixture separation, the C_3H_6 permeance and C_3H_6/C_3H_8 selectivity decreased by about 67% and 19%, respectively. This was due to the blockage of zeolitic pores by the hydrocarbon deposits formed from the decomposition reactions of hydrocarbons caused by the strong basicity of ETS-10.

1.5.4 ZIF-8 membranes

ZIF-8 membrane is an emerging membrane with superior separation performances towards propylene/propane separation. The functional pore size of ZIF-8 is around 0.4 nm, with potential to molecularly sieve propylene from propane. Adsorption studies showed that the ZIF-8 gives almost identical equilibrium adsorption capacity for propylene and propane, but the diffusivity of propylene is more than 100 times higher than that of propane due to the strong molecular sieving effects (Li et al., 2009). Thus, high quality ZIF-8 membranes were synthesized and studied for propylene/propane separation by several groups, and their work was summarized in Table 1.2. It can be seen that in general, a mixture selectivity above 30 and a propylene gas permeance in the

range of 1.0-4.0×10^{-8} mol/(m^2·s·Pa) can be achieved for ZIF-8 membranes with a thickness smaller than 3 μm. In Lin's studies, the ZIF-8 membranes demonstrated stable separation performances under both off-stream storage conditions (lab air, 10~30% humidity) and on-stream propylene/propane separation conditions under room temperature.

Table 1.2

Summary of the propylene/propane separation properties of ZIF-8 membranes reported in literature

Synthesis method	Membrane thickness	C_3H_6 permeance (mol/m^2·s·Pa)	C_3H_6/C_3H_8 selectivity	Reference
Secondary growth	2.5 μm	1.1×10^{-8}	30	Liu et al., 2014
Secondary growth	2.2 μm	2.0~3.0 ×10^{-8}	31~45	Pan et al., 2012
In Situ counter diffusion	1.5 μm	~2.0×10^{-8}	50	Kwon & Jeong, 2013
Counter diffusion	80 μm	~2.5×10^{-9}	59 (ideal)	Hara et al., 2014

1.6 Research objectives and significance

As reviewed in this chapter, MFI type zeolite membrane and carbon molecular sieve membrane are currently considered to be the most stable microporous membrane for gas separation. Several challenges regarding to the synthesis and characterization of these promising membrane candidates still remain to be solved. The use of membranes for propylene/propane separation is a relatively new but very promising direction in membrane area. However, MFI type zeolite membrane has not been explored for this separation. CMS membranes have shown good propylene/propane separation

performances above the upper bound trade off curve of polymer membranes. In order to meet the requirements for industrial application, the performance, especially the propylene gas permeance needs to be further improved through delicate structure design and membrane synthesis. The objective of this dissertation is to present a systematic study into the synthesis, characterization, and propylene/propane separation properties of MFI zeolite membrane and 6FDA-derived carbon molecular sieve membrane.

1.6.1 Research objective 1

Characterizing the micropore structure, especially the intercrystalline micropores of supported polycrystalline MFI zeolite membranes is difficult to be achieved, due to the limitations of current characterization techniques. To address this, for the first time, two positron annihilation spectroscopy (PAS) techniques, positron annihilation lifetime spectrocopy (PALS) and Doppler broadening energy spectroscopy (DBES), were used in our work to characterize non-destructively the hierarchical microporous structure of polycrystalline MFI zeolite membranes on inorganic supports. The structure information obtained from PAS was correlated to the xylene separation performance of the zeolite membranes. Template free method was found to produce a membrane with highest quality, as evaluated by the PAS analysis. Propylene/propane separation properties of these template free synthesized membranes were explored.

1.6.2 Research objective 2

In preparing supported CMS membranes, improvements in gas permeance brought about by reducing membrane thickness are usually accompanied by decreased selectivity brought about by forming non-selective defects in the thinner membrane. We proposed to prepare CMS membrane on macroporous α-alumina support coated with a

sol-gel derived mesoporous γ-alumina layer. The mesoporous γ-alumina layer can eliminate the surface imperfections of α-alumina support, allowing the formation of a thinner, defect-free polymer film and subsequently a thin, high quality CMS membrane. The synthesis and gas permeation properties of CMS membranes on both γ-alumina modified and bare α-alumina supports were compared. The propylene/propane mixture separation performance was studied and compared with other reported CMS membranes.

1.6.3 Research objective 3

In order to further improve the propylene gas permeance without compromising the selectivity, the thickness of CMS membranes was changed through varying the conditions for the coating of polymer precursor film on support. Based on the gas permeation and separation results of polymer and CMS membranes of different thicknesses, the mechanism for the thickness dependence of micropore structure formation for CMS membrane was discussed. The impacts of several industrial related factors, including the feed pressure, feed composition and operation temperature on the performances of CMS membrane were systemically studied. Finally, the stability of CMS membrane was also investigated under both off-stream storage and on-stream separation conditions.

1.7 Structure of the dissertation

The following chapters in this dissertation will serve to accomplish the objectives mentioned above. Chapter 2 addresses objective 1 to study the synthesis, pore structure characterization and propylene/propane separation property of MFI zeolite membranes. Chapter 3 addresses objective 2 by introducing a novel CMS/ceramic composite membrane structure. The membrane synthesis, characterization, and gas permeation

properties were discussed in detail. Objective 3 are fulfilled by Chapters 4 and 5. These two chapters focused on systematic studies on the effect of membrane thickness on pore structure and gas transport properties of CMS membrane, the effect of operation conditions on propylene/propane separation performances, as well as the stability of CMS membrane. Chapter 6 summarizes all the work presented in this dissertation and provides some recommendations for the future development of microporous inorganic membranes for propylene/propane separation.

CHAPTER 2

MFI ZEOLITE MEMBRANES: PORE STRUCTURE CHARACTERIZATION BY POSITRON ANNIHILATION SPECTROSCOPY AND PROPYLENE/PROPANE SEPARATION PROPERTY

2.1 Introduction

Literature reviews described in Chapter 1 has showed that polycrystalline zeolite membranes, especially MFI type zeolite membranes offer many attractive properties, such as excellent separation capability and high structural stability for several industrially important gas separations (Tavolaro & Drioli, 1999; Caro & Noack, 2008; Lin et al., 2013). The separation properties and stability of the zeolite membranes are derived from their unique crystalline pore structure, pore surface chemistry and bulk inorganic material characteristics (Caro et al., 2000; Lin and Duke, 2013; Caro et al., 2000). However, polycrystalline zeolite membranes contain grain-boundary or intercrystalline gaps, which, if larger than the zeolitic pores, provide non-selective pathways for mass transport, degrading the overall performance of the membrane (Xu et al., 2000; Korelskiy et al., 2014). Researchers have tried to minimize or eliminate these intercrystalline defects through manipulation of crystal orientation (Lai et al., 2004), template-free secondary growth (Pan & Lin, 2001), template removal by rapid calcination (Choi et al., 2009), and post-synthesis defect repairing (Hong et al., 2011). The details of these methods have been reviewed in Chapter 1.

It is expected that the intercrystalline pore structure of the polycrystalline zeolite membrane depends on the synthesis methods, so a good understanding of the microstructure of polycrystalline zeolite membrane is key to ensure synthesis of high

quality zeolite membranes. However, it is difficult to directly characterize the intercrystalline gaps of supported zeolite membranes, and the effectiveness of a synthesis or post-treatment method to prepare zeolite membranes with intercrystalline pores minimized or eliminated. As a result, the research on synthesis of high quality zeolite membranes was largely performed in try-and-error fashion.

Direct observation of the complex hierarchical microporous structure of polycrystalline zeolite membranes remains a major challenge in the membrane community, because the intercrystalline pores are in micropore range (< 2nm) and of highly irregular topologic structure (Wegner et al., 1999). Nitrogen adsorption porosimetry is a destructive means to characterize the pore structure of zeolite membranes by measuring the powdery samples of the zeolite membrane layer scratched off from the support (Sano et al., 1994). Permporometry uses condensable gas like water or hexane in the process, both of which could induce microstructure change by strong adsorption and affect the measurement accuracy (Noack et al., 2005). Molecular probing method relies on the permeance cutoff of a series of probing gases (or liquids) with different molecular sizes to estimate the critical pore size of the membrane (Hedlund et al., 1999). All these methods could not provide information of the hierarchical pore structure of the supported polycrystalline zeolite membranes.

Positron annihilation spectroscopy (PAS), based principally on the annihilation phenomena of positron and positronium due to pickoff in open-volume defects, is an emerging nondestructive technique to probe the pore structure of various materials (Gidley et al., 2006). Among the many PAS techniques, positron annihilation lifetime spectroscopy (PALS) has proven to be effective in quantifying the free-volume in

polymers (Geise et al., 2014; Wang et al., 2011), micro/meso pores in silica (Duke et al., 2008), and cage and cavity size in zeolite crystals (Lo et al., 2011; Cabral-Prieto et al., 2013). Recently, Yan and co-workers reported using PALS to obtain pore size and pore connectivity information in zeolite low-k films (Li et al., 2004). Duke and co-workers reported the use of PALS to characterize the pore structure of MFI zeolite powders (Zhu et al., 2013; Zhu et al., 2010). The results revealed a hierarchical trimodal porous structure of the MFI zeolite powders containing intrinsic zeolite crystalline pores, intercrystalline micropores and interparticle mesopores. The work shows promise of using the PAS technique to study pore structure of supported zeolite membranes.

In this chapter, we present the use of two PAS techniques, PALS and Doppler broadening energy spectroscopy (DBES), to characterize non-destructively the hierarchical microporous structure of inorganic supported polycrystalline MFI type zeolite membranes, one of the most studied zeolite membranes in the literature because of its industrial importance. DBES was used to detect the free-volume variation and the multilayer structure of composite polymer membranes (Chen et al., 2007; Huang et al., 2008), but it has never been used to characterize zeolite membranes. Such structure information is important to guide the membrane synthesis and to explain the separation performance of the zeolite membranes. The objectives of this chapter are to demonstrate that PALS and DBES are effective in revealing the complex hierarchical structure of MFI zeolite membranes composed of both intra and intercrystalline micropores and use of these techniques to help determine synthesis-structure-properties relationship of polycrystalline zeolite membranes. Based on the information provided by PAS, template-free synthesized membrane has the best membrane quality with the least amount of

intercrystalline gaps. The propylene/propane separation performance of the high quality membranes synthesized by template free method was also evaluated.

2.2 Experimental

2.2.1 Membrane synthesis and characterization

The following four supported MFI zeolite membranes of different microstructure, as summarized in Table 2.1, were synthesized on macroporous α-alumina support by the seeded secondary growth methods under different conditions as reported in the respective literature: (a) randomly oriented MFI zeolite membrane (TR) prepared with the use of a TPABr template in the secondary growth step (O'Brien-Abraham et al., 2007); (b) randomly oriented MFI zeolite membrane (TFR) prepared without an organic template in the secondary growth step (template-free method) (Wang & Lin, 2012); (c) h0h-oriented MFI zeolite membrane (TH) prepared with a template by performing sequential secondary growth at a moderate temperature of 130 ℃ (Gouzinis & Tsapatsis, 1998); and (d) c-oriented MFI zeolite membrane (TC) prepared with a template at a high secondary growth temperature of 175 ℃ (Xomeritakis & Tsapatsis, 1999).

The disk supports were pressed from A16 powders (Almatis), and then sintered at 1150 ℃ for 30 h in air. One side of the disk was polished using SiC sandpaper (#500, #800 and #1200) to smooth the surface. Silicalite seeds were prepared by hydrothermal synthesis at 120 ℃ for 12 h using a synthesis solution of 10 SiO_2: 2.4 TPAOH: 1 NaOH: 110 H_2O. Figure 2.1 shows the SEM images of the prepared seeds, which have a particle size of around 100 nm. Silicalite seeds layer were dip-coated onto the polished side of α-alumina supports, dried in humid oven at 40 ℃ for 2 days and then calcined at 550 ℃ in air for 8 h to strengthen the bonding between seeds layer and support.

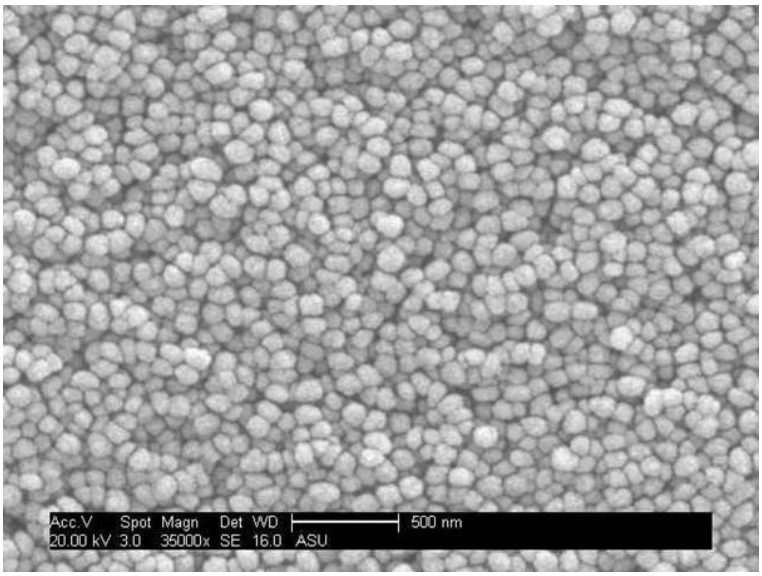

Figure 2.1 SEM image of silicalite seeds

The secondary growth solution for three templated membranes with different orientations had a molar composition of 1 KOH: 1 TPABr: 4.5 SiO_2: 16 C_2H_5O: 1000 H_2O. The composition of the synthesis solution for template-free secondary growth was 5 g SiO_2: 60 g H_2O: 1.15 g NaOH: 0.65 g $Al_2(SO_4)_3 \cdot 18H_2O$. The solution and seeded supports were transferred to a Teflon-lined stainless steel autoclave and hydrothermally treated at different conditions as listed in Table 2.1. The seeded support was vertically held in the autoclave using a Teflon holder. After synthesis, the autoclave was quenched using water and the membranes were washed with de-ionized water for several times and dried at room temperature for one day. The TR, TH, TC membranes synthesized using templated method were calcined at 550 ℃ in air for 8 h to remove the templates trapped inside zeolite pores. The template-free synthesized membrane (TFR) was dried at 200 ℃ for 8 h to remove any adsorbed water and other impurities in the membranes. The membranes were stored in desiccator before characterization and separation measurements.

Table 2.1

Secondary growth conditions for MFI zeolite membranes

Membrane type	Structure and synthesis method	Secondary growth conditions		
		Temperature (℃)	Duration (h)	Number of growths
TR	Ramdomly oriented with template	175	4	1
TFR	Randomly oriented without template	175	24	1
TH	*h0h*-oriented with tempalte	130	24	2
TC	*c*-oriented with template	175	24	2

The surface and cross-section of the membranes were characterized by scanning electron microscopy (SEM) (Philips, XL 30) to evaluate the morphology and to estimate the membrane thickness. X-ray diffraction (XRD) (Bruker AXS-D8, Cu Kα radiation) was used to analyze the crystal structure, especially the orientation of the four membranes prepared at different conditions.

2.2.2 Positron annihilation spectroscopy

Two PAS techniques, positron annihilation lifetime spectroscopy (PALS) and Doppler broadening energy spectroscopy (DBES), were conducted by using a PAS coupled with a variable monoenergetic positron slow beam. The detailed description of the experimental set up can be found in literature (Huang et al., 2008). The surface of zeolite film of each of the four supported zeolite membranes was subjected to positron irradiation, as illustrated in Figure 2.2.

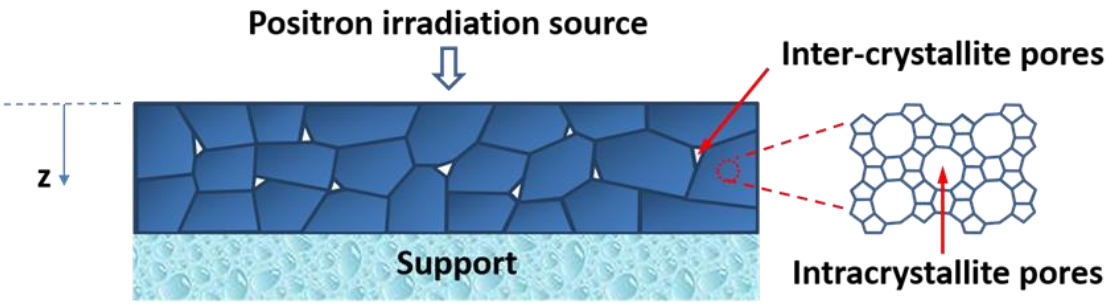

Figure 2.2 Schematics of the transport of positrons in a polycystalline MFI zeolite membrane

The PALS measures the pore size and the distribution at a certain depth, while the DBES qualitatively examines the pore profiles as a function of depth from the membrane surface. Both of them were conducted under a vacuum level lower than 10^{-6} torr. The PALS measurements were carried out at fixed incident energy of 5 keV with a counting rate of 50 cps for each membrane. This corresponds to a mean depth of around 0.49 μm in the membrane. In the measurement, the secondary electrons emitted from the membrane surface detected by the multichannel plate (MCP) were taken as the start signal while the photons detected by a BaF_2 detector were the stop signal. The PALS spectra were obtained by counting the coincident events of the two signals.

The obtained raw PALS spectrum was analyzed by both the program MELT based on a continuous decay function and the program PATFIT which carries out the finite analysis by a discrete function. MELT usually shows information about the pore size and its distribution, and PATFIT provides the details about the average lifetime for the pick-off ortho-positronium (o-Ps) (τ_3) and its intensity (I_3). The mean pore radius is correlated to τ_3 by the semi-empirical equation as shown in Equation 2.1.

$$\tau_3 = \frac{1}{2}\left[1 - \left(\frac{R}{R + \Delta R}\right) + \frac{1}{2\pi}\sin\left(\frac{2\pi R}{R + \Delta R}\right)\right]^{-1} \quad (2.1)$$

where R is the pore radius and ΔR is an empirical parameter determined by calibration on materials with known free volume sizes. 1.656 Å was used for ΔR in this work. This equation was reported to be valid for o-Ps lifetime smaller than ~20 ns or pore radius smaller than 1 nm (Ito et al., 1999).

For DBES, a total of 29 spectra measured at different positron incident energies in the range of 0.1 to 27 keV were recorded by a HP Ge solid-state detector for a sample membrane. Each spectrum carried 1 million counts with a counting rate of 800-1000 cps. The incident energy of the slow positron beam (E+) is correlated to the positron penetration depth in a membrane (Z) by Equation 2.2:

$$Z = \frac{40}{\rho} \times E_+^{1.6} \quad (2.2)$$

where Z is in nm, E+ is in keV and ρ refers the density of the film (1 g/cm^3 was used in this work). As indicated, the positron could penetrate into the membrane at different depths by varying E+. Therefore, the depth profile of the pores in the membrane as a function of depth is investigated by DBES analyses. Three parameters, S, W and R were collected from DBES.

2.2.3 Membrane separation performance measurement

The single component xylene isomers separation performance was measured using a home-made pervaporation setup. The membrane was placed in the stainless steel pervaporation cell with the membrane layer facing up to the feed reservoir, which was filled with pure *p*-xylene (99%, Sigma-Aldrich) or *o*-xylene (99%, Sigma-Aldrich). The

downstream side was evacuated by a vacuum pump, and the permeated vapors were collected by a cold trap placing in liquid nitrogen. Before collecting the sample, the setup was evacuated for at least 0.5 h to reach the equilibrium of the set up. The duration of each run was kept at 4 h. The flux of each component was calculated by Equation 2.3,

$$J = \frac{W}{At} \tag{2.3}$$

where w is the weight of collected sample (kg), A is the permeation area (m^2), t is the total time for the run (hr). The ideal selectivity was determined by the ratio of the *p*-xylene flux to the *o*-xylene flux. The propylene/propane mixture separation measurement was conducted with a 50/50 propylene/propane mixture with a total feed pressure of 14.69 psi. The downstream side was swept with nitrogen gas. Detailed experiments will be described in the next chapter.

2.3 Results and discussion

2.3.1 Membrane Morphology and PALS Characterization Results

The structure, orientation and morphology of the four zeolite membranes were examined by the surface and cross-sectional SEM images and XRD patterns given in Figure 2.3 and Figure 2.4, respectively. The SEM images in Figure 2.3 show that these membranes, with a thickness of 5 to 15 μm, are of high integrity and contain no surface macroscopic defects. The zeolite membrane layer and the alumina support region can be clearly distinguished in the cross-sectional images. The difference in the membrane thickness was due to the different synthesis conditions used for each membrane. XRD patterns in Figure 2.4 confirm random orientation for the TR and TFR membranes, *h0h* orientation for the TH membrane and *c*-orientation for the TC membrane. These data of

morphology and crystal structure and orientation of the MFI membranes are consistent with those reported in the literature (O'Brien-Abraham et al., 2007; Wang & Lin, 2012; Gouzinis & Tsapatsis, 1998; Xomeritakis & Tsapatsis, 1999). It should be noted that these characterizations are unable to reveal the pore structure of the zeolite membranes.

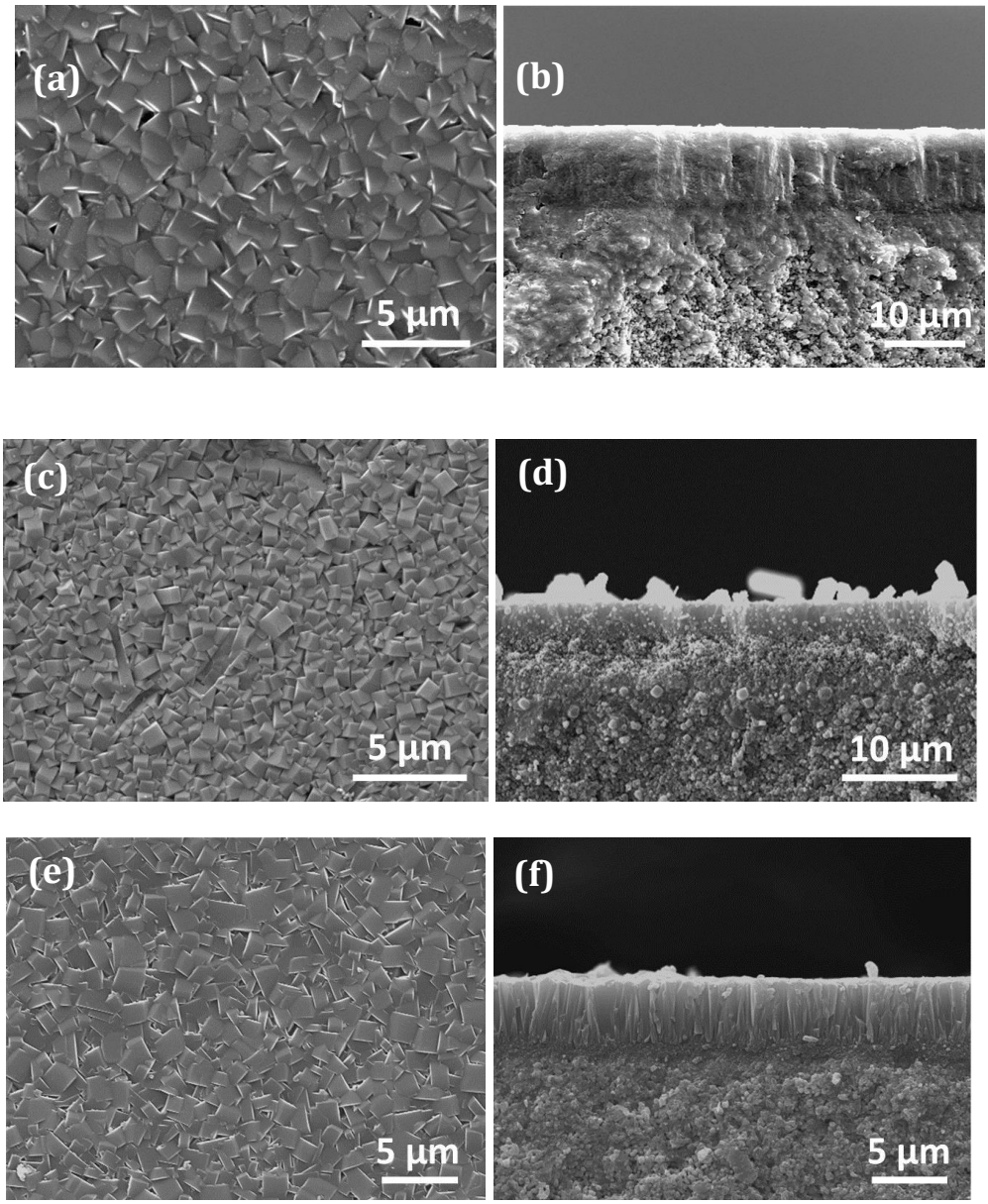

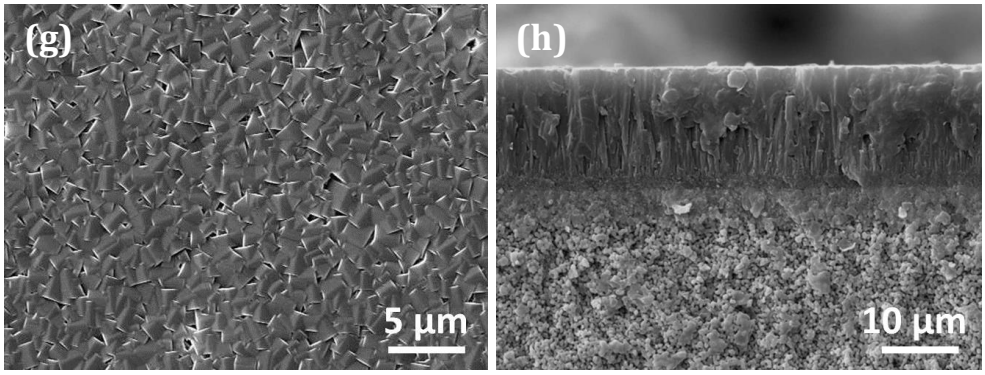

Figure 2.3 Surface and cross-section SEM images of (a, b) templated synthesized random oriented MFI membrane (TR), (c, d) template free synthesized random oriented MFI membrane (TFR), (e, f) templated synthesized h0h-oriented MFI membrane (TH), and (g, h) templated synthesized c-oriented MFI membrane (TC)

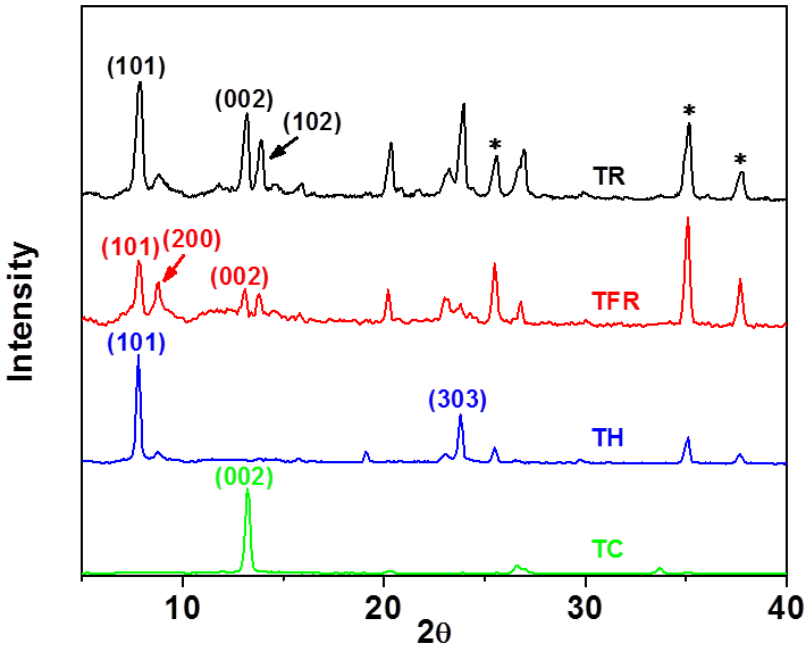

*Figure 2.4 XRD patterns of templated synthesized random oriented MFI membrane (TR), template free synthesized random oriented MFI membrane (TFR), templated synthesized h0h-oriented MFI membrane (TH), and templated synthesized c-oriented MFI membrane (TC). The asterisks * in the XRD spectra indicate the peaks of alumina substrate*

In PAS measurements, the positronium with a Bohr radius of 0.53 Å was able to access all pore spaces in the zeolite layer without altering the pore structure. In this work, PALS measured the pores at a mean depth of 0.49 μm from the surface of the zeolite membrane. The collected positron annihilation lifetime spectra are shown in Figure 2.5. These spectra were best fitted with four discrete lifetime components based on PATFIT program. The third lifetime τ_3 and the fourth lifetime τ_4 are on the order of a few ns and are due to ortho-positroniums (o-Ps) annihilation by pickoff inside the pores. Assuming the pores are of spherical shape, the calculated pore sizes from τ_3 and τ_4 are in the micropores range.

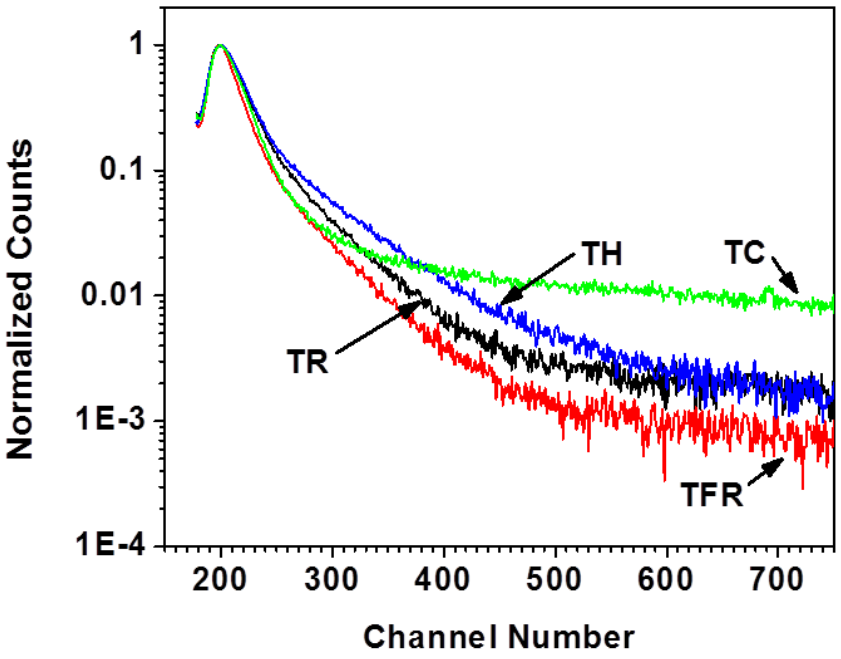

Figure 2.5 Normalized positron annihilation lifetime spectra for TR, TFR, TH and TC MFI-type zeolite membranes

It should be noted that five lifetime components were reported to be the best fit for PAL spectra of zeolite powders, with the fifth long lifetime (>50 ns) suggesting the

existence of mesopores between zeolite particles (Zhu et al., 2013; Zhu et al., 2010). Our PAL results here clearly show that for a high quality zeolite membrane, the pore structure is composed of bimodal micropores with the absence of any mesopores.

Table 2.2 and Table 2.3 show the average values for τ_3, τ_4 and their respective intensities I_3, I_4 based on the PATFIT program, as well as the calculated pore radius (R) and pore volume fractions. The smaller pores calculated from τ_3 have a pore radius ranging from 2.7 to 3.6 Å, which agree well with the crystallographically defined MFI zeolitic pore size of 0.55 nm (pore radius of about 2.8 Å). These are intracrystalline zeolitic micropores in the membranes. The slightly larger value for the pore size measured from PAL is probably due to assumption of the sphere shape for the pores in the model, which also accounts the presence of channel intersections. Similar finding was reported for the pore size analysis on different types of zeolite crystals using PAL (Schultz & Lynn, 1988). On the other hand, the larger pores with radius in 7.43 Å-9.17 Å are found for all four MFI zeolite membranes, and these pores most likely belong to the intercrystalline micropores. The fractions of intra and intercrystalline pores can be represented from $I_3/(I_3+I_4)$ and $I_4/(I_3+I_4)$ for each membrane, as shown in Table 2.3. It can be seen that for the two randomly and the *h0h*- oriented zeolite membranes, the intrinsic zeolitic pores contribute to above 90% of the total pore volume. However, the *c*-oriented zeolite membrane contains much less intrinsic pores. This will be discussed next with the DBES results.

Table 2.2

Positron lifetime results including lifetime and intensity for TR, TFR, TH and TC membranes

Sample name	Lifetime (ns)		Intensity (%)	
	τ_3	τ_4	I_3	I_4
TR	2.30 ±0.02	17.51 ±0.68	38.36 ±0.38	2.32 ±0.07
TFR	2.22 ±0.02	13.34 ±0.59	32.56 ±0.28	1.56 ±0.07
TH	3.01 ±0.02	16.05 ±0.44	38.26 ±0.23	3.48 ±0.10
TC	1.87 ±0.05	22.11 ±0.16	16.17 ±0.69	18.45 ±0.09

Table 2.3

Positron lifetime results including calculated pore radius and pore faction for TR, TFR, TH and TC membranes

Sample name	Pore radius (Å)		Pore volume fraction (%)	
	Intracrystalline (from τ_3)	Intercrystalline (from τ_4)	Intracrystalline ($I_3/(I_3+I_4)$)	Intercrystalline ($I_4/(I_3+I_4)$)
TR	3.11 ±0.01	8.33 ±0.03	94.3	5.7
TFR	3.05 ±0.01	7.43 ±0.04	95.4	4.6
TH	3.64 ±0.01	8.04 ±0.02	91.7	8.3
TC	2.73 ±0.04	9.17 ±0.01	46.7	53.3

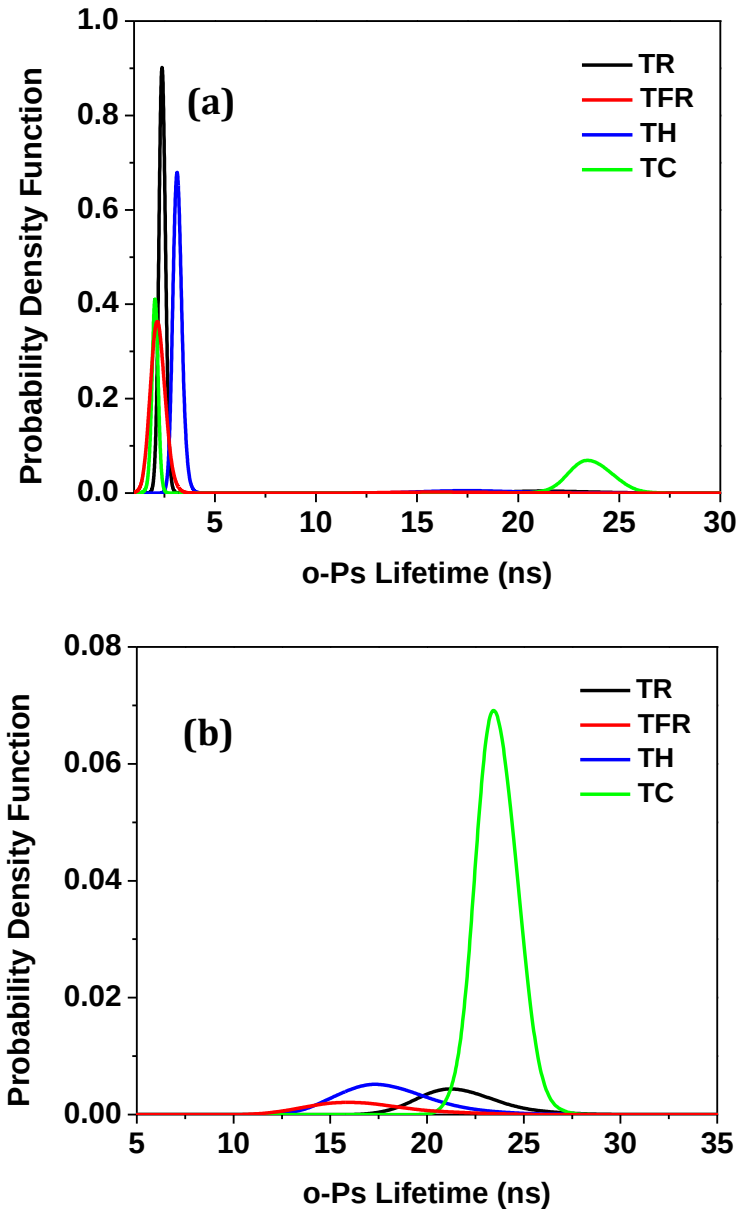

Figure 2.6 (a) Distribution curves of o-Ps with lifetime in the range from 1 to 30 ns representing all the micropores in the four membranes, (b) Enlarged distribution curves of o-Ps with longer lifetime in the range from 5 to 35 ns representing the larger micropores (intercrystalline micropores) in the four membranes

Figure 2.6 shows the lifetime distribution curves obtained by MELT program for the four membranes. As shown, the larger intercrystalline pores are much more broadly

distributed than the intracrystalline pores, which is consistent with the highly irregular topologic structure of the intercrystalline micropores and the well-defined nature of zeolitic pores.

The results of PAL analysis show that intercrystalline pores are different in size and quantity for these zeolite membranes of different structure synthesized under different conditions. The template-free, randomly oriented membrane contains intercrystalline micropores with smaller size (7.43 Å) and lowest amount (4.6%), confirming the advantage of template free synthesis method in minimizing the intercrystalline pores of the zeolite membranes. It was suggested that removing templates from zeolitic pores by high temperature calcination (>500 ℃) creates and/or enlarges the intercrystalline gaps due to the shrinkage in zeolite framework. On the other hand, the *c*-oriented MFI zeolite membrane (TC membrane) contains smaller measured intracystalline pores (2.73 Å), but bigger intercrystalline pores (9.17Å) in larger pore fraction (53.3%) than the other three membranes. We hypothesized that the differences in intracrystalline pore sizes for the four membranes may be caused by the asymmetric intracrystalline pore structure of MFI-type zeolites. The pore structure consists of two channels: a straight channel along the *b*-axis with circular openings of 0.54×0.56 nm and a sinusoidal channel along the *a*-axis with elliptical openings of 0.51×0.55 nm. Along *c*-direction, which is the channel intersections, the molecules will diffuse through either the straight channel and/or the sinusoidal channel. And the Ps will probably take the same tortuous path during their transport through the *c*-oriented membrane. In this case, the empirical equation which assumes the pores are of spherical in shape may be not as accurate for *c*-oriented membrane as for the other membranes. The larger intercrystalline

pores are possibly attributed to the highly columnar, asymmetrical microstrucure of the *c*-oriented MFI zeolite membrane.

2.3.2 Membrane structure by DBES analysis and separation performance

The DBES analysis was performed on these zeolite membranes as a function of the incident energy, and S, R and W parameters were collected to give the pore structure distribution along the direction normal to the membrane surface (z direction shown in Figure 2.2). According to the use of DBES for characterizing polymer membranes, S parameters are associated with the Ps pick-off annihilation in free volumes (Å to nm), while R parameters are related to the existence of large pores (nm to μm). The pores in the four zeolite membranes can be divided into three groups: (1) intracrystalline pores; (2) intercrystalline pores with radius smaller than 1nm and (3) intercrystalline pores with radius larger than 1nm. Therefore, we believe S parameter is a combination of pores from group (1) and (2), while R parameter is associated with group 3 pores. The S and R parameters versus incident energy (or the depth from the zeolite membrane surface) for the four membranes are shown in Figure 2.7a and 2.7b. Considering that all these membranes possess similar intracrystalline pores, the S parameter results show that the intercrystalline pores with radius smaller than 1 nm in the zeolite membrane layer for the four membranes decreases in the order: TC > TH > TR > TFR. This agrees well with the order of intercrystalline pore fractions (in Table 2.3) from PALS which measured the pores at a mean depth of 0.49 μm.

The R vs E plot shows a sharp decrease in the range of < 1 kV. This indicates that the concentration of large voids/pores decreases at the surface (~ 100 nm range) or the membrane is denser at the surface. For our case, this may be caused by the large surface

roughness of the inorganic membranes. As shown in the SEM images, the membrane surface is very rough. In this case, when the positrons reach the membrane surface, they form the positronium in the rough open area, which contributes to higher R value. The results of R parameters as a function of the membrane thickness show that the TC membrane has much more intercrystalline pores with radius larger than 1 nm than the other three membranes. This explains the much larger fraction of the intercrystalline pores for the TC membrane measured by the PALS as compared to the other three membranes. Furthermore, for the TC membrane the amount of these larger intercrystalline pore increases from the zeolite membrane surface towards the zeolite/support interface. This is consistent with the columnar microstructure for the TC membrane observed by SEM, as discussed above. W parameter shown in Figure 2.8a can provide information about the type of chemical environment where the positron annihilation takes place. Only one slope was observed for the W vs S parameters shown in Figure 2.8b, indicating no changes of chemical composition or void type in the four membranes along the membrane thickness direction.

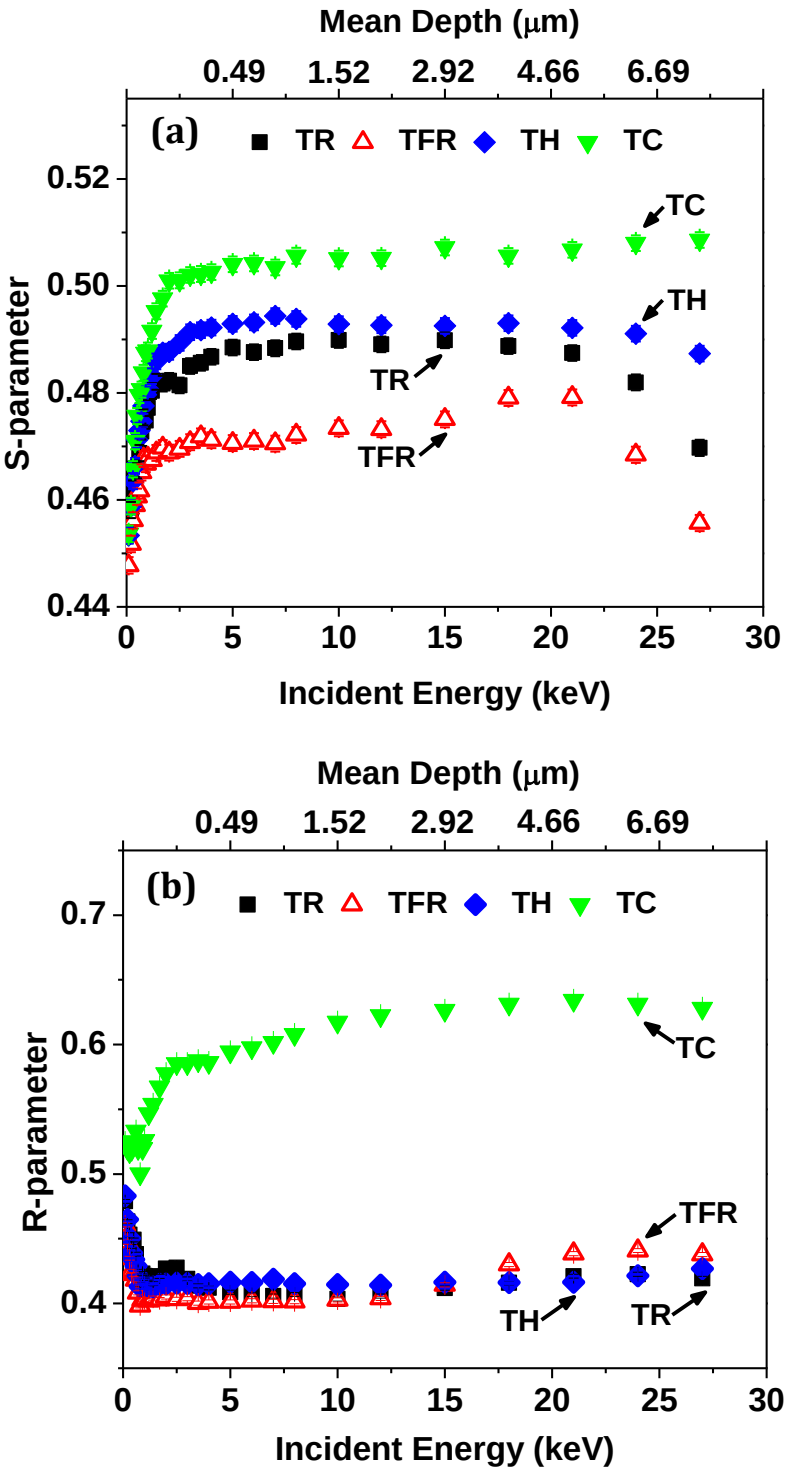

Figure 2.7 (a) S parameters vs positron incident energy and depth, and (b) R parameters vs positron incident energy and depth for TR, TFR, TH, and TC MFI zeolite membranes

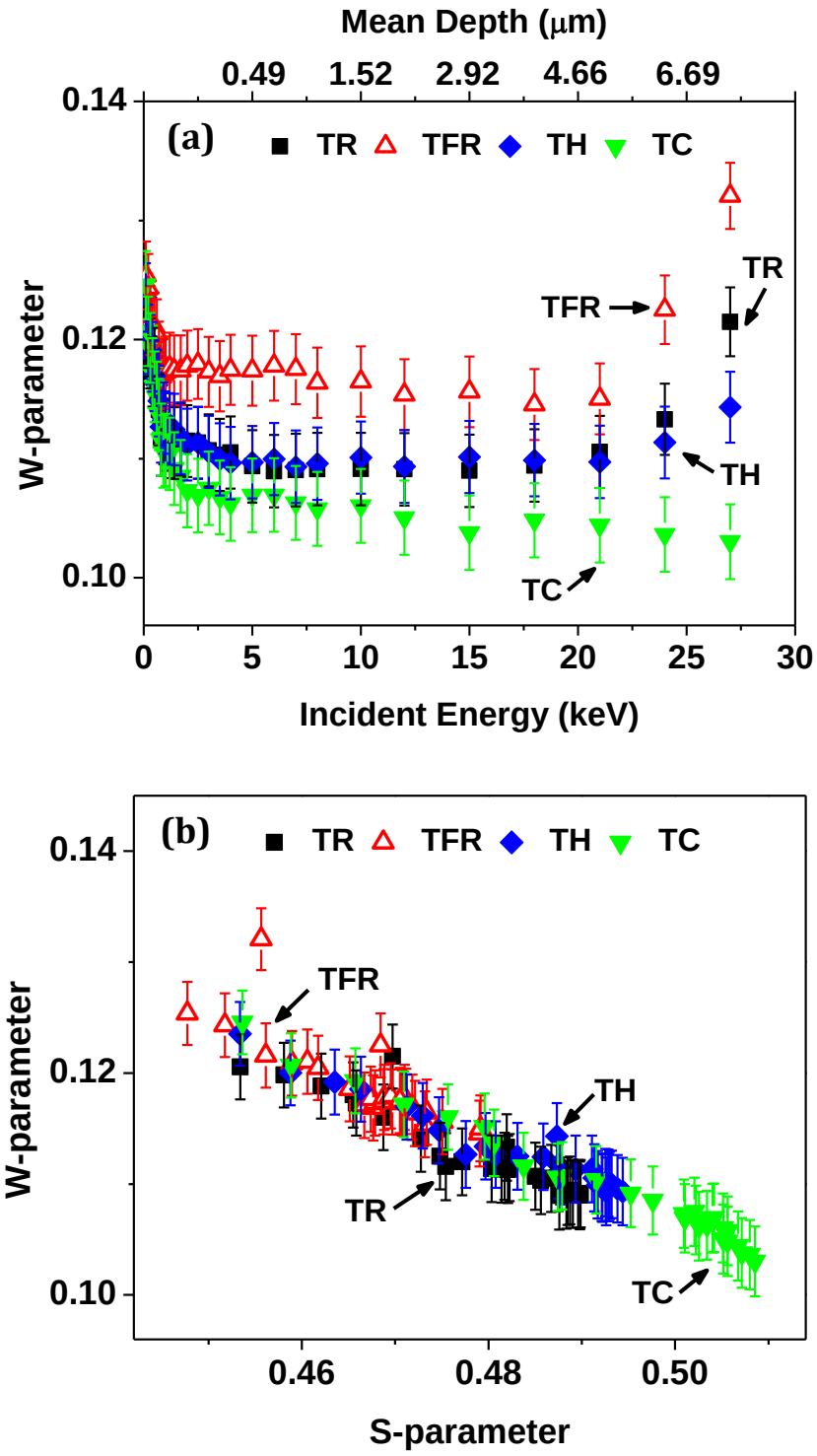

Figure 2.8 (a) W parameters vs positron incident energy and depth, (b) W parameters vs S parameters for TR, TFR, TH, and TC MFI-type zeolite membranes

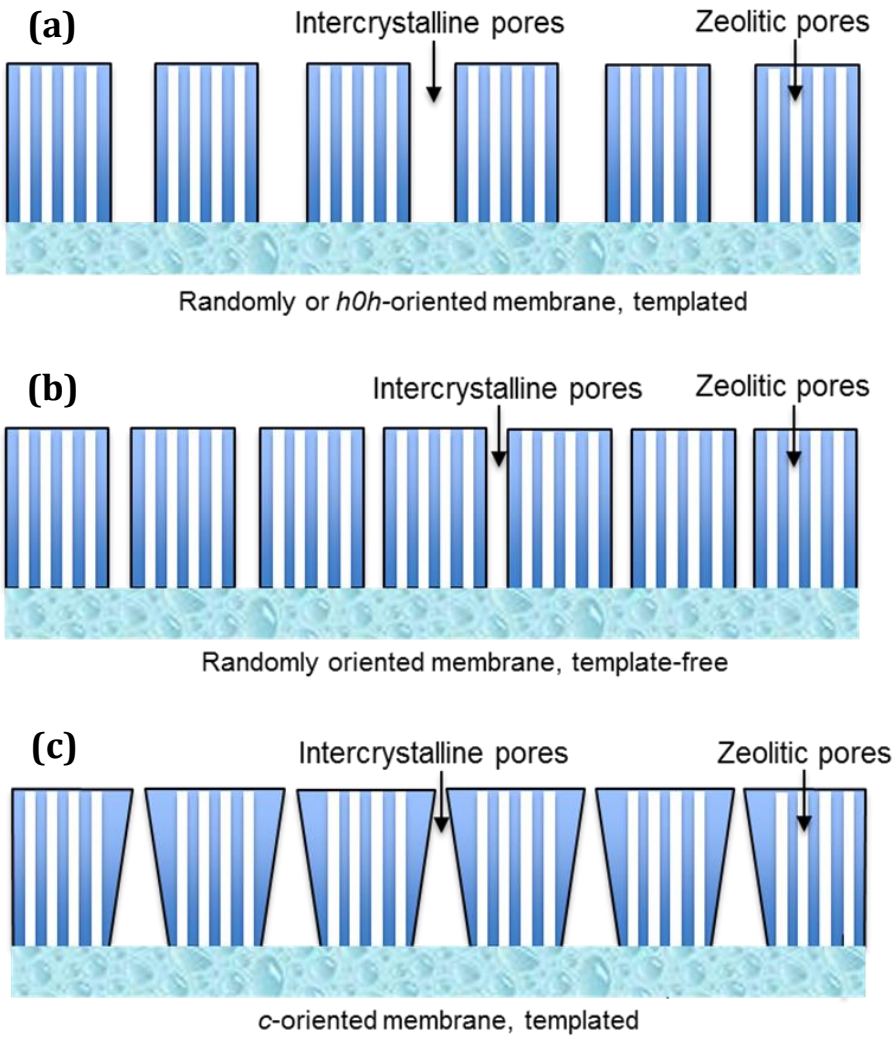

Figure 2.9 Schematic showing three types of microstructure of MFI zeolite membranes: (a) Templated synthesized random and h0h-oriented MFI membranes (TR and TH) containing a moderate amount of intercrystalline micropores with medium pore size, (b) Template-free synthesized MFI membrane (TFR) containing a small amount of intercrystalline micropores with smaller pore size, and (c) Templated synthesized c-oriented MFI membrane with substantially larger amount of large intercrystalline pores

The structures of these four MFI zeolite membranes identified by PAS are schematically represented in Figure 2.9. Among these four membranes, random and *h0h*-

oriented MFI membranes synthesized by templated method contain a moderate amount of intercrystalline micropores with medium pore size. The randomly oriented template-free synthesized membrane has a small amount of intercrystalline micropores with smaller pore size. The microstructure of the *c*-oriented MFI membrane synthesized by templated method is featured with a substantially large amount of large intercrystalline pores with the pore amount increasing from the zeolite membrane surface towards the zeolite-support interface.

The specific microporous features can be correlated to the xylene separation properties of the membranes. Table 2.4 shows the performance of xylene isomers pervaporation of the four MFI-zeolite membranes prepared in this work. The template-free membrane (TFR) exhibits highest p/o-xylene ideal selectivity of 24, about 6~13 times higher than the other three membranes synthesized with the template. This can be explained by the more desirable microstructure of TFR membrane as examined from our PAS analysis. The intracrystalline pores for the four studied membranes are of around 0.6 nm in diameter, and is selective to *p*-xylene (kinetic diameter ~0.58 nm) over the bulkier *o*-xylene (~0.68 nm) through molecular sieving effect. However, diffusion of *p*- and *o*-xylene through the relatively large intercrystalline pores (1.4-1.8 nm) follows Knudsen-like diffusion mechanism, which is not selective to molecules with the same molecular weight. The template-free MFI zeolite membrane contains intercrystalline micropores in smaller size and lower quantity than the other three MFI zeolite membranes. Hence a better overall separation performance is achieved for the TFR membrane due to the less non-selective flow from the intercrystalline pores.

Table 2.4

Pervaporation separation results of single component p-xylene and o-xylene at room temperature for TR, TFR, TH and TC membranes

Membranes	*p*-xylene flux (kg/m^2 ħr)	*o*-xylene flux (kg/m^2 ħr)	*p*/*o*-xylene ideal selectivity
TR	0.71	0.39	1.8
TFR	0.17	0.007	24
TH	0.24	0.10	2.4
TC	0.22	0.06	3.6

As revealed by the PAS analysis and the xylene isomers separation, the random oriented membrane synthesized by template free method has the highest quality with the fewest non-selective intercrystalline pores. Therefore, this membrane was tested for propylene/propane separation performance. Table 2.5 shows the performances of three MFI zeolite membranes prepared using the template free secondary growth method. These membranes show a high propylene gas permeance of $3\sim4.0\times10^{-8}$ $mol/(m^2 \cdot s \cdot Pa)$ However, the selectivity is relatively low, with the highest value of 1.5 observed for membrane #3. This is because the intracrystalline pore of ZSM-5, which is larger than the molecular size of both propylene and propane, is unable to provide a strong molecular sieving effect to these two gases. However, high gas permeances were achieved for both gases due to the low transport resistance provided the relatively large pore size of zeolitic channels. It should be noted that, the selectivity values of these membranes are still higher than the selectivity determined from Knudsen diffusion mechanism, which is about 1.02. This is likely due to the preferential adsorption of propylene molecules in the

zeolite membrane from the interaction between the double bonds in propylene and the cations in zeolite framework.

Table 2.5

Propylene/propane mixture separation results of MFI zeolite membranes synthesized by template free method

Membranes	C_3H_6 permeance ($mol/m^2 \cdot s \cdot Pa$)	C_3H_8 permeance ($mol/m^2 \cdot s \cdot Pa$)	C_3H_6/C_3H_8 selectivity
#1	4.1×10^{-8}	3.4×10^{-8}	1.2
#2	3.5×10^{-8}	2.5×10^{-8}	1.4
#3	3.8×10^{-8}	2.5×10^{-8}	1.5

2.4 Conclusions

The work in this chapter demonstrated that PAS techniques, including PALS and DBES, are effective non-destructive methods to characterize the pore structure of supported polycrystalline zeolite membranes. The MFI zeolite membranes feature a bimodal pore structure consisting of intracrystalline zeolitic micropores of around 0.6 nm in diameter and irregular intercrystalline micropores of 1.4 to 1.8 nm in size. The quantity and size of the intercrystalline pores and their distribution along the membrane thickness of the zeolite membranes are determined by the synthesis conditions including the usage of template which give MFI zeolite of different crystal orientation. The quantity and size of the intercrystalline pores are largest for the *c*-oriented membrane and smallest for the template free random oriented membrane, consistent with the xylene separation results. PAS results provide distribution of the bimodal pores along the membrane growth direction. The *c*-oriented MFI zeolite has asymmetric structure with the amount of intercrytalline pores increasing from the zeolite membrane surface towards the zeolite-

support interface. The template free synthesized MFI zeolite membrane showed a high C_3H_6 permeance, but a relatively low selectivity for the separation of C_3H_6/C_3H_8 mixture.

CHAPTER 3

GAMMA-ALUMINA SUPPORTED CARBON MOLECULAR SIEVE MEMBRANE FOR PROPYLENE/PROPANE SEPARATION

3.1 Introduction

Although being considered to be the most stable inorganic microporous membrane, MFI zeolite membranes did not possess promising propylene/propane separation properties as demonstrated in Chapter 1. The reason for the low selectivity is the relatively large pore size of MFI framework (~0.6 nm) which is unable to provide strong molecular sieving effect. In comparison, the pore size of carbon molecular sieve (CMS) membrane can be adjusted by the selection of polymer precursors and/or varying pyrolysis conditions. CMS membranes derived from 6FDA-based polyimides with good propylene/propane separation performance have been reported in literature. Therefore, the following three chapters will present our systematically studies into the CMS membrane system.

CMS membranes can be fabricated into the geometry of free-standing hollow fiber membrane and ceramic supported composite membrane. Hollow fiber membrane has the advantage of high packing density. The major drawback of the hollow fiber CMS membranes is their brittleness, making them difficult to handle in practical applications. Propylene/propane separations are often needed on the output of industrial crackers or on petrochemical purge streams, both of which are typically at elevated pressures, making mechanical strength an important membrane attribute. If thin and defect-free CMS membranes could be formed on inorganic substrates, such as alumina or stainless steel supports, mechanical strength could be improved without sacrificing high permeance.

Shiflett and Foley (2000) applied the ultrasonic deposition method to prepare CMS membranes on a macroporous stainless steel tube for O_2/N_2 separation. The thickness of the CMS membrane ranged from 5 μm to 20 μm, depending on the number of coatings and the concentration of polymer solution. They found that the thinner membrane exhibited a higher permeance but a lower selectivity. Morooka and co-workers (1996) prepared a CMS membrane by the pyrolysis of BPDA-pp'ODA polyimide coated on a macroporous (pore size 140 nm) α-alumina tubular support at an optimized temperature of 700 ℃. The polymer film was imidized in nitrogen at 300 ℃ before being pyrolyzed. The coating/imidization/pyrolysis process was repeated two or three times to obtain a membrane with a thickness of 5~6 μm. At 35 ℃, their membrane showed a C_3H_6/C_3H_8 selectivity of 46 and a C_3H_6 permeance of 7.9×10^{-10} mol m^{-2} s^{-1} Pa^{-1} (2.4 gpu) for a C_3H_6/C_3H_8 mixture separation.

In preparing supported CMS membranes, improvements in gas permeance brought about by reducing membrane thickness are usually accompanied by decreased selectivity brought about by forming non-selective defects in the thinner membrane. In this chapter, CMS membranes were prepared on macroporous α-alumina support coated with a sol-gel derived mesoporous γ-alumina layer. The mesoporous γ-alumina layer can eliminate the surface imperfections of α-alumina support, allowing the formation of a thinner, defect-free polymer film and subsequently a thin, high quality CMS membrane. The objective of this chapter is to report and compare the synthesis and gas permeation properties of CMS membranes on mesoporous γ-alumina modified and bare α-alumina supports. The C_3H_6/C_3H_8 mixture separation performance of the γ-alumina supported CMS membrane was also studied.

3.2 Experimental

3.2.1 Preparation of γ-alumina support

Macroporous α-alumina supports with thickness of 2 mm and diameter of 20 mm (porosity: 45%, average pore diameter: 0.20 μm) were prepared by pressing and sintering the alumina powder. The sintering temperature is 1150 ℃ and the sintering time is 30 hrs. The α-alumina supports were polished with three types of sandpaper (#500, #800 and #1200) to smooth the surfaces and remove any major imperfections. The mesoporous γ-alumina was prepared by the sol-gel method. The boehmite sol was prepared by hydrolysis and the condensation of aluminum-tri-butoxide, according to the procedure reported previously (Chang et al., 1994; Cooper & Lin, 2002). The γ-alumina layer was coated on the polished side of α-alumina support by dip-coating the boehmite sol which had been sonicated for 0.5 hr prior to dip-coating. The coated support was dried in a humidity camber (40 ℃, relative humidity: 60%) for 2 days, followed by calcination at 550 ℃ for 3 hrs with a heating and cooling rate of 0.5 ℃/min. The dip-coating and calcination was repeated 3 times to obtain a defect-free γ-alumina layer. Detailed procedures of the preparation of alpha-alumina and gamma-alumina supports can be found in the Appendix.

3.2.2 Preparation of polymer film

An appropriate 6FDA-based polyimide polymer (molecular weight >30,000) provided by Membrane Technology and Research, Inc. (MTR) was used as the precursor for CMS membrane. The polymers were dissolved in acetone to prepare a 2 wt% polymer solution for dip-coating. The polymer film was formed on the surface of the alpha and gamma-alumina supports, respectively, by dip-coating with the polymer solution. The

supported polymer films were dried at room temperature for 3 hrs, then at 100 ℃ for 12 hrs, and finally annealed at 140 ℃ for 5 hrs before conducting pyrolysis. For some samples, the dip-coating, drying and annealing were repeated twice to obtain polymer films on both the α-alumina and γ-alumina supports.

3.2.3 Preparation of CMS membranes

After drying and annealing, the supported polymer films were pyrolyzed in ultra high purity (UHP, 99.999% purity) argon gas to form the CMS membrane using a high temperature tubular furnace. The flow rate of UHP argon was controlled by a mass flow meter and was set at 100 mL/min in this work. The membranes were pyrolyzed at a final temperature in the range of 550 to 750 ℃ to study the effect of pyrolysis temperature on the separation performances of the membrane. The heating and cooling rate was 4 ℃/min. The thermal soak time was 2 hrs. It has been reported that exposure to water vapor or oxygen can change the properties of CMS membranes (Menendez & Fuertes, 2001; Lagorsse et al., 2008). Therefore, the CMS membranes obtained after pryolysis were stored in UHP argon gas before the characterization, gas permeation and separation measurements.

3.2.4 Characterization of membranes

The surface morphology and cross-section of the γ-alumina support, polymer membrane, and CMS membrane were characterized by scanning electron microscopy (SEM, Philips, XL 30) at an accelerating voltage of 20 kV on samples with gold deposition. The thicknesses information can be obtained from the cross-section images of the support and membranes. FTIR spectra for the polymer and CMS membrane were obtained by a Nicolet 4700 FT-IR spectrometer. Thermal decomposition behavior of the

polyimide precursor was studied by a thermogravimetric analyzer (TGA, TA Instruments SDT Q-600) under the flow of UHP argon at a flow rate of 100 mL/min, from 25 ℃ to 550 ℃ with a heating/cooling rate of 4 ℃/min. The condition used for the TGA measurement was the same with that for pyrolysis.

3.2.5 Single gas permeation test

The single gas permeances through the γ-alumina support, polymer membrane and CMS membrane were measured using a new unsteady-state permeation setup, as shown in Figure 3.1. The molecular weights and sizes of the gases tested are listed in Table 3.1. The kinetic diameter was used for He, H_2, CO_2, O_2 and N_2 (Tang et al., 2009). For C_3H_6 and C_3H_8, the critical diameter was used (Zhu et al., 1999). Before each gas permeation measurement, both the feed and permeate sides were evacuated for at least one hour to remove all the gases in the setup. The gas permeance was calculated by the following equation:

$$Q = \frac{V}{SRT(P'-P'')}\left(\frac{dP''}{dt}\right) \tag{3.1}$$

where V is the volume of the gas tank, S is the permeation area of the membrane, T is room temperature, P′ and P″ are the upstream and downstream pressure, R is the ideal gas constant, and dP″/dt is the pressure increase rate in the gas tank. The ideal separation factor for component A vs. B, which is equal to the ratio of permeances of two pure penetrants, was calculated and used to examine the quality of membrane.

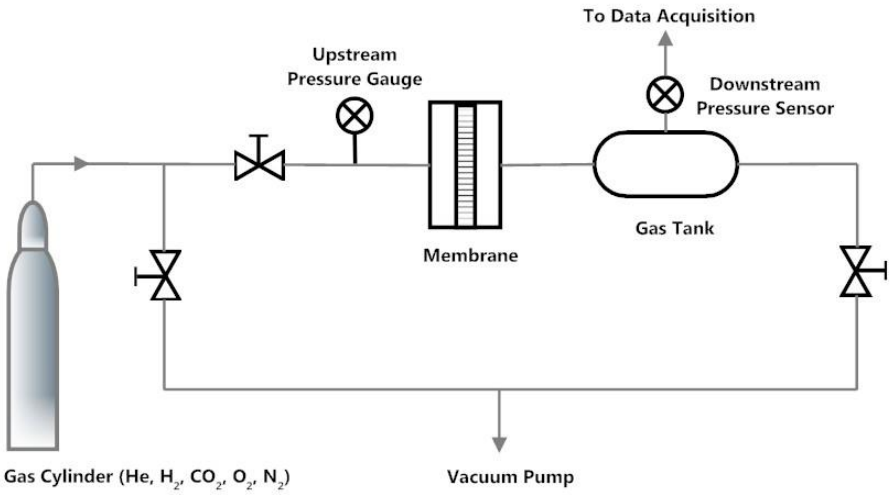

Figure 3.1 Schematic diagram of the unsteady state setup for single gas permeation test

Table 3.1

Molecular properties of gases used for single gas permeation tests

Gas	He	H_2	CO_2	O_2	N_2	C_3H_6	C_3H_8
Molecular weight	4	2	44	32	28	42	44
Molecular dimension (Å)	2.6	2.89	3.3	3.46	3.64	4.31	4.46

3.2.6 Propylene/propane mixture separation tests

The mixed-gas performance of the CMS membranes for C_3H_6/C_3H_8 separation was measured using a previously reported cross-flow setup (Zhao et al., 2012), with some modifications shown in Figure 3.2. Detailed measurement procedures can be found in the Appendix. For the measurement in this chapter, the feed was an equimolar C_3H_6/C_3H_8 mixture at a total flow rate of 50 mL/min, and the permeate side was swept by N_2 at a flow rate of 10 mL/min. The total gas flow rate on the permeate side was measured by a bubble flow meter, and the gas composition was measured by gas chromatography (GC) (SRI Instruments, SRI 8610C) equipped with a flame ionization detector (FID) and a

silica gel column. The carrier gas for the GC measurement is He gas with a flow rate of 20 mL/min. The column and detector temperature of the GC was set at 130 ℃. The mixture selectivity was defined as the ratio of the permeances of C_3H_6 and C_3H_8 in the mixture separation measurements. With this setup, the feed pressure can be varied by a needle valve on the retentate line to study the pressure dependence on the separation performance. The two mass flow controllers on the feed side are used to control the feed composition.

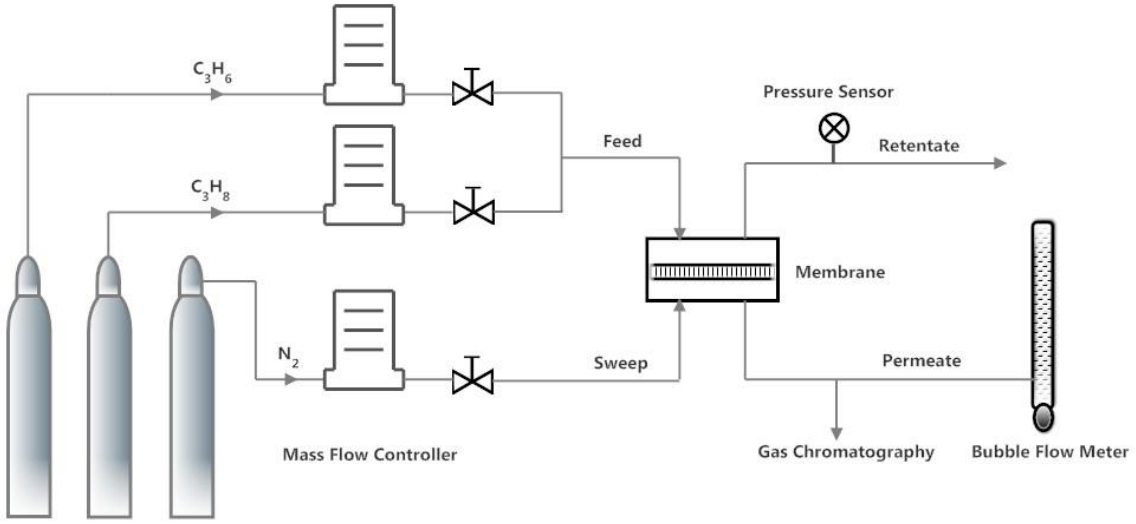

Figure 3.2 Schematic diagram of the cross-flow membrane separation setup for studying the C_3H_6/C_3H_8 mixture gas separation properties of a CMS membrane

3.3 Results and Discussion

3.3.1 Preparation and characterization of polymer membrane

Figure 3.3 shows the surface (a) and cross section (b) SEM images of a γ-alumina support. The surface of the γ-alumina is smooth and no cracks or pinholes can be observed. As shown in Figure 3.3(b), the thickness of a one-time coated γ-alumina layer is approximately 2 μm. The thickness of γ-alumina layer will increase with the times of

dip-coating. The α-alumina support has a macroporous morphology with pore size of around 200 nm. Due to the small mesopores, the γ-alumina layer looks relatively dense, compared to the α-alumina.

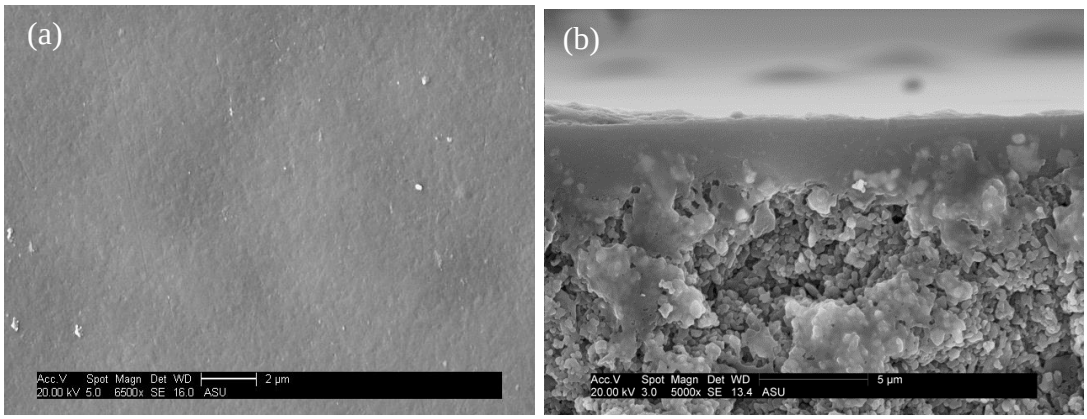

Figure 3.3 Surface and cross-section SEM images of a mesoporous γ-alumina coated α-alumina support

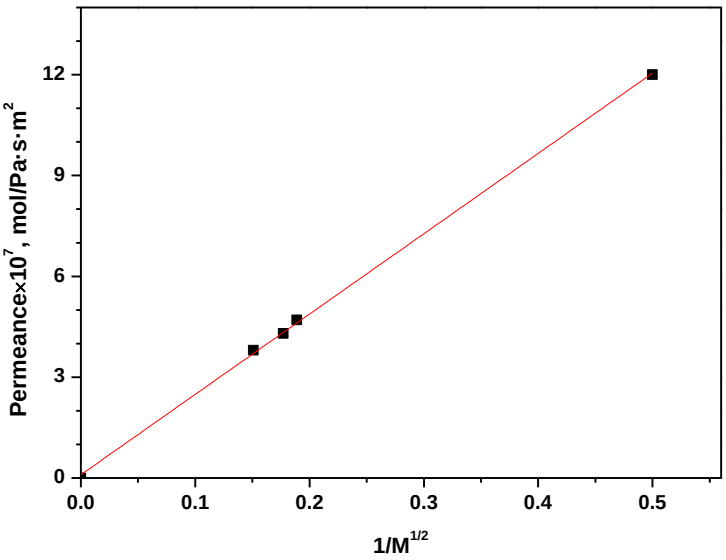

Figure 3.4 Gas permeance for He, N_2, O_2, and CO_2 versus the reciprocal of the square root of the molecular weight for a γ-alumina support membrane. The data indicate that gas transport is by Knudsen diffusion

Figure 3.4 is a plot of the gas permeance for He, N_2, O_2 and CO_2 versus the reciprocal of the square root of the molecular weight. The data can be correlated by a straight line, indicating Knudsen diffusion as the gas transport mechanism for the gamma-alumina support. Knudsen diffusion is a typical mechanism for the transport of gases through mesoporous membranes or supports. This confirms the good quality of the mesoporous γ-alumina layer for the support.

Figure 3.5 shows the SEM images of the surface and cross-section of polymer membranes prepared on α-alumina and γ-alumina supports. No visible defects or pin-holes were observed in the polymer films from the SEM images. Although the preparation conditions are the same, the polymer layer on the α-alumina support is about 6.5 μm thick, at least two times thicker than the layer on the γ-alumina support (~3 μm). The difference in thickness is probably due to the different surface properties of the two supports, especially the roughness. Wei et al. (2010) reported that the larger contact area presented by a rough ceramic support increased the mechanical interlocking and interfacial chemical bonds between the polymer and the support, resulting in stronger interfacial adhesion. The α-alumina support is rougher than the γ-alumina. As a result, a larger amount of polymer solution will adhere to the surface of the α-alumina support, resulting in a polymer film with a larger thickness. Recently, Tseng et al. (2012) reported a similar finding that, as the roughness of the support increases, the membrane thickness for a CMS membrane on an α-alumina support also increases.

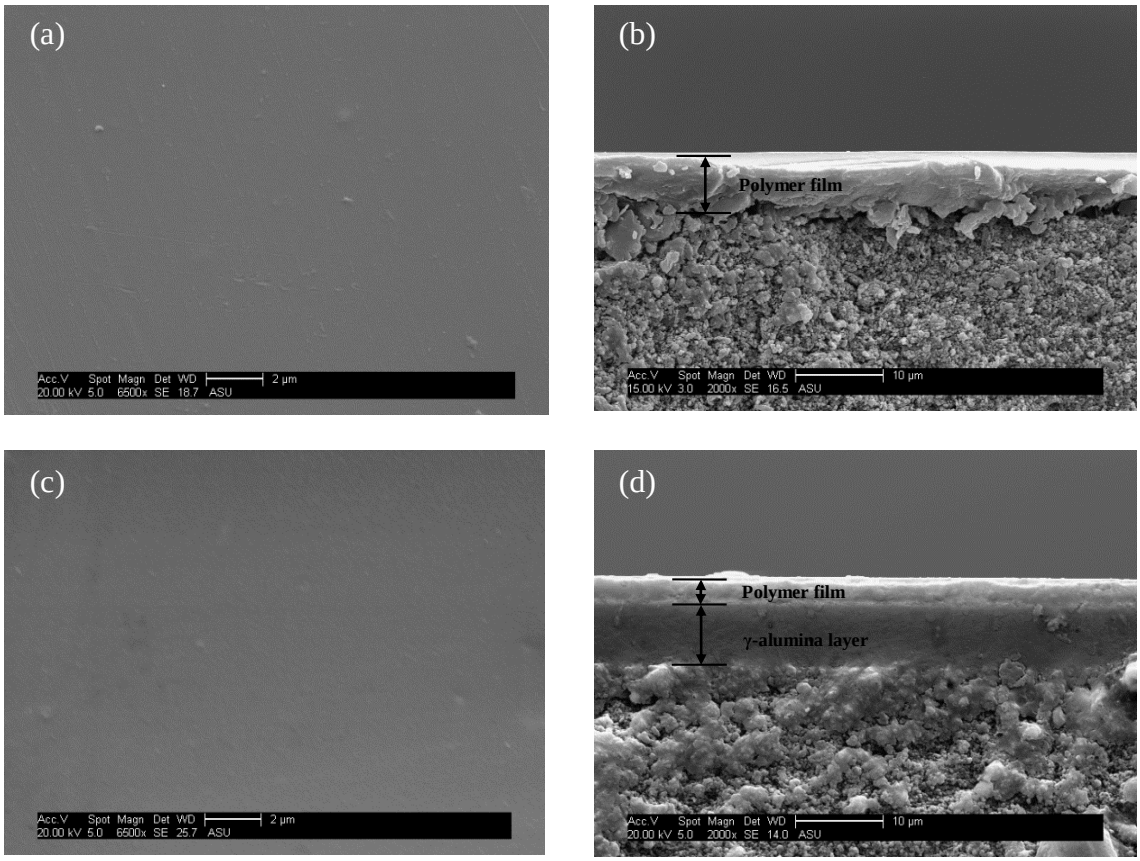

Figure 3.5 Surface and cross-section SEM images of polymer membranes prepared on α-alumina (a and b) and γ-alumina (c and d) supports

The quality of the polymer membranes was further examined by comparing their gas permeation properties with that of the bulk polymer. Table 3.2 lists the gas permeances and ideal separation factors of the prepared polymer membranes on α-alumina and γ-alumina supports. The one-time coated polymer membrane on γ-alumina shows a He/N_2 ideal separation factor of 24.9 and O_2/N_2 ideal separation factor of 4.2, which are close to the values of the bulk polymer, indicating the absence of defects in the polymer film. The permeance of the α-alumina supported membranes is less than half that of the γ-alumina supported membranes, because the thickness of the former is more than twice that of the latter. Also, the one-time coated α-alumina supported membrane

showed a smaller ideal separation factor, probably due to some minor defects in the membrane.

Table 3.2

Gas permeation properties of the polymer membranes prepared on α and γ-alumina supports

Support	Number of coating	Permeance (mol/Pa s m^2)			Ideal separation factor	
		He	O_2	N_2	He/N_2	O_2/N_2
α-alumina	1	7.32×10^{-9}	1.21×10^{-9}	3.41×10^{-10}	21.5	3.5
α-alumina	2	5.34×10^{-9}	9.45×10^{-10}	2.21×10^{-10}	24.2	4.3
γ-alumina	1	1.55×10^{-8}	2.62×10^{-9}	6.22×10^{-10}	24.9	4.2
γ-alumina	2	1.18×10^{-8}	2.07×10^{-9}	4.69×10^{-10}	25.2	4.4

The multiple dip-coating procedure has been widely used to eliminate or minimize possible defects in membranes prepared by the dip-coating method (Wang et al., 2012; Zhao et al., 2011). As shown in Table 3.2, the selectivity of the γ-alumina supported polymer membrane, which already matched well the intrinsic polymer properties, was not improved by multiple coatings, and the permeance decreased because of the increase of membrane thickness. However, an improvement in the ideal separation factors for He/N_2 and O_2/N_2 was observed for the α-alumina supported membrane, with the defects repaired by the second coating. This additional repair process is not preferred for industrial application, because it not only complicates the membrane preparation procedures, but also reduces the gas permeance by increasing the membrane thickness. In contrast, by taking advantage of the γ-alumina support, defect-free, thin polymer membranes can be successfully prepared by just one-time coating. CMS membranes were obtained by pyrolysis of these good quality polymer membranes.

3.3.2 Formation and characterization of CMS membranes

Figure 3.6 shows the TGA curve of the polymer precursor under the pyrolysis condition used in this work. The slight weight loss from 100 ℃ to 200 ℃ is most likely attributed to boiling off of adsorbed water. The major chemical decomposition of the polymer occurred around 450 ℃, with a large weight reduction observed in the TG curve. The final weight of carbon after the pyrolysis is around 60% of the original weight of polymer precursor.

The FTIR spectra of the polymer membrane and CMS membrane are shown in Figure 3.7. For the polyimide precursor membrane, the characteristic bands at 1786 cm^{-1} and 1723 cm^{-1} come from the symmetric and asymmetric C=O stretch. The typical band for the C-N stretch is located at approximately 1350 cm^{-1}. After pyrolysis, almost all of the sharp peaks observed for the polymer membranes disappeared completely, due to the decomposition of those chemical groups. The small broad band at 1605 cm^{-1} is ascribed to the C=C, characteristic of carbon materials. Other tiny bands can still be observed, such as the peaks at 1723 cm^{-1} and 1350 cm^{-1}. This result is not surprising, as CMS membranes usually contain some residual oxygen and nitrogen heteroatoms (Liao et al., 2012). It also should be noted that ultra high purity Ar gas instead of vacuum condition was used for the pyrolysis in this work. It has been reported that trace oxygen in the pyrolysis atmosphere can chemisorb onto the carbon surface forming oxygen containing bonds (Kiyono et al., 2010).

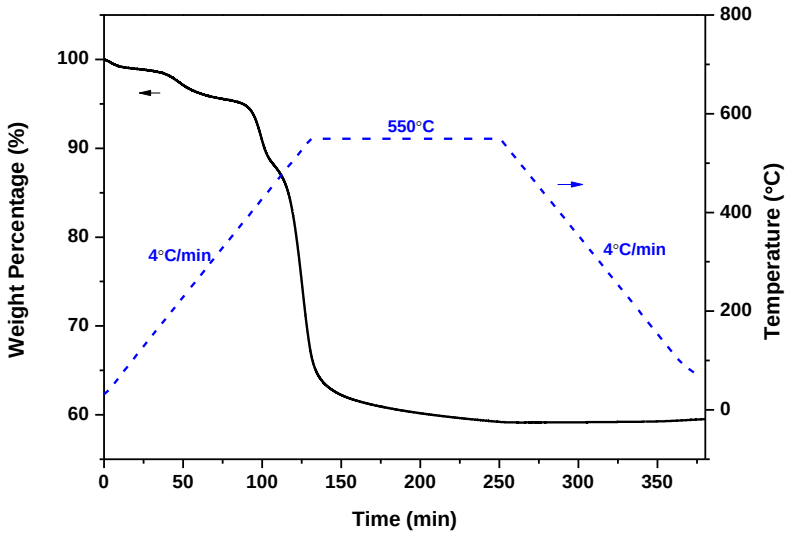

Figure 3.6 TGA curve for the polyimide precursor material under pyrolysis conditions. The pyrolysis time and temperature profile is also shown

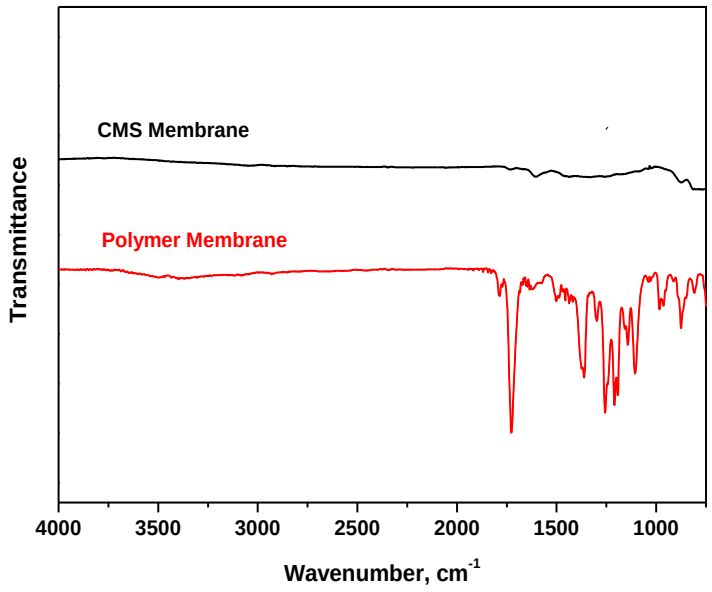

Figure 3.7 FTIR spectra of polymer membrane and CMS membrane pyrolyzed at 550 ℃

Figure 3.8 shows surface and cross-section SEM images of CMS membranes on α-alumina and γ-alumina supports. Both membranes are free of any large defects. The three distinct regions —α-alumina support, intermediate γ-alumina layer, and top CMS layer—were clearly observed in the cross-section image of the γ-alumina supported CMS membrane (Figure 3.8(d)). The top selective carbon layer has a symmetric structure of approximately 1.6 μm thick. The carbon layer formed on the α-alumina support prepared under the same conditions has a thickness of 4 μm. The CMS membranes on both supports are thinner than their polymer membrane counterparts, due to the shrinkage of the membrane layer caused by the decomposition of the polymer during pyrolysis.

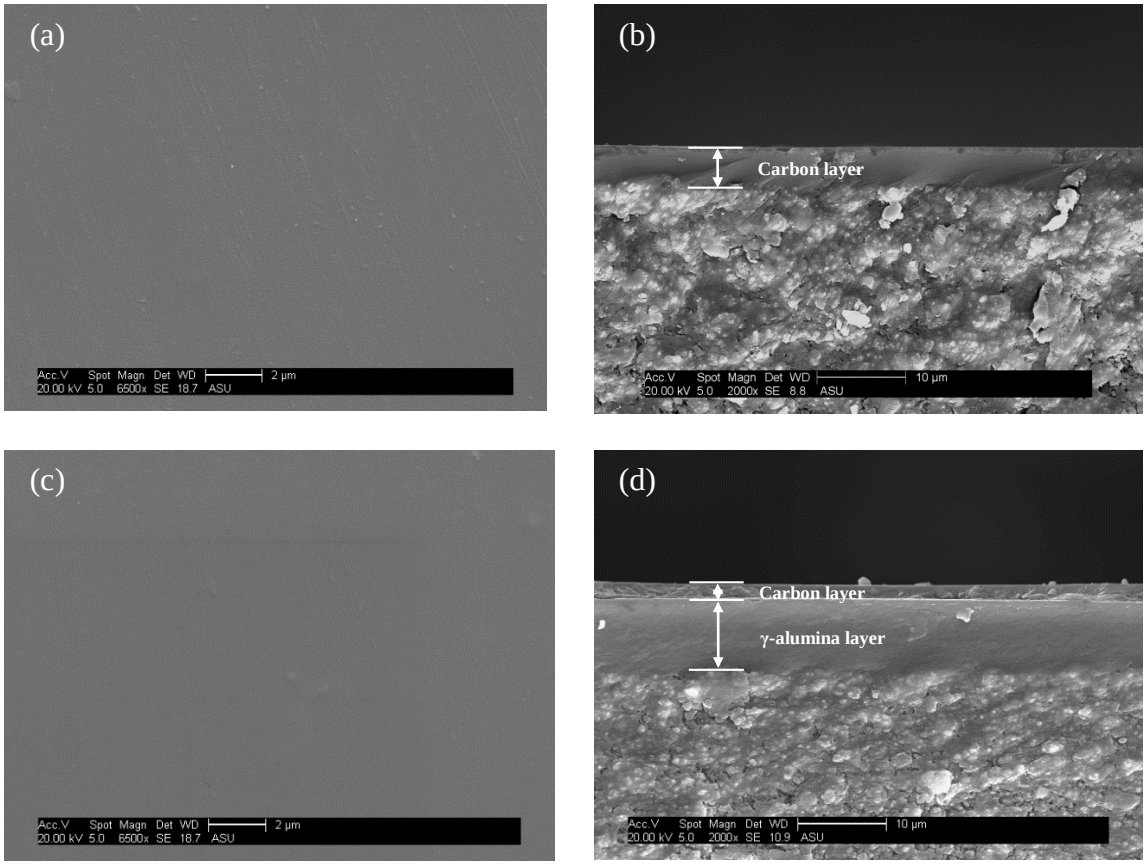

Figure 3.8 Surface and cross-section SEM images of CMS membranes prepared on α-alumina (a and b) and γ-alumina (c and d) supports

During pyrolysis in an inert gas environment, some by-products of small volatile gases, such as H_2, CO_2, CO, and CH_4, were released from the membrane, creating slit-like micro-pore structures in the CMS membrane (Salleh et al., 2011). As a result, the gas permeation mechanism changed from solution diffusion for the precursor polymer membrane to molecular sieving diffusion for the CMS membrane. Table 3.3 lists gas permeation and separation data for CMS membranes prepared at different pyrolysis temperatures. Compared with the data for the precursor polymer membrane in Table 3.2, the He/N_2 ideal separation factor was considerably improved for the CMS membranes prepared at 550 ºC on both α-alumina and γ-alumina supports. Furthermore, the CMS membranes exhibit He permeances around five times higher than those of polymer membranes.

Table 3.3

Gas permeation properties of CMS membranes prepared on α-and γ-alumina supports at different temperatures

Support	Temperature (℃)	Permeance (mol/Pa s ṁ^2)		Ideal separation factor
		He	N_2	He/N_2
α-alumina	550	3.61×10^{-8}	1.09×10^{-9}	33.1
γ -alumina	550	8.54×10^{-8}	1.91×10^{-9}	44.7
γ-alumina	650	2.13×10^{-8}	3.72×10^{-10}	57.3
γ-alumina	750	3.86×10^{-9}	$<1.0\times10^{-10}$	/

The relationship between the gas permeation properties and the pyrolysis conditions, which include pyrolysis temperature, heating/cooling rate, thermal soaking time, and pyrolysis atmosphere, have been widely studied (Fu et al., 2011; Geiszler &

Koros, 1996) Because the pyrolysis temperature is the most critical parameter in determining the final structure of CMS membranes, its effect was studied to determine the optimal condition for preparing the membranes. As shown in Table 3.3, increasing the pyrolysis temperature from 550 ℃ to 750 ℃ caused a decrease in both the He and N_2 permeance, but an increase in He/N_2 ideal separation factor. This was expected, because CMS membranes treated at higher pyrolysis temperatures have smaller pore sizes. Considering both permeance and selectivity, 550 ℃ was selected as the optimum pyrolysis temperature.

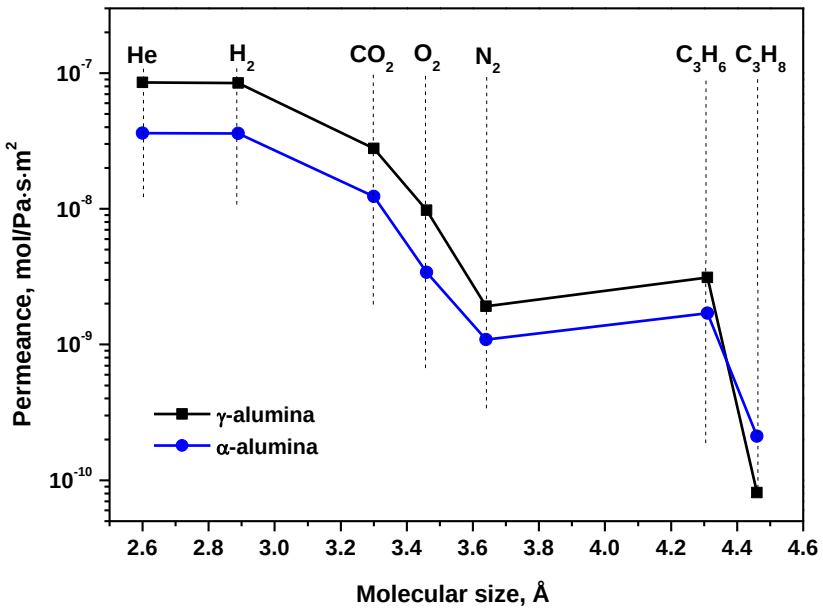

Figure 3.9 Molecular sieving effect characterization of CMS membranes prepared at 550 °C on γ-alumina and α-alumina supports

Molecular probing, based on single gas permeation experiments, was used to further examine the quality of the CMS membranes prepared at 550 ℃. Figure 3.9 shows the single gas permeance through the CMS membranes as a function of molecular size.

For membranes prepared on both γ-alumina and α-alumina supports, the permeance of the gases with a kinetic diameter smaller than 4 Å decreases with increasing kinetic diameter in the order of $P(He)>P(H_2)>P(CO_2)>P(O_2)>P(N_2)$, showing molecular sieving characteristics. Larger C_3H_6 molecules have a higher permeance than the smaller N_2 molecules, because of preferential adsorption of hydrocarbons. The γ-alumina supported membrane has a higher He/N_2 and O_2/N_2 ideal separation factor (45 and 5.1 respectively) than the α-alumina supported membranes, due to the better quality of the membrane on the γ-alumina surface. This improvement in ideal separation factor is more significant for the C_3H_6/C_3H_8 gas pair. A high ideal separation factor of 38 was observed for the γ-alumina supported membrane, as compared to the low value of 8 for the α-alumina support. Propylene (4.31Å) and propane (4.46Å) have very similar molecular sizes, so non-selective defects will greatly inhibit the membrane separation performance. As a result, the γ-alumina supported membranes, with fewer defects, offer a C_3H_6/C_3H_8 ideal separation factor 475% higher than that of the α-alumina supported membranes, although the difference in He/N_2 ideal separation factor is only around 25%. The better quality of the membranes on γ-alumina is due to the improved quality of the polymer precursor membrane on this support. The reduced membrane thickness may also reduce stresses in the carbon layer that develop from the thermal expansion mismatch between the carbonizing layer and the alumina support during pyrolysis.

3.3.3 Propylene/propane mixture gas separation

Most studies of CMS membranes for propylene/propane separation report only their pure-gas performance, although a few papers have reported mixed-gas data. These limited studies reported that the mixture gas selectivity is usually smaller than the ideal

selectivity calculated from pure gas permeance. Table 3.4 lists the performances of different γ-alumina supported CMS membranes prepared in this work for the separation of 50/50 C_3H_6/C_3H_8 mixture at 25 ℃. These membranes were prepared under the same conditions, but from different batches. All of them have a mixture selectivity of above 30 and a C_3H_6 permeance of around 3.0×10^{-9} mol/Pa s ㎡ (9.0 gpu), indicating good manufacturing reproducibility.

Table 3.4

Permeances and C_3H_6/C_3H_8 mixture selectivity of γ-alumina supported CMS membranes pyrolyzed at 550 ℃ for 2hrs

Membranes	Permeance (mol/Pa s ㎡)		C_3H_6/C_3H_8 Mixture Selectivity
	C_3H_6	C_3H_8	
M1	3.2×10^{-9}	8.9×10^{-11}	36
M2	2.7×10^{-9}	7.7×10^{-11}	35
M3	3.0×10^{-9}	9.4×10^{-11}	32

3.4. Conclusions

High quality alumina supported CMS membranes have been successfully prepared by a single coating/pyrolysis step. An intermediate mesoporous γ-alumina layer is effective in improving the surface quality of the support. Thinner and higher quality CMS membranes can be obtained by using the γ-alumina intermediate layer than by use of a bare α-alumina support. The single gas permeance through the CMS membrane decreases with increasing kinetic diameter of the molecules in the order of $P(He)>P(H_2)>P(CO_2)>P(O_2)>P(N_2)$, indicating its molecular sieving characteristics. A 1.6 μm thick CMS membrane on a γ-alumina support offers He/N_2 and O_2/N_2 perm-selectivities of 45 and 5.1 respectively. Due to significantly fewer defects, the γ-alumina

supported CMS membrane offers a C_3H_6/C_3H_8 ideal separation factor of 38, which is almost five times higher than that of an α-alumina supported CMS membrane. When tested with a 50/50 C_3H_6/C_3H_8 mixture at room temperature, the CMS membrane exhibits a C_3H_6/C_3H_8 mixture selectivity up to 36 with a C_3H_6 permeance of around 3.0×10^{-9} mol/Pa s m^2 (9.0 gpu), with no plasticization observed.

CHAPTER 4

ULTRA-THIN CARBON MOLECULAR SIEVE MEMBRANE FOR PROPYLENE/PROPANE SEPARATION: EFFECTS OF MEMBRANE THICKNESS ON SEPARATION PERFORMANCE

4.1 Introduction

The CMS membrane prepared in Chapter 3 showed a high mixture selectivity up to 36 for propylene/propane separation. The membrane has a thickness of 1.6 μm, offering a reasonably good propylene permeance. It should be noted that thin membrane is especially preferred in industry application, because it offers high gas permeance and hence high productivity and lower cost of membrane separation process. There is still a potential to further reduce the thickness of the CMS membrane prepared in our work to achieve high gas permeance.

It is challenging to fabricate thin, high quality CMS membrane in either hollow fiber or ceramic supported geometry without compromising the membrane selectivity. Several researchers have tried to prepare thin CMS membranes through pyrolysis of the polymer hollow fiber membrane with asymmetric pore structure, in which a thin dense membrane layer is on the surface. Okamoto et al. (1999) prepared hollow fiber CMS membranes with a thin selective layer of approximately 200 nm, which exhibited a high C_3H_6 permeance of 8.7×10^{-9} mol/(m^2·s·Pa) (26 gpu) at 35 ℃. But the relatively low selectivity of 11 for C_3H_6/C_3H_8 mixture separation suggested the existence of non-selective defects in the membrane. Recently, Koros and co-workers (2011) found a collapse behavior of the porous substructure into a dense separation layer during the pyrolysis of Matrimid hollow fiber membrane. In their following study, a novel pre-

pyrolysis treatment using a sol-gel crosslinking reaction to induce vinyl crosslinked silica on precursor fiber walls was developed to restrict the morphology collapse. The treated membranes possessed an apparent membrane skin thickness of ~5-6 μm for Matrimid derived membrane and ~3-4 μm for 6FDA derived membrane, both of which were reduced up to 5-6 fold compared to the CMS membranes from untreated precursors.

The CMS membrane prepared on ceramic support has a symmetric pore structure with the thickness essentially being determined by the thickness of the coated polymer layer. In order to cover the surface flaws and the macropores (~200 nm) of ceramic substrate, a thick membrane layer (>2 μm) is usually required to achieve a defective free membrane. For example, Hayashi et.al (1996) and Yamamoto et.al (1997) have synthesized CMS membranes with good C_3H_6/C_3H_8 selectivity above 20, but these membranes are of 4-6 um thick and only offered less attractive C_3H_6 permeances lower than 3.0×10^{-9} mol/(m^2·s·Pa).

On the other hand, when the membrane thickness decreases toward the submicron or nanometer range, very different gas transport properties were noticed for several glassy polymer membrane (Huang & Paul, 2004; Rowe et al. 2009). For example, as compared to thick films, thin polymer films undergo a more rapid physical aging, and more extensive and faster plasticization. In their recent studies, Paul and co-workers (2014) found that the thermal rearrangement of an ortho-functional polyimide and the gas transport properties of thermal rearranged (TR) films are also strongly film thickness dependent. Thin TR film has a higher degree of chemical conversion, and experienced a much greater rate of physical aging than the thick films. The lower glass transition temperature, the higher segmental chain mobility for the thinner polymer film is believed

to be the reason behind these phenomena. It is well known that the glass transition temperature is also a key factor influencing the development of micropore structure in CMS membrane during pyrolysis. However, no studies have been reported on the change in pore structure and gas transport properties of CMS membranes associated with the change in the membrane thickness.

Despite the extensive work on the synthesis of CMS membranes, no literature has reported high quality CMS membrane with membrane thickness smaller than 500 nm. As demonstrated in the previous chapter, high quality, thin CMS membrane can be prepared on mesoporous γ-alumina support compared to the more commonly used macroporous α-alumina support. The mesoporous γ-alumina support is also effective in avoiding the undesirable infiltration of polymer chains into the support pores, as found when α-alumina support is used, as shown in Figure 4.1. The objective of this chapter is to synthesize ultra-thin CMS membranes with high C_3H_6 gas permeance for C_3H_6/C_3H_8 separation, and study the effect of membrane thickness on the structure and gas transport properties of CMS membranes. The thickness of CMS membranes was changed through varying the conditions for the coating of polymer precursor film on support including the dip-coating time and the concentration of the polymer precursor solution. Based on the gas permeation and separation results of polymer and CMS membranes of different thicknesses, the mechanism for the thickness dependence of micropore structure formation for CMS membrane was discussed.

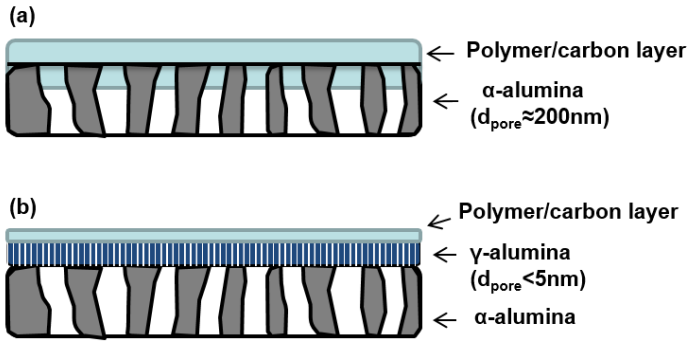

Figure 4.1 Schematic composite membrane structure for (a) α-alumina supported and (b) γ-alumina supported polymer/carbon membranes

4.2 Experimental

4.2.1 Preparation of ceramic support

Ceramic support with an asymmetric structure consisting of a γ-alumina top layer and α-alumina substrate were used as the support for membrane preparation. The α-alumina supports with a porosity of ~45% and an average pore diameter of ~200 nm were prepared by sintering α-alumina disk at 1150 °C for 30 h. One side of the α-alumina support was polished with sandpaper (#500, #800, and #1200). The boehmite sol was prepared following previous reported procedures, and then coated onto the polished side of α-alumina support. The whole support was then calcined at 550 ℃ for 3 h with a heating and cooling rate of 0.5 ℃/min. If necessary, the coating and calcination was repeated to get a final good quality γ-alumina layer.

4.2.2 Preparation of polymer membranes

The polymer precursor used in this work is a proprietary 6FDA based polyimide polymer (molecular weight >30000) provided by Membrane Technology and Research, Inc. The precursor was dissolved in acetone to prepare polymer coating solutions with different concentrations from 1wt% to 0.02 wt%. The polymer membranes were formed

on the surface of γ-alumina support by dip-coating method. The dip-coating time was varied from 15 s to 30 s and 60 s. Different polymer concentration and different dip-coating time were used to give polymer membranes with different thicknesses. The polymer membranes were named in the form of P-concentration of polymer solution-dip coating time. These supported polymer membranes were first dried at room temperature for 3 h, then at 100 ℃ for 12 h, and finally annealed at 140 ℃ in air for 5 h.

4.2.3 Preparation of CMS membranes

CMS membranes with different thicknesses were formed by pyrolysis of the supported polymer membranes under ultra high purity (UHP) argon gas environment. The oxygen level in the pyrolysis gas is crucial to the quality of CMS membranes prepared by this method. Depending on the concentrations, the oxygen could damage the membrane due to excessive decomposition of the polymer film, or improve the membrane performance through oxygen doping in the micropores. In order to avoid any effects from oxygen and to maintain the same pyrolysis conditions for all membranes, an additional oxygen removal step using copper-based catalyst (Research Catalysts, Inc.) as "oxygen getter" was applied in this work.

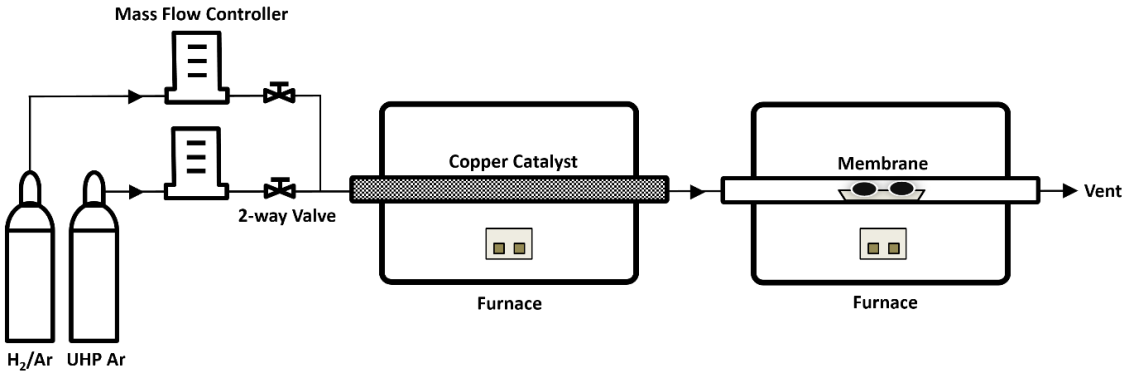

Figure 4.2 Schematic setup for the oxygen removal assisted pyrolysis of CMS membranes

Figure 4.2 shows the schematic setup for the oxygen removal and pyrolysis process. The copper catalysts were closely packed inside the left tubular furnace to form a fixed-bed reactor. The catalysts, which came as copper oxides, were first activated by reduction of the copper oxides to metallic copper using a reducing 2% H_2/Ar mixture at a flow rate of 100 mL/min at 175 ℃ for 24 h. After the activation, the polymer membranes were placed inside the furnace on the right side and UHP Ar gas at a flow rate of 100 mL/min was used for pyrolysis. The copper catalyst reacted with the oxygen impurities existing in the UHP Ar to form copper oxide. As a result, an almost oxygen free environment was created for the downstream pyrolysis process. The pyrolysis was typically conducted at 550 ℃ for 2 h with a heating and cooling rate of 4 ℃/min. The pyrolysis conditions including the final pyrolysis temperature and thermal soak time were varied for the ultra thin CMS membrane. All the CMS membranes prepared were stored in ultra high purity Ar atmosphere before gas permeation and separation test, to avoid any water or oxygen adsorption on membrane.

4.2.4 Membrane characterization

The surface morphology and cross-section of the polymer membranes and CMS membranes were characterized by scanning electron microscopy (SEM, Philips, XL 30) at an accelerating voltage of 20 kV. The thicknesses were determined from the cross-section SEM images of these membranes.

4.2.5 Single gas permeation and physical aging measurements

The He and N_2 single gas permeances through the polymer membranes and CMS membranes were measured by a previously reported steady state method at room temperature, with a feed pressure of 45 psi. The He/N_2 perm-selectivity was calculated

based on the ratio of He and N_2 single gas permeance, and was used to examine the membrane quality. In the physical aging test of polymer membranes, the permeances of He and N_2 were monitored over 72 h. To facilitate comparison of the rate of physical aging, the He, N_2 permeances and He/N_2 perm-selectivity were normalized by the corresponding initial values of the membranes.

4.2.6 C_3H_6/C_3H_8 mixture separation measurement

The C_3H_6/C_3H_8 mixture separation performance of the CMS membranes was measured using a previously reported cross-flow setup. The feed side was a 50%/50% C_3H_6/C_3H_8 mixture at a total flow rate of 50 mL/min, and N_2 at a flow rate of 50 mL/min was used as sweeping gas on the permeate side. The feed pressure was maintained at 45 psi (310 kPa) by a needle valve on the retentate line. The gas flow rate on the permeate side was measured by a bubble flow meter. The gas composition on the permeate side was measured by gas chromatography (SRI Instruments, SRI 8610C) equipped with a flame ionization detector (FID) and a 6'×1/8" silica gel packed column, using He as carrier gas. All the measurements were conducted at room temperature.

4.3. Results and discussion

4.3.1 Polymer membranes with different thicknesses

The mesoporous γ-alumina supports prepared are all of good quality with the gas transport showing Knudsen diffusion behavior. They have been characterized in the previous chapter. Table 4.1 and Figure 4.3 shows the He and N_2 gas permeation properties of the polymer membranes prepared at different conditions. As shown for membranes P-2-60 to P-2-15, with the decrease of dip-coating time, the permeance of both He and N_2 increases while the perm-selectivity keeps essentially constant. The

increase in gas permeance is more obvious for the membranes prepared with a more diluted polymer precursor dip-coating solution. At a fixed dip-coating time of 15 s, the permeance increases by about 35 times as the concentration of the dip-coating solution decreases from 2 wt% to 0.02 wt%. These membranes all show a good He/N_2 perm-selectivity above 26, suggesting the absence of any large defects. The differences in the gas permeance for various membranes are essentially due to different membrane thickness. The results clearly indicate that using a shorter dip-coating time and a more diluted polymer solution leads to polymer membranes with smaller thickness.

Table 4.1

Gas permeation properties of polymer membranes prepared at different conditions

Polymer membrane	Polymer concentration (wt%)	Dip-coating time (s)	He permeance ($mol/m^2 \cdot s \cdot Pa$)	N_2 permeance ($mol/m^2 \cdot s \cdot Pa$)	He/N_2 perm-selectivity
P-2-60	2	60	6.05×10^{-9}	2.33×10^{-10}	26.0
P-2-30	2	30	8.80×10^{-9}	3.22×10^{-10}	27.3
P-2-15	2	15	1.87×10^{-8}	7.06×10^{-10}	26.5
P-1-15	1	15	3.34×10^{-8}	1.23×10^{-9}	27.2
P-0.5-15	0.5	15	6.76×10^{-8}	2.41×10^{-9}	28.1
P-0.2-15	0.2	15	1.58×10^{-7}	5.36×10^{-9}	29.5
P-0.1-15	0.1	15	2.63×10^{-7}	8.98×10^{-9}	29.3
P-0.05-15	0.05	15	4.95×10^{-7}	1.85×10^{-8}	26.8
P-0.02-15	0.02	15	6.42×10^{-7}	2.35×10^{-8}	27.3

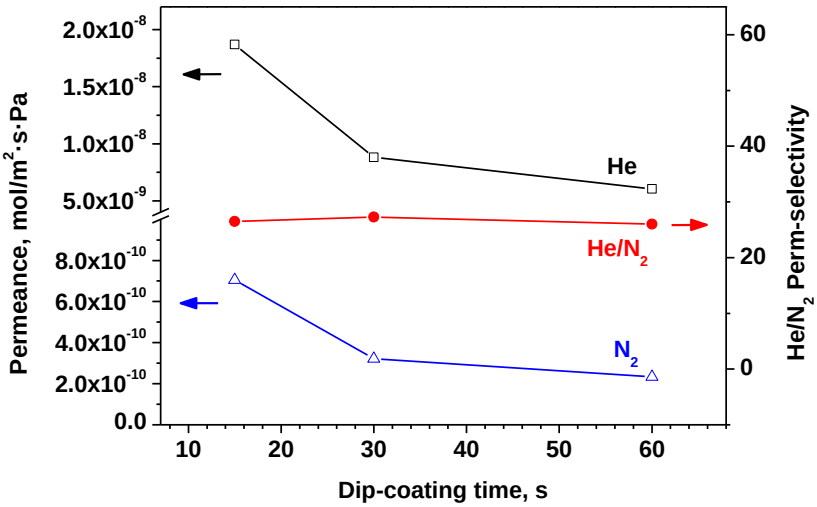

Figure 4.3 He, N_2 permeances and He/N_2 perm-selectivity of the polymer membranes as a function of dip-coating time

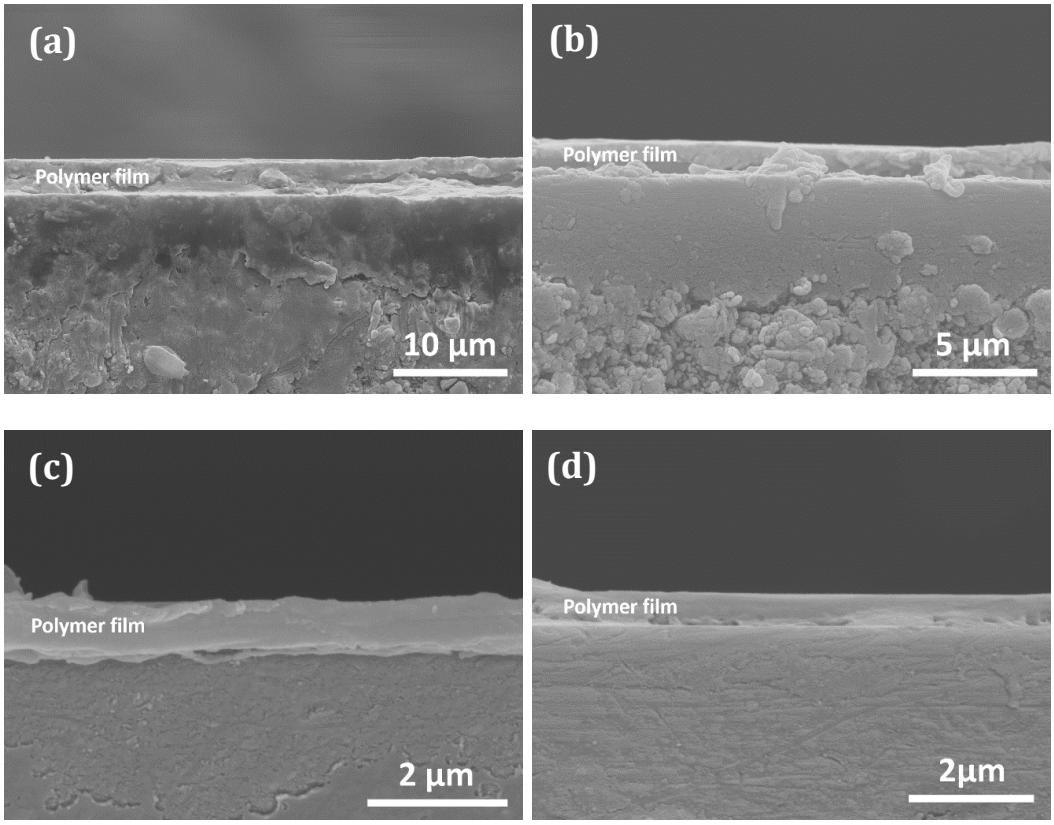

Figure 4.4 Cross-section SME images of γ-alumina supported polymer membranes with different thicknesses: (a) P-2-15, (b) P-1-15, (c) P-0.5-15 and (d) P-0.2-15

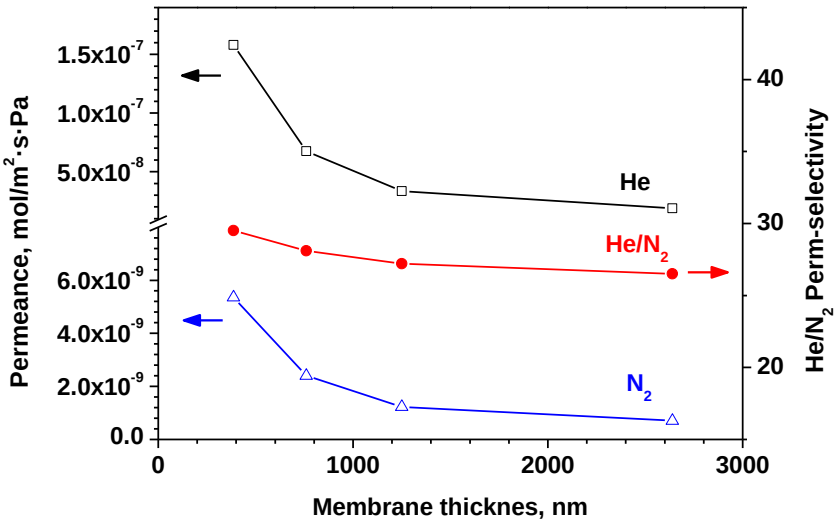

Figure 4.5 He, N_2 permeances and He/N_2 perm-selectivity of the polymer membranes as a function of membrane thickness

Figure 4.4 shows the cross-section SEM images of some polymer membranes in Table 4.1. Polymer membranes P-0.1-15, P-0.05-15 and P-0.02-15 were not characterized, because the CMS membranes generated from these membranes are of low quality. Figure 4.5 shows the He, N_2 gas permeances and He/N_2 perm-selectivity as a function of the membrane thickness determined from SEM images. A clear inverse proportional relationship between the permeance and membrane thickness was observed. This indicated no penetration of polymer chains into the support pores even under the conditions of using very diluted polymer solutions. These high quality polymer membranes were pyrolyzed to form CMS membranes with different thicknesses.

4.3.2 CMS membranes with different thicknesses

Figure 4.6 shows the cross-section SEM images of the CMS membranes with different thicknesses after pyrolysis at 550 ℃ for 2 h. The three layers structure consisting of carbon layer, γ-alumina layer and α-alumina support can be clearly

distinguished from the SEM images. These membranes are of high integrity with no macroscopic defects found on the surface SEM images (not shown here). As shown in Figure 4.7, with the thickness decreasing from 2.1 μm to 520 nm, both He and N_2 permeances increases accordingly with the He/N_2 perm-selectivity maintaining at around 40. However, it is interesting to observe a decrease in the permeances when the membrane thickness was reduced from 520 nm to 300 nm. Meanwhile, the He/N_2 perm-selectivity greatly increased from 39 to 52, which seems to suggest a reduction in the effective pore size for the 300 nm CMS membrane.

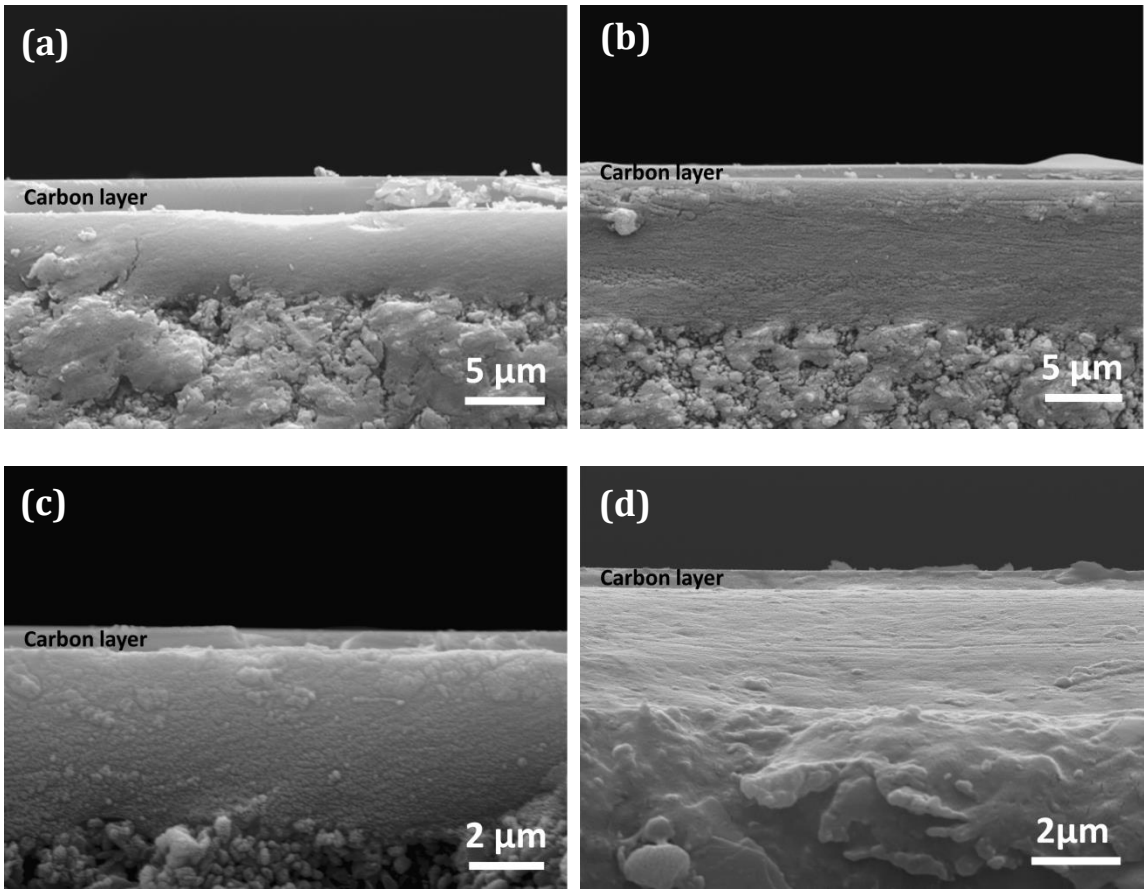

Figure 4.6 Cross-section SME images of γ-alumina supported CMS membranes with different thicknesses: (a) 2.1 μm, (b) 850 nm, (c) 520 nm and (d) 300 nm

Figure 4.8 shows the C_3H_6/C_3H_8 separation performance as a function of membrane thickness. Similar to the trend for He/N_2 system, the C_3H_6 permeance is improved without compromising the selectivity through reducing the membrane thickness to 520 nm. However, the 300 nm membrane shows a dramatically decreased C_3H_6/C_3H_8 selectivity, due to a decrease in C_3H_6 permeance but an increase in C_3H_8 permeance. These results suggest some pore structure change taking place when the membrane thickness was reduced to 300 nm. This will be explained after discussing the effect of pyrolysis conditions on the structure of polymer film next.

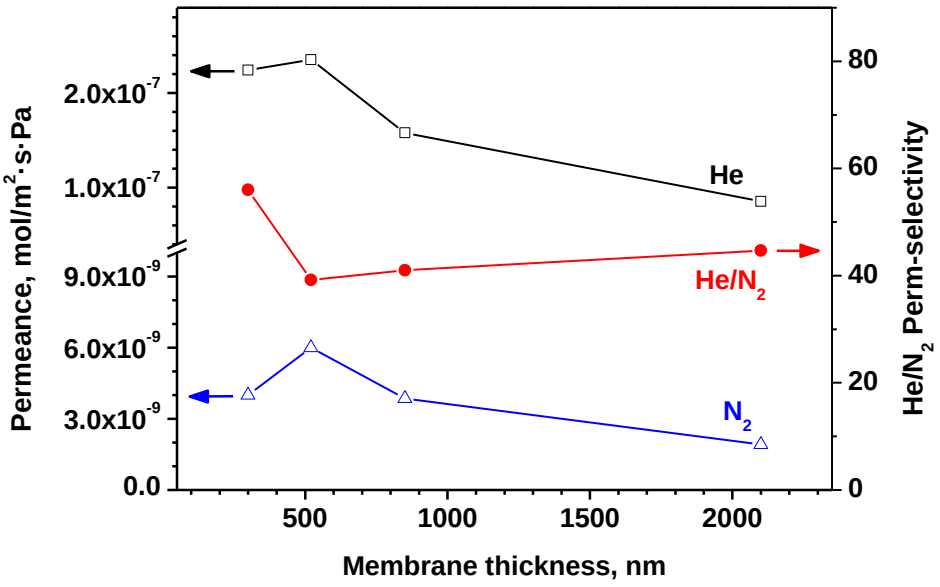

Figure 4.7 He, N_2 permeances and He/N_2 perm-selectivity of CMS membranes as a function of membrane thickness

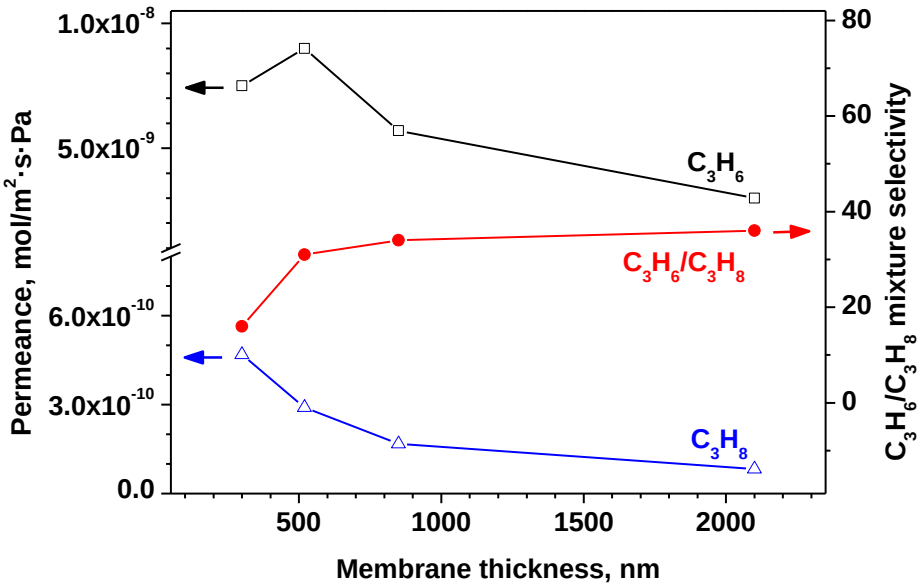

Figure 4.8 C_3H_6, C_3H_8 gas permeances and C_3H_6/C_3H_8 mixture selectivity of CMS membranes as a function of membrane thickness

The micropores in CMS membranes were formed by the misalignment/imperfect packing of the aromatic domains/carbon sheets. The piling of polymer precursor chains on support before pyrolysis has been reported to have influences on the final CMS pore structure. Irregularly arrayed polymer chains tend to form bigger CMS pores, while orderly and tightly arranged polymer chains will result in a smaller distance between the carbon sheets. For the polymer membranes prepared in our work, the polymer chains are more uniformly dispersed and less tangled together in the more diluted solution, which consequently leads to a more closely packed polymer chains in the thinnest polymer film coated on the support. This can be confirmed by the slight higher He/N2 perm-selectivity for the P-0.2-15 membrane (Table 4.1) compared to the other membranes. Thus a smaller pore size can be expected for the derived CMS membrane counterpart.

The glass transition temperature Tg, which is directly related to the chain segmental mobility of the polymer, is another key factor influencing polymer-carbon transition during the pyrolysis and the pore structure of the final CMS membrane. Polymer precursor with higher Tg possesses higher chain rigidity to prevent pore collapses in the intermediate stage during pyrolysis and help the membrane retain the desirable pore structure. On the other hand, lower Tg, which implies higher molecular mobility, facilitates the reorganization of carbon chains and leads to a more closely packed carbon sheets. Although the same polymer precursor was used in our work, these polymer membranes still differ in terms of membrane thickness. It is well known that for free standing polymer films and supported polymer films on non-attractive substrates, the glass transition temperature for the polymer decreases as the film thickness decreases. This film thickness dependence of Tg causes a faster physical aging for a polymer membrane with a smaller thickness. The physical aging behavior of our γ-alumina supported polymer membranes was measured by tracking the gas permeances and selectivity over time. As shown in Figure 4.9 and Figure 4.10, the thinner the membranes, the more rapid rate for the decrease of normalized He, N_2 permeancee, and the higher the normalized He/N_2 perm-selectivity over aging time. This effect is more pronounced for the 386 nm membrane. These results reflect a much higher chain segmental mobility for the 386 nm polymer membrane, which allows the aromatic domains/carbon chains extra freedom to become more closely packed and form smaller micropores in the 300 nm CMS membrane.

In addition, the release of volatile products during pyrolysis might also play some role in the structure change. The thinner film clearly provides a shorter pathway for the

diffusion and release of volatile products from the membrane. Under the same pyrolysis condition, the thinner film may eventually end up with a higher degree of graphitization and smaller pore size. However, more experiments are required to verify this possible reason.

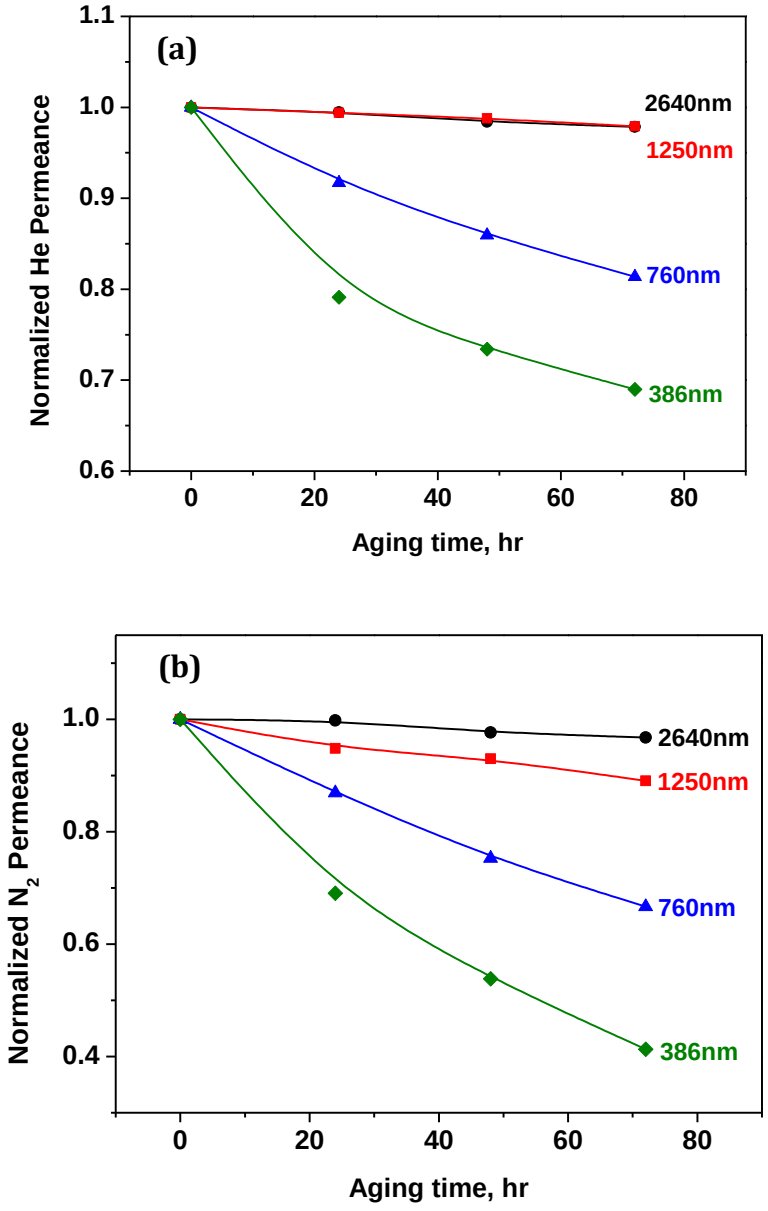

Figure 4.9 Normalized He (a) and N_2 (b) gas permeances of polymer membranes with different thickness as a function of aging time

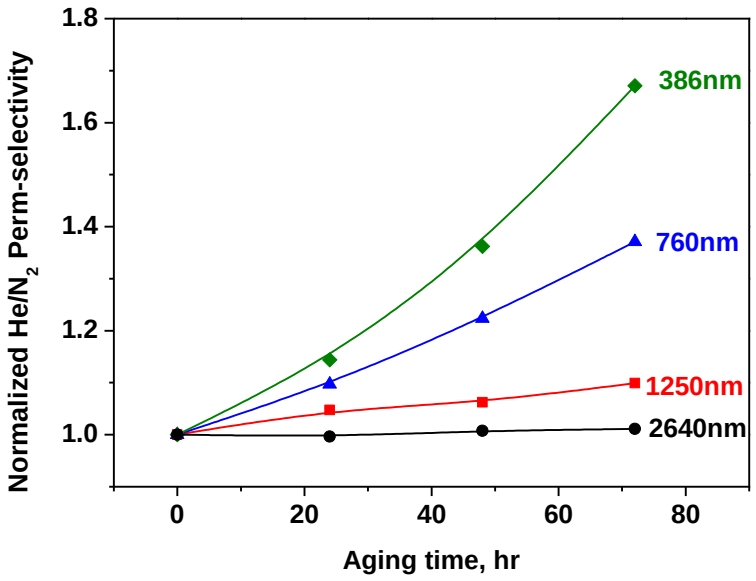

Figure 4.10 Normalized He/N_2 perm-selectivity of polymer membranes with different thickness as a function of aging time

The combined effects from the packing of polymer chains, chain segmental mobility and the diffusion of volatile by-products resulted in a smaller effective micropore size and smaller amount of these pores for the 300 nm CMS membrane. A hypothetical qualitative micropore size distribution model proposed by Koros to explain the unusual gas permeation and separation properties of the 300 nm CMS membrane. Based on Koros's model, the pore size distributions for the CMS membranes prepared in this work were generated and illustrated in Figure 4.11. When the membrane thickness was reduced to 300 nm, the distribution curve is very likely to transfer from type (a) to type (b). The four solid straight lines indicate the molecular size of He, N_2, C_3H_6 and C_3H_8, which have a van der Waals diameter respectively of 2.66, 3.13, 4.03, 4.16 Å.

The micropores locating on the right side of the straight lines represent the corresponding pores accessible for the transport of each gas. The membrane with type (b)

distribution is expected to be more selective but less permeable to the He/N_2 gas pair. However, the permeation of the relatively large C_3H_6 and C_3H_8 molecules through the CMS membrane largely depends on the micropores locating on the tail end of the distribution. As illustrated by the rea area, the shift from distribution type (a) to type (b) leads to a significant reduction in the total number of micropores accessible for the transport of C_3H_6, but only has a minor effect on the pores responsible for the permeation of C_3H_8. Therefore, a decreased C_3H_6/C_3H_8 selectivity was observed for the 300 nm CMS membrane due to the relatively large decrease in C_3H_6 permeance as compared to that for C_3H_8.

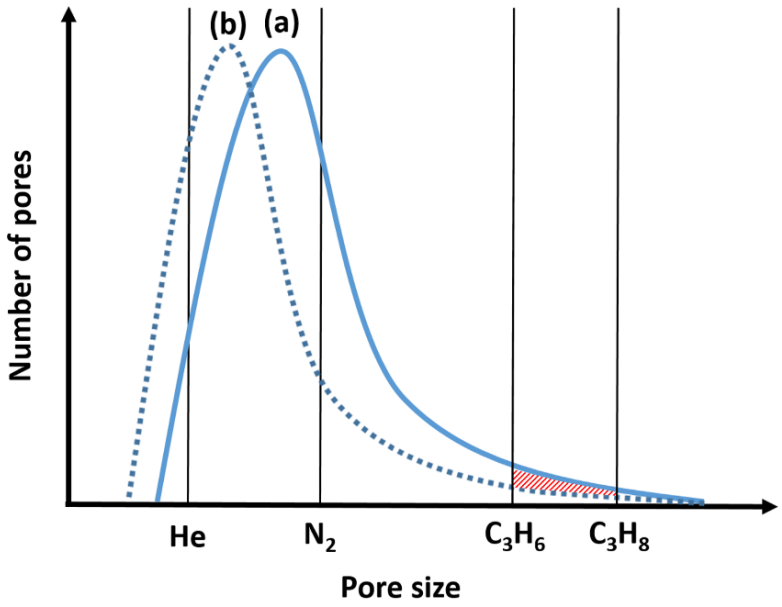

Figure 4.11 Schematic micropore size distribution for CMS membranes based on the hypothetical semi-quantitative model proposed by Koros and co-workers (2005)

4.3.3 Performances improvement through tuning pyrolysis conditions

It was reported that for a given type of polymer precursor pyrolysis treatment at a higher temperature for a longer thermal soak time leads to a smaller effective pore size of

the pyrolysis-derived CMS membrane. Iin order to obtain thinnest membrane with high C_3H_6/C_3H_8 selectivity, pyrolysis was performed at lower temperature for short timer to minimize reduction in the pore size. As shown in Table 4.2, when the final pyrolysis temperature lowered to 500 ℃ and the thermal soak time reduced to 0.5 h, membrane M3 showed both improved permeance and selectivity, as compared to membrane M1. The improvement is most likely caused by forming a more favorable pore structure with the pore distribution close to type (a) in Figure 4.11. However, the selectivity is still much lower than the other three CMS membranes with thickness above 500 nm, suggesting that the pore structure was not completely retained even under the more gentle pyrolysis condition. This is not surprising because mild pyrolysis can only help compensate the structure change caused by the aforementioned effects, instead of completely eliminating these effects. Therefore, more detailed studies are required to further understand how the pore structure change of CMS membranes depends on membrane thickness, and to identify effective approaches to avoid the closure of the C_3H_6-accessible micropores, so as to improve the separation performance.

Table 4.2

C_3H_6/C_3H_8 separation results of CMS membranes with thickenss of ~300 nm prepared at different pyrolysis condtions, ramping rate is 4 ℃/min for all membranes

Membranes	Pyrolysis temperature (℃)	Thermal soak time (h)	C_3H_6 permeance ($mol/m^2 \cdot s \cdot Pa$)	C_3H_6/C_3H_8 selectivity
M1	550	2	7.5×10^{-9}	16
M2	550	0.5	8.7×10^{-9}	17
M3	500	0.5	1.4×10^{-8}	23

Figure 4.12 compares the C_3H_6/C_3H_8 mixture selectivity and C_3H_6 permeance (at <50 ℃) for the CMS membranes prepared in this work with various other membranes reported in literature. The upper-bound trade-off curve for CMS membranes was generated based on reported data, and the curve for polymer membranes was created by using the reported permeability and selectivity upper-bound curve assuming the membrane thickness to be around 500 nm. The CMS membranes with the thickness of around 520 nm prepared in this work showed a mixture selectivity of around 31, and a C_3H_6 permeance up to 1.0×10^{-8} mol/(m^2·s·Pa). As shown, the performances of the CMS membranes prepared in this work are above the upper-bound curve for the reported CMS membranes and polymer membranes, and close to the performances of ZIF-8 and silica based membranes.

Despite the excellent separation performance of the silica based membrane, the hydrothermal stability still remains a major problem to be solved before the industrial application of the silica membrane. Besides the promising performance, ZIF-8 membrane was also reported to be stable under off-stream storage in air and on-stream propylene/propane separation conditions. CMS membranes prepared in our work show comparable mixture selectivity, but lower gas permeance than ZIF-8 membrane. Membrane thickness is not the reason for the difference in permeance, because our CMS membrane is already thinner than the reported ZIF-8 membranes. It is probably due to the three dimensional pore structure and high porosity of ZIF-8, offering high solubility and thus high permeability to propylene gas. However, it is usually difficult to fabricate defect-free zeolite or ZIF membranes with large membrane area because of the crystalline

nature. In comparison, amorphous CMS membrane has the advantage of easier fabrication for industrial application.

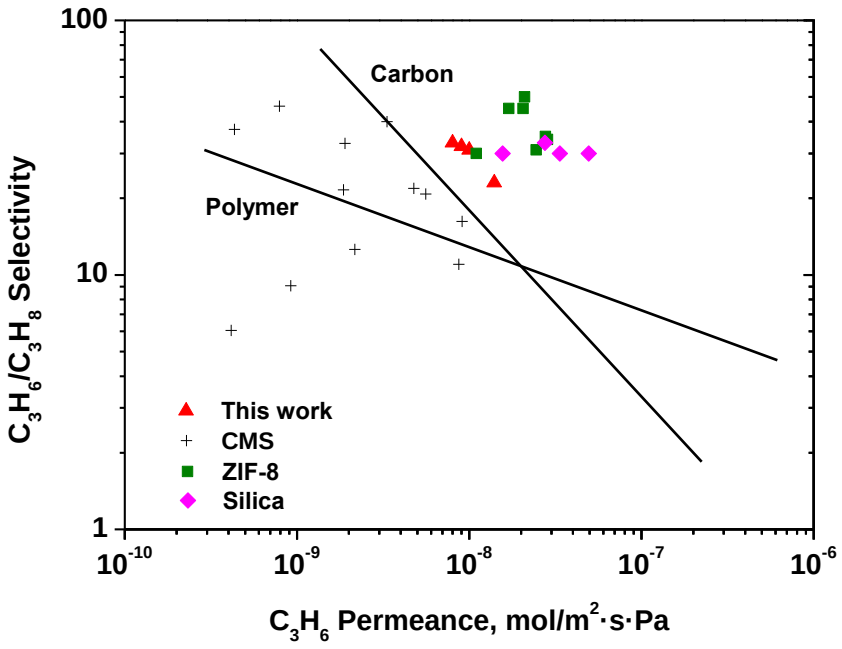

Figure 4.12 C_3H_6/C_3H_8 mixture selectivity as a function of C_3H_6 permeance (at <50 ℃) for polymer, CMS, ZIF-8 and silica membranes. The solid line shows the upper-bound trade-off curve for polymer membranes and CMS membranes reported in the literature to date

4.4 Conclusions

Ultra-thin, high quality CMS membranes of various thickness (300-2100 nm) were synthesized on mesoporous γ-alumina support by pyrolysis of polymer films of different thicknesses. The gas permeation properties and micropore structure of the CMS membranes depend on membrane thickness. With the membrane thickness decreasing from 2.1 μm to 520 nm, the gas permeance of the studied gases He, N_2, C_3H_6 and C_3H_8 increase and He,/N_2, C_3H_6/C_3H_8 selectivities decrease with decreasing membrane

thickness. However, further reduction in thickness to 300 nm causes an increase in He/N_2 perm-selectivity, but a decrease in C_3H_6/C_3H_8 mixture selectivity. These findings suggest that the 300 nm CMS membrane contains micropores in smaller size and lower quantity as compared to the other membranes with larger thickness. The change in micropore structure might be due to the more close packing of polymer chains, higher chain segmental mobility, and the faster release of volatile products during pyrolysis for the thinner polymer films. The CMS membranes prepared in our work show excellent C_3H_6/C_3H_8 mixture separation performances, especially a high C_3H_6 permeance offered by the ultra-thin membrane layer.

CHAPTER 5

PROPYLENE/PROPANE MIXTURE TRANSPORT AND SEPARATION PROPERTIES, AND STABILITY OF CARBON MOLECULAR SIEVE MEMBRANE

5.1 Introduction

The results in the previous chapters have demonstrated the promise of carbon molecular sieve membrane (CMS) for propylene/propane separation which is of great commercial importance. Most of efforts reported in literature are mainly focused on the optimization of membrane synthesis in producing membrane with improved separation performances. CMS membranes fabricated by our group and several other groups have shown performance above the upper-bound trade off curve of polymer membranes.

Only A few work has studied the permeation and separation properties of propylene/propane mixture through CMS membrane. Gas transport through microporous carbon materials can be described using a sorption-diffusion mechanism. Adsorption studies have shown similar adsorption capacity of propylene and propane on carbon molecular sieve materials (Jarvelin & Fair, 1993). Despite an adsorption selectivity around 1.1, the propylene/propane diffusion selectivity is as high as 90 for the 6FDA/BPDA-DAM derived CMS membrane, as reported by Koros's group (2005). Hayashi et al. (1996) studied the temperature dependence of the single-component permeance of propylene and propane through CMS membrane derived from BPDA-ppODA polyimide precursor. The obtained activation energy values are positive and comparable to those for the other non-hydrocarbon gases like oxygen and nitrogen, suggesting an activated diffusion rather than a surface diffusion dominated mechanism for the permeation of propylene and propane. These reported work has showed that the

separation mechanism of propylene/propane by CMS membrane is based on the strong molecular sieving effect of the membrane.

Although thermally and chemically resistant, CMS membranes appear to suffer some instability issues in the separation performance as described in Chapter 1. In summary, there are three possible causes for the aging of CMS membrane: (1) physical adsorption of water and other species with low diffusivity in the pores, blocking the permeation of the targeted gas molecules through membrane; (2) oxygen chemisorption onto the active sites in micropores, forming oxygen containing groups on pore edges and reducing the effective pore size; (3) recently reported physical aging of CMS membrane (Xu et al. 2014), which is analogously to the physical aging of polymer membranes (Cui et al., 2011, Rowe et al., 2010, Kim, et al., 2006). The adsorption of water is reversible and can be avoided through coating a hydrophobic polymer layer on the membrane surface. Oxygen chemisorption is irreversible and can only be regenerated by heat treatments at high temperature in a reducing atmosphere. Therefore, it was suggested that the use of CMS membrane for the separation of oxygen-free gas mixtures, like the olefin/paraffin separation is a more reliable option. The physical aging appears to be more obvious for those CMS membranes derived from polymer precursors with large free volume.

Propylene/propane separation is often operated on the output of industrial steam crackers or on petrochemical purge streams, both of which are typically at elevated pressures (100-150 psig) with varied propylene/propane composition. The separation properties of CMS membrane under these critical industrial operating conditions have not been reported in literature. Despite some studies on the stability of CMS membrane, the

long term stability of CMS membrane under propylene/propane on-stream separation conditions is still not clear. The objective of this chapter is to systematically study the effects of several important factors including feed pressure, feed composition and operation temperature on the propylene/propane mixture permeation and separation properties of CMS membrane. Furthermore, the on-stream stability behavior, aging mechanism and accelerated pre-aging treatments of CMS membrane were also explored. The CMS membranes used for these studies were prepared on alpha-alumina supports modified with a mesoporous gamma-alumina layer.

5.2 Experimental

5.2.1 Membrane synthesis and characterization

The membrane synthesis procedures followed those described in Chapter 3. Alpha-alumina supports were first prepared by pressing/sintering technique, followed with the coating of gamma-alumina layer by a sol-gel method. The polymer film was coated onto the mesoporous gamma-alumina layer, and pyrolyzed in an ultra high purity argon gas atmosphere to form the final CMS membrane. Membranes with two different thicknesses were prepared. A relatively thicker membrane was prepared using a 2wt% polymer solution for the permeation and separation study, because this condition produced CMS membrane with the fewest defects and highest selectivity. Thinner membranes were synthesized using a 1wt% polymer solution, and used for stability study. Because the aging resulted in a significant reduction in gas permeance, a starting membrane with higher permeance provided by the thinner thickness gave less error in the permeance measurements of aged membranes.

5.2.2 Gas permeation and separation measurements

The mixed-gas performance of the CMS membranes for propylene/propane separation was measured using a cross-flow setup shown in Chapter 3, and the effects of feed pressure, feed composition and temperature on the separation performance were studied in details. During the tests, the feed was a propylene/propane mixture at a total flow rate of 50 mL/min, and the permeate side was swept by N_2 at a flow rate of 50 mL/min. On the feed side, the gas flow rates for propylene and propane were controlled by two mass flow controllers, so as to control the feed composition. The total pressure was controlled by a needle valve on the retentate line. The gas compositions on both feed side and permeate side were measured by gas chromatography (GC) equipped with a flame ionization detector (FID) and a silica gel column. The temperature of the membrane cell was controlled by a temperature programmed furnace. For the study on the effect of feed pressure, the total feed pressure was changed from 32 to 100 psi at a feed composition fixed at 50/50 and room temperature. The feed composition was varied by the flow meter, with a total feed pressure controlled at 30 psi to study the effect of feed composition on separation properties. A temperature range from room temperature to 100 ℃ was used to study the performance at different temperatures.

5.2.3 Stability test

Fresh CMS membrane was used for each stability test. One membrane was used for on-stream propylene/propane separation performance stability study. The feed is a 50/50 propylene/propane mixture with a total feed pressure of ~30 psi. Both permeances and selectivity were measured during the studied time period. The stability of 50/50 He/N_2 system was also studied using another fresh membrane. Same setup was used

except that argon gas was used as the sweeping gas for the He/N_2 system. Two additional membranes were used to study the effect of oxygen concentration on the aging: (1) The first membrane was subjected to industrial grade nitrogen with 500 ppm oxygen, and the nitrogen gas permeance was continuously measured; (2) The second membrane was exposed to dry air for a certain amount of time, during which the nitrogen gas permeance was monitored over the aging time.

5.2.4 Regeneration and pre-aging of membrane

The pre-aging was conducted at four different conditions: (1) Dry air conditions at room temperature; (2) Dry air conditions at 50 ℃; (2) Propylene/propane mixture stream at 100 ℃ and 120 ℃.

5.3 Results and discussion

5.3.1 Effect of operation parameters on performances

Figure 5.1 shows the effect of feed pressure on C_3H_6 and C_3H_8 permeances and the C_3H_6/C_3H_8 mixture selectivity. Both the permeances and selectivity decreased with increasing feed pressure. The adsorption of propylene and propane on CMS membrane is likely to follow the Langmuir isotherm. With the increase of feed pressure, the solubility coefficients for both gases decrease, resulting in a decrease in gas permeance. The propylene probably experienced a larger decrease in the solubility than that for propane, causing a decreased selectivity with the increase of the feed pressure. It should be noted that polymer membranes usually suffer severe plasticization problem under exposure to high pressure hydrocarbon gas. In contrast, due to the high rigidity of the inorganic pore structure, our CMS membrane exhibited excellent performance even at a feed pressure up to 100 psi.

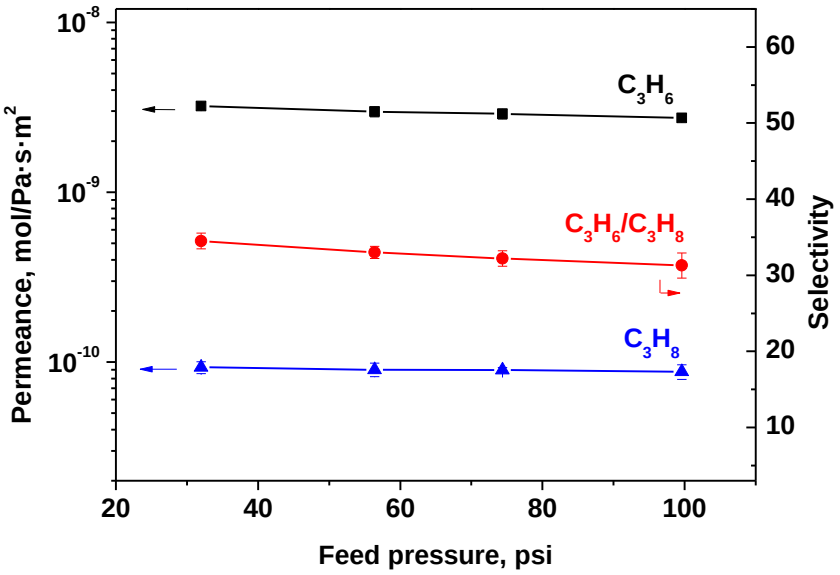

Figure 5.1 Effect of feed pressure on C_3H_6/C_3H_8 separation performance for a CMS membrane at 25 ℃ with 50:50 C_3H_6/C_3H_8 feed

Figure 5.2 shows the effect of feed composition on the separation performances. At a given total feed pressure, the change in feed composition essentially causes the change of partial pressure for each gas on the feed side, as well as the transmembrane pressure. As shown, with the increase of C_3H_6 fraction on the feed side, the C_3H_6 permeance decreased due to the reduced solubility coefficient with the increase of C_3H_6 partial pressure. At the same time, the C_3H_8 permeance increased because of the increase of solubility coefficient brought by the declined C_3H_8 partial pressure on the feed side. Consequently, the C_3H_6/C_3H_8 selectivity decreased with the increase of C_3H_6 fraction on the feed side. Overall, the membrane exhibited excellent performances under the wide feed composition range studied in this work.

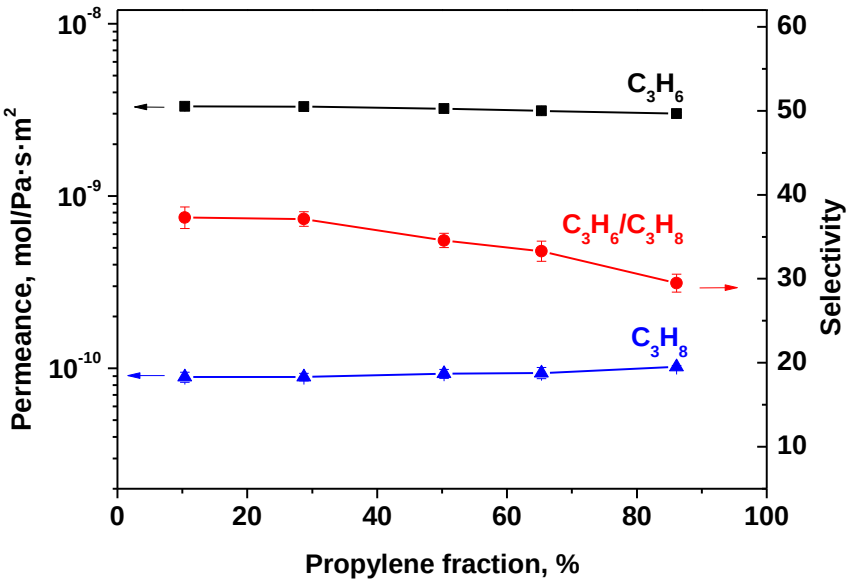

Figure 5.2. Effect of propylene fraction on the feed side on C_3H_6/C_3H_8 separation performance for a CMS membrane at 25 ℃, and a feed pressure of 30 psi

Figure 5.3 shows the effect of operation temperature on the permeances and selectivity. It can be seen that the separation of C_3H_6/C_3H_8 showed a strong dependence on the operation temperature. With the increase of temperature, both C_3H_6 and C_3H_8 permeances increased and the selectivity decreased. The C_3H_6 permeance at 100 ℃ is about 4 times the permeance at 25 ℃. The activation energies for the permeation of C_3H_6 and C_3H_8 were calculated to be 15.3 and 25.4 kJ/mol, respectively. The temperature dependence and the activation energies suggest a diffusion controlled mechanism for the transport of C_3H_6 and C_3H_8 through the CMS membrane prepared in our work.

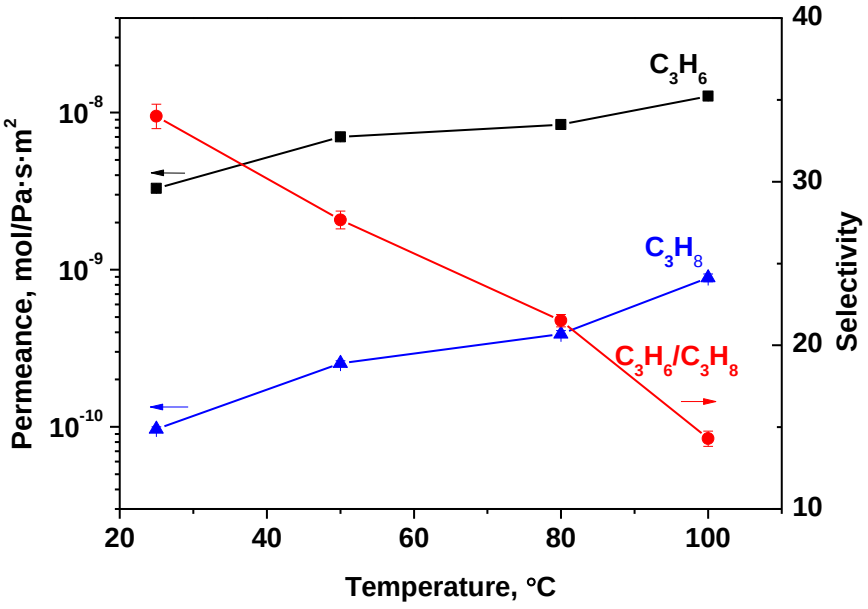

Figure 5.3. Effect of temperature on C_3H_6/C_3H_8 separation performance for a CMS membrane at with 50:50 C_3H_6/C_3H_8 feed and a feed pressure of 30psi

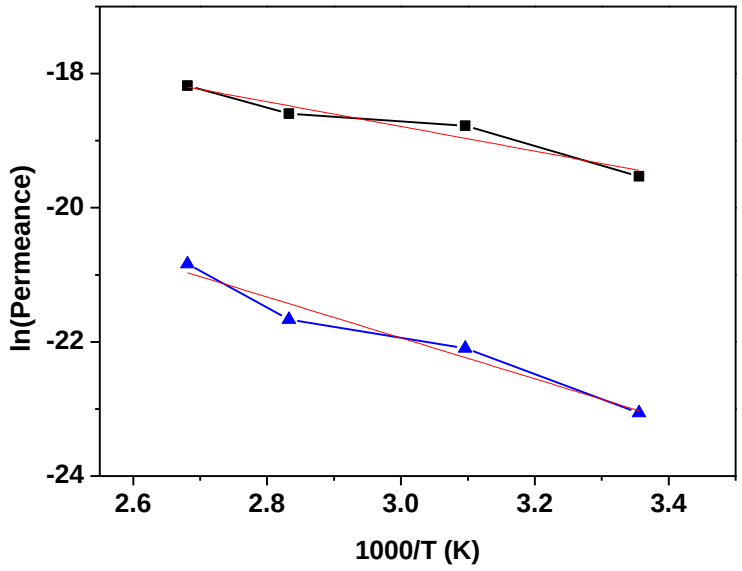

Figure 5.4. Arrhenius plot of the permeances through CMS membrane

5.3.2 On-stream stability of CMS membrane

Figure 5.5 shows the long term stability of separation performances for a 50/50 C_3H_6/C_3H_8 feed at room temperature. The membrane was not stable under the long term on-stream separation test, and experienced an aging behavior in the separation performances, with both propylene and propane permeances decreasing with testing time. The decline in the permeance for propane is faster than that for propylene gas, resulting in a slow increase in the mixture selectivity during aging. It can be seen that the aging became smaller in rate with the aging time, but did not reach stabilized even after 13 days continuous test.

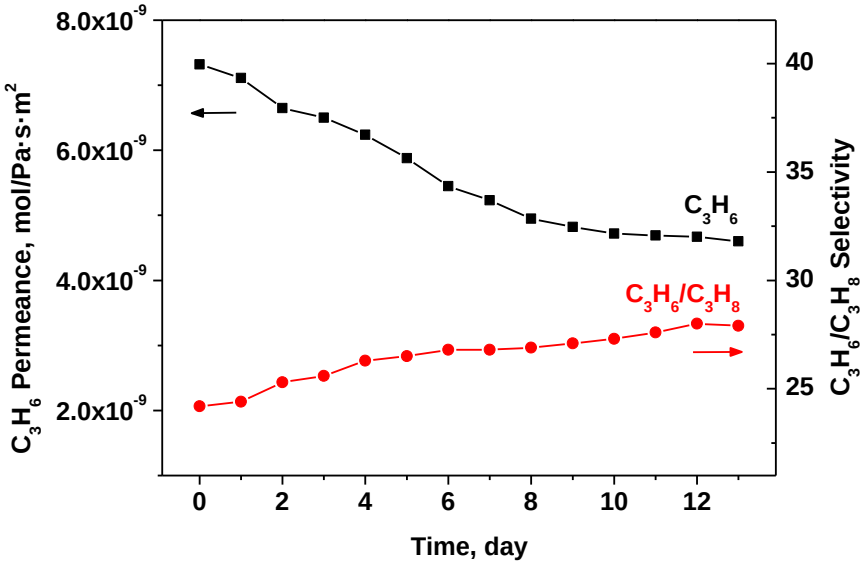

Figure 5.5. On-stream C_3H_6/C_3H_8 separation test of a freshly prepared CMS membrane

To further confirm the aging of our membrane, the stability of He/N_2 mixture separation through another freshly prepared CMS membrane was tested and the results were shown in Figure 5.6. It can be seen that similar aging treads in the permeance and selectivity were observed for the He/N_2 system.

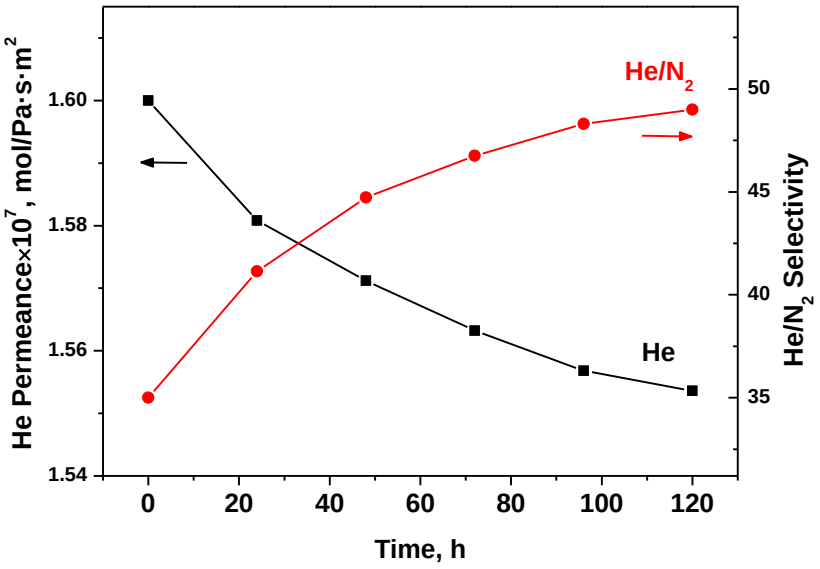

Figure 5.6. On-stream He/N_2 separation test of a freshly prepared CMS membrane

There are three possible reasons for the aging of the CMS membrane: (1) adsorption of water vapor; (2) oxygen chemisorption; and (3) physical aging. The first reason is the pore blockage caused by physical adsorption of water vapor or other larger hydrocarbon species with extremely low diffusivity in the membrane pores. As reported in literature, the adsorption of water only takes place when the relative humidity reaches a certain value. This is unlikely to happen in our measurement based on the fact that the propylene/propane mixture only contains water and other impurities in ppm level. On the other hand, the adsorption of water usually caused a reduction in both permeance and selectivity, as opposed to the increase in selectivity observed in this work. Furthermore, the adsorption of water and other hydrocarbon species is reversible. The permeance and selectivity of the aged membrane were not recovered after a heat treatment in ultra high purity argon or vacuum conditions at 120 ℃ for 24hrs. These results have excluded the

possibility of any physical adsorption causing the aging in the on-stream propylene/propane or He/N_2 separation process.

Chemisorption of oxygen is another reason for the aging of CMS membranes. The formation of oxygen containing groups at the windows of micropores narrowed the effective pore size of the membrane, causing a reduction in permeances but an increase in the selectivity. These oxygen containing groups can only be removed by heat treatment at high temperature in a reducing atmosphere. These phenomena are consistent with the aging behavior found for our CMS membrane. The third reason for the aging of CMS membrane is the physical aging recently proposed by Koros. Analogous to the unrelaxed free volume in glassy polymers, the micropores in CMS membrane tend to shrink over time to reach a thermodynamically more stable state. As a result, their CMS membrane exhibited a decreasing permeances and an increasing selectivity over testing time, similar to the aging behaviors found in our work. Besides, the 6FDA-based polymer precursor used in our work also possesses a relatively large free volume. Therefore, we believe that besides the oxygen chemisorption, the physical aging of CMS membrane is another possible cause for the aging of our membrane. However, it is still difficult to tell which one or if both of them are contributing to the aging of our membrane.

To confirm the presence of oxygen chemisorption, two fresh membranes were subjected to atmospheres with different concentrations: (1) industrial grade N_2 gas with O_2 concentration of ~500 ppm; (2) dry air with 21% O_2. Figure 5.7 shows the normalized nitrogen permeances as a function of aging time for the two membranes. The membrane subjected to the 21% oxygen atmosphere experienced a much faster aging than the membrane subjected to 500 ppm oxygen. This strong oxygen concentration dependence

was usually found for the chemisorption of oxygen onto active carbons, suggesting that our CMS membrane material is extremely reactive to oxygen. Because the physical aging of CMS membrane is independent of the oxygen concentration, we can confirm the presence of oxygen chemisorption in affecting the aging of our membrane. Although the oxygen in the gas mixture is in ppm level, the oxygen chemisorption probably still takes place very slowly to narrow the effective pore size of the membrane.

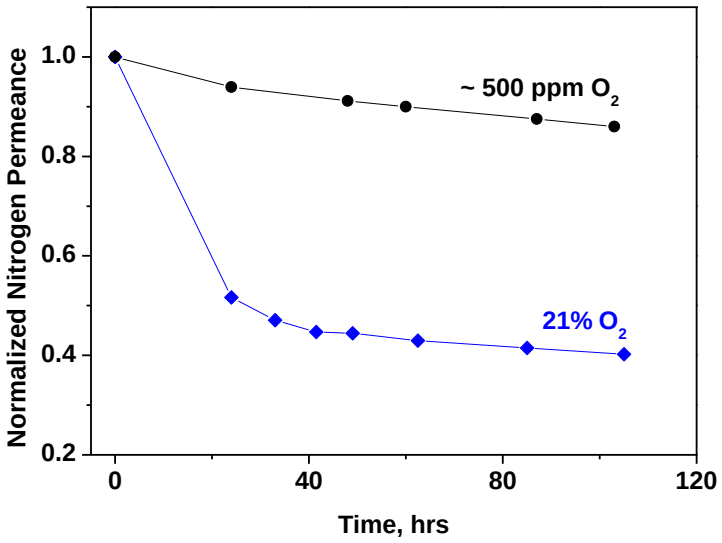

Figure 5.7 Effect of oxygen concentration on the stability

The oxygen containing groups formed from the oxygen chemisorption can be removed by high temperature treatment in reducing atmosphere. Figure 5.8 shows the normalized nitrogen permeance history of the membrane aged in dry air condition for an extended period and the permeance after regeneration. After aging in 21% O_2 for 50 days, the membrane eventually becomes stabilized with a final permeance only ~10% of the fresh value. This aged membrane was regenerated through a heat treatment in 5% H_2 atmosphere at 300 ℃ for 24 h. Nitrogen permeance was partly recovered to 83% of the

fresh permeance by the heat treatment under reducing environment. The 17% difference from the original permeance could be due to the pore structure change caused by the removal of oxygen groups which take one carbon atom and leave the membrane as CO or CO_2. This process is accompanied with the loss of carbon atoms and consequently the formation of additional defects in the aromatic or graphene sheet. It is not clear how this will affect the pore structure of the membrane, but we believe these defects will probably enlarge the pore size and increase the permeance. Therefore, the 17% difference in the permeance is more likely due to the permanent structure change caused by the physical aging of the CMS membrane.

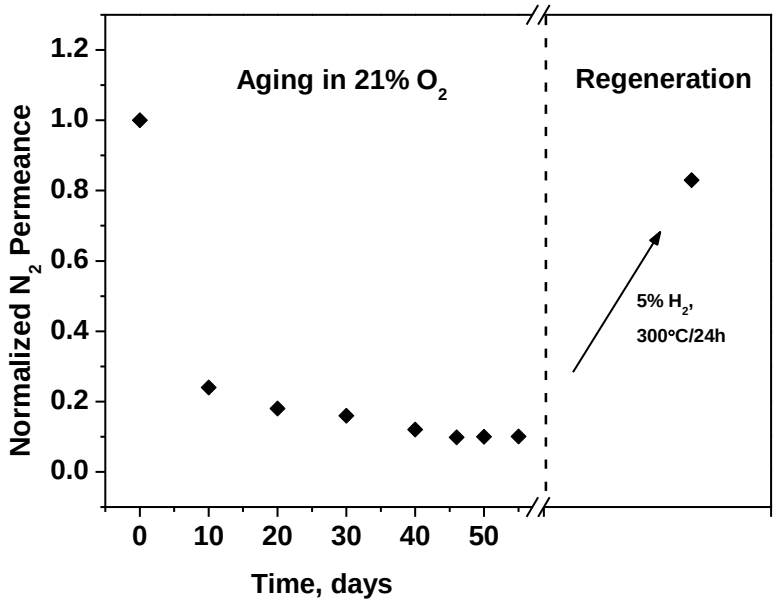

Figure 5.8 N_2 permeances of a CMS membrane at fresh state, different aging time in dry air, and after regeneration

Therefore, we can conclude that both oxygen chemisorption and physical aging are playing a role in the aging of our membrane. The chemical adsorption of oxygen onto the active site of carbon inside the pore channels of CMS membrane, reducing the

porosity of micropores. One the other hand, the formation of species on the pore constrictions narrows the pore size. The physical aging causes the disordered graphene sheets to be more closely packed. It can be seen that both oxygen chemisorption and physical aging lead to a reduction in the effective pore size and porosity of the CMS membrane, increasing the gas transport resistance. This effect is more pronounced for the larger molecules with kinetic diameter close to the critical pore size of membrane. As a result, the selectivity for gas mixtures, like He/N_2, and propylene/propane studied in this work increased over the aging time.

5.3.3 Pre-aging of CMS membrane

Figure 5.9 shows the on-stream stability of the membrane that has aged in dry air at room temperature for 50 days. A stable propylene/propane separation performance was observed for at least three days for this aged membrane, indicating that a final stabilized state can be achieved for CMS membrane after a long time aging process. This result is consistent with the theories behind the aging of the membrane. The aging caused by oxygen chemisorption will stop after all the active sites on the CMS membrane have reacted with oxygen. The physical aging, as demonstrated in Koros's work for their 6FDA/BPDA-DAM derived CMS membrane, eventually reached a stable state after several months' aging period. The CMS membrane after aging could still be used in industry if it exhibits reasonably good stabilized separation performance. However, two problems remain to be solved for industrial application based on the results shown in Figure 5.9: (1) The 50 days pre-aging is too long; (2) The propylene/propane separation performance of this aged membrane is not attractive.

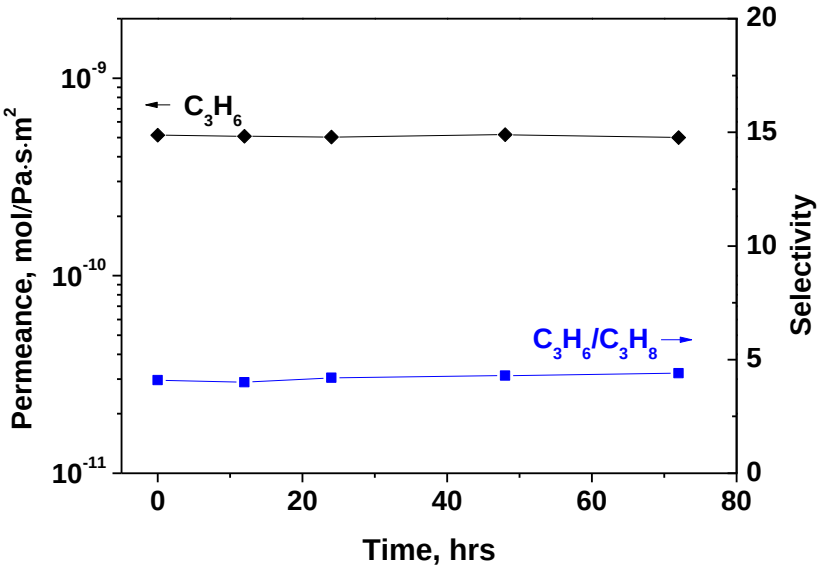

Figure 5.9 On-stream propylene/propane separation performance of one membrane after aging in dry air at room temperature for 50 days

The rate of oxygen chemisorption onto activated carbon is dependent on not only the oxygen concentration, but also the temperature. Higher oxygen concentration and higher temperature are expected to accelerate the aging of CMS membrane caused by oxygen chemisorption. On the other hand, although it has not been reported, we believe that higher temperature will also accelerate the physical aging of CMS membrane through facilitating the structure rearrangement of the imperfectly packed graphene sheets in membrane. Therefore, in order to accelerate the aging process, we proposed to age the membrane under a high oxygen concentration atmosphere at high temperature.

One fresh CMS membrane was aged in air at 50 ℃ for 24 h. Afterwards, the propylene permeance dropped from 9.9×10^{-9} to 7.15×10^{-10} mol/(m^2·s·Pa) (only 7% of the fresh permeance). The reduction in the permeance is much larger than that of the membrane aged in the on-stream propylene/propane gas mixture at room temperature

(shown in Figure 5.5), suggesting a significantly accelerated aging in air at 50 ℃. However, this propylene permeance is too low for any separation application. It was also found that despite the large reduction in the gas permeance, this membrane continued to age with a lower rate during the following on-stream propylene/propane separation test. The reason might be the gasification reaction of those oxygen containing groups, in which new active sites were created and continued to react with oxygen upon exposure to any gas mixtures containing trace oxygen.

We then proposed to pre-age the membrane at a higher temperature under low oxygen partial pressure. The higher temperature will accelerate the chemisorption of oxygen onto the carbon, and the low oxygen partial pressure will avoid the creation of new active sites. And the best condition for this will be the propylene/propane mixture stream. One membrane was heat treated under propylene/propane stream at 100 ℃ for 6 days, and 120 ℃ for one day. Thereafter, as shown in Figure 5.10, the membrane showed stable propylene/propane separation performance in the following several days' test at 120 ℃. It should be noted that, we are not concluding that this membrane will stay stable for the future test, because 4 days might be not enough to justify the stability. However, these results indicated that, heat treatment of the membrane under a low oxygen concentration condition seems to be a good approach to accelerate the aging with a minimum sacrifice in the separation performance before the long-term propylene/propane separation operation.

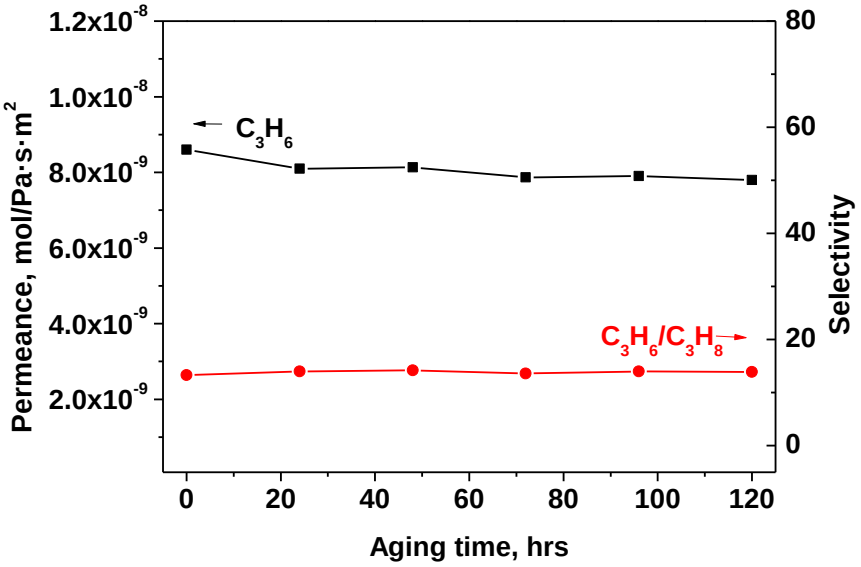

Figure 5.10. On-stream propylene/propane separation performance at 120 ℃ of one membrane which was pre-aged at 100 ℃ for 6 days in propylene/propane stream before being heated up to 120 ℃

Based on these results, a shorter pre-aging time should be expected if an even higher heat treatment temperature, like 200 ℃ or 300 ℃ was used. It is also plausible to believe that high temperature pre-treatment under other gas phases with low oxygen concentration should provide similar pre-aging effect. This pre-aging approach might be a useful option for industrial application. More work should be done in this area to search an effective and reliable accelerated pre-aging process.

5.4 Conclusion

CMS membranes prepared in our work demonstrated excellent separation performance toward propylene/propane mixture separation over a wide range of feed pressure, feed composition and operation temperature. Trends of the changes of gas permeance and selectivity at different feed pressure and composition can be explained by

Langmuir adsorption isotherm. No plasticization effect was observed for the CMS membrane at a feed pressure up to 100 psi. The permeation and separation of propylene and propane through CMS membrane is mainly controlled by diffusion instead of adsorption. Activation energy for the permeance of propylene and propane is 15.3 and 25.4 kJ/mol, respectively. CMS membrane experienced an aging behavior featured a decline in permeance, and an increase in selectivity under on-stream propylene/propane and He/N_2 separation process. This is due to the reduction in both effective pore size and porosity as a consequence of oxygen chemisorption onto carbon active sites in membrane and the physical aging of the CMS membrane structure.

CHAPTER 6

SUMMARY AND RECOMMENDATIONS

6.1 Summary

This dissertation presented the synthesis and characterization of microporous inorganic membranes for propylene/propane separation. Two membrane systems: MFI-type zeolite membrane and carbon molecular sieve (CMS) membrane were systematically studied. MFI zeolite membranes were synthesized on alpha-alumina supports by secondary growth method under different conditions. Besides the conventional characterization including XRD and SEM, a novel technique PAS was used to characterize the pore structure of the zeolite membranes of different microstructures. CMS membranes with different thicknesses were prepared on mesoporous gamma-alumina support by a coating/pyrolysis method. The composite membrane exhibited excellent propylene/propane mixture separation performance, with a mixture selectivity of ~30. High propylene permeance was realized through reducing the membrane thickness, which was found to have a significant effect on the pore structure and gas transport properties of CMS membrane. Systematic studies were also conducted on the effects of operation parameters on separation properties, and the on-stream stability of CMS membrane.

The first objective is to address the challenge in characterizing the hierarchical microporous structure of zeolite membranes, and explore the propylene/propane separation properties of high quality zeolite membrane. In Chapter 2, for the first time, two positron annihilation spectroscopy (PAS) including positron annihilation lifetime spectroscopy (PALS) and Doppler broadening energy spectroscopy (DBES) were used to

expose the zeolite membranes with different microstructure prepared at different conditions. They were proved to be powerful tools in non-destructively revealing the intracrystalline and the intercrystalline micropores of zeolite membranes. PAS analysis reveals a bimodal pore structure consisting of intracrystalline zeolitic micropores of around 0.6 nm in diameter and irregular intercrystalline micropores of 1.4 to 1.8 nm in size for the four MFI zeolite membranes studied. Distributions of the micropores along the membrane thickness direction can be inferred from Doppler broadening energy spectroscopy results, illustrating development of intercrystalline gaps during the growth of the zeolite layer. The amount and size of the intercrystalline micropores of the zeolite membranes vary with the synthesis method, and are the smallest for the randomly oriented MFI zeolite membrane synthesized without template and largest for the *c*-oriented MFI zeolite membrane synthesized with template. The *c*-oriented membrane has an asymmetric distribution of intercrystalline pores along the film growth direction as compared to the uniform distribution of the bimodal structure for the other three membranes. The pore structure data obtained by PAS are consistent with the xylene isomer separation performance of these membranes.

The propylene/propane separation performance of MFI zeolite membranes were explored in Chapter 2 as well. Membranes synthesized by template free method was chosen as the membrane for propylene/propane mixture separation test, because this method produces membranes with the fewest non-selective intercrystalline pores. The membrane exhibited a high propylene permeance but a low mixture selectivity. The intracrystalline pores of zeolite membrane, which are larger than both the molecular size of propylene and propane, provides a low transport resistance and high permeances for

both gases. The mixture selectivity, which is still larger than the Knudsen selectivity, is due to the preferential adsorption to propylene molecules of the cations in zeolite membrane framework.

Chapter 3 addressed the second object of this dissertation through developing a novel CMS/ceramic composite membrane with improved membrane quality. The ceramic support used is a macroporous α-alumina support coated with a sol-gel derived mesoporous γ-alumina layer. The mesoporous γ-alumina layer is effective in improving the surface quality of α-alumina support, allowing the formation of a final thinner, high quality CMS membrane layer on top. SEM, FTIR and molecular probing method were used to characterize the morphology and gas transport properties of the membrane. Based on the strong molecular sieving capability, the membrane showed excellent performances to propylene/propane mixture separation, with the selectivity above 30.

The third objective of this dissertation is to conduct further studies on the CMS membrane system, including performance improvement, membrane thickness dependence of membrane structure and properties, effect of operation parameters on the performances, as well as the membrane stability. Chapter 4 focused on improving membrane performance through reducing the membrane thickness, and studying the effect of membrane thickness on the micropore structure, gas transport and C_3H_6/C_3H_8 separation properties of CMS membranes. Defect free polymer films with thickness ranging from 2.6 μm to 386 nm were first prepared on γ-alumina support with no penetration of polymer chains into the support pores. These films were pyrolyzed in an oxygen free inert gas environment to form CMS membranes with thickness in the range of 2.1 μm-300 nm. For separation of He/N_2 and C_3H_6/C_3H_8 mixtures, these membranes

showed increasing gas permeance and increasing selectivity with decreasing membrane thickness down to 500 nm. The 500 nm CMS membrane exhibits a C_3H_6/C_3H_8 mixture selectivity of ~31 and a C_3H_6 permeance up to 1.0×10^{-8} mol/(m^2·s·Pa). Further reduction in membrane thickness from 500 nm to 300 nm causes an increase in C_3H_8 permeance and He/N_2 selectivity, but a decrease in the permeance of He, N_2 and C_3H_6 and C_3H_6/C_3H_8 selectivity. These results can be explained by the thickness dependent chain mobility of the polymer film resulting in final CMS membrane of reduced pore size with different effects on transport of gas of different sizes, including possible closure of C_3H_6-accessible micropores.

Chapter 5 studied the effects of several industrially important operation parameters including the feed pressure, feed composition and temperature on membrane performances. The membrane exhibited excellent performances over the wide range studied. Change in permeance and selectivity with the feed pressure and feed composition can be explained by the Langmuir isotherm adsorption of propylene and propane to the membrane. The temperature dependence, and the calculated activation energies suggests a diffusion controlled transport of propylene and propane through the CMS membrane. The membrane is not stable under on-stream propylene/propane separation process. The cause for the aging is a combined effect of the oxygen chemisorption and physical aging of CMS membrane structure.

6.2 Recommendations

6.2.1 Introducing PAS to other microporous membrane systems

Our work has demonstrated the excellent capability of PAS techniques in non-destructively characterizing the complex microporous structure of MFI zeolite membrane.

MFI type zeolite membrane was chosen as the membrane system because of its well-established synthesis methods and industrial importance for the separation of several challenging gas mixtures. We believe these powerful PAS techniques can also be used to study other zeolite membrane, and MOF/ZIF membrane systems. Similar to the MFI type zeolite membranes, the other zeolite, MOF and ZIF membrane are all polycrystalline membranes containing both the intracrystalline pores and the irregular intercrystalline pores. The detailed hierarchical micropore structure of those membranes remains unexplored. It is important to characterize these pore information so as to study the synthesis/structure/property relations, and provide insights into developing new synthesis method to improve the membrane property. Additionally, the PAS can also be used to study the pore structure changes of membrane associated with the specific separation application.

6.2.2 Performance improvement of MFI zeolite membrane for propylene/propane separation

As found in this dissertation, although the MFI zeolite membrane exhibited a high propylene gas permeance in propylene/propane separation, the mixture selectivity is still too low for industrial application. Considering the extremely high thermal and chemical stability of the MFI zeolite membrane, it is certainly worth of trying to develop novel approaches to improve the selectivity. One recommendation is to exchange the membrane with silver ions. The as-synthesized MFI zeolite membrane contains sodium ions in the framework, which can be readily exchanged to other cations through an ion exchange process. Silver ions has been reported to be able to interact with the double bonds in propylene molecules. The adsorption or solubility of propylene gas will be improved if

the silver ions are incorporated into the membrane structure. Therefore, it is a good approach to ion exchange the zeolite membrane with the silver ions and use for propylene/propane separation.

6.2.3 Further study into the effect of membrane thickness on CMS membrane

The impacts of membrane thickness have been studied for polymer membranes and thermal rearranged membranes in literature. Our work has shown that the membrane thickness is also an important factor in influencing not only the membrane permeance, but also the pore structure and gas transport properties of CMS membranes. Further and more systemically studies are required to understand the detailed membrane structure transformation process during the pyrolysis. It is also important to find effective ways to avoid the negative impact of the thickness on the separation performance. One promising direction is to improve the rigidity of the polymer membranes before pyrolysis. Several methods can be tried, such as crosslink the polymer membrane and stabilization through oxidation.

6.2.4 Aging of CMS membrane caused by oxygen chemisorption

The stability of CMS membrane is an important issue that needs to be studied and solved before the industry application of CMS membrane. Some reported work and the work conducted in this dissertation have found that the CMS membrane is extremely sensitive to oxygen. However, some other groups reported stable separation performances of CMS membrane even under oxygen/nitrogen separation, suggesting the resistance of the membrane to oxygen adsorption. These inconsistent results reported by different groups might arise from the different precursors and pyrolysis conditions used for the preparation of CMS membranes. The relationship between those membrane preparation

factors and the oxygen chemisorption is worth further studies. On the other hand, it is important to study the kinetics of the changes in separation performances during aging under atmospheres with different oxygen concentrations and at different temperatures, and correlate it to the kinetic of oxygen chemisorption of oxygen onto the carbon materials used for membrane.

6.2.5 Physical aging of CMS membrane

The physical aging of CMS membrane is a very new phenomenon that was recently discovered by Koros's group. The work conducted in this dissertation confirmed the presence of physical aging of CMS membrane derived from polymer precursor with large free volume. More work is necessary to further understand and develop this new theory. In both Koros and our work, only gas permeation and separation results were used to study the physical aging. There is no direct observation on the structure change associated with the physical aging. Several materials characterization methods can be used to characterize the membrane before and after the physical aging to help understand the structure change. One method is the small angle XRD, which can provide information about the d-spacing between graphene sheets in the membrane structure. This information is directly related to the micropore size of the membrane. The other method, Raman spectroscopy, is able to characterize the degree of disorder packing of the graphene sheets. The Raman spectra should be able to reflect the structure change associated with the physical aging, which is believed to lead to a more orderly packing of the graphene sheets.

REFERENCES

Anderson, M., Wang, H., & Lin, Y. S. (2012). Inorganic membranes for carbon dioxide and nitrogen separation. *Reviews in Chemical Engineering, 28*, 101-121.

Baker, W. B. (2002). Future directions of membrane gas separation technology. *Industrial & Engineering Chemistry Research, 41*, 1393-1411.

Barsema, J. N., Klijnstra, S. D., Balster, J. H., Van der Vegt, N. F. A., Koops, G. H., & Wessling, M. (2004). Intermediate polymer to carbon gas separation membranes based on Matrimid PI. *Journal of Membrane Science, 238*, 93-102.

Betard, A., & Fischer, R. A. (2011). Metal-organic framework thin films: from fundamentals to applications. *Chemical Reviews, 112*, 1055-1083.

Bhuwania, N., Labreche, Y., Achoundong, C. S., Baltazar, J., Burgess, S. K., Karwa, S., Xu, L. R., Henderson, C. L., & Koros, W. J. (2014). Engineering substructure morphology of asymmetric carbon molecular sieve hollow fiber membranes. *Carbon, 76*, 417-434.

Bowen, T. C., Noble, R. D., & Falconer, J. L. (2004). Fundamentals and applications of pervaporation through zeolite membranes. *Journal of Membrane Science, 245*, 1-33.

Briceño, K., Garcia-Valls, R., & Montané, D. (2010). State of the art of carbon molecular sieves supported on tubular ceramics for gas separation applications. *Asia-Pacific Journal of Chemical Engineering, 5*, 169-178.

Burns, R. L., & Koros, W. J. (2003). Defining the challenges for C3H6/C3H8 separation using polymeric membranes. *Journal of Membrane Science, 211*, 299-309.

Cabral-Prieto, A., García-Sosa, I., López-Castañares, R., & Olea-Cardoso, O. (2013). Positronium annihilation in LTA-type zeolite. *Microporous and Mesoporous Materials, 175*, 134-140.

Caro, J., Noack, M., Kölsch, P., & Schäfer, R. (2000). Zeolite membranes-state of their development and perspective. *Microporous and Mesoporous Materials, 38*, 3-24.

Caro, J., & Noack, M. (2008). Zeolite membranes-recent developments and progress. *Microporous and Mesoporous Materials, 115*, 215-233.

Castricum, H. L., Sah, A., Kreiter, R., Blank, D. H., Vente, J. F., & Johan, E. (2008). Hydrothermally stable molecular separation membranes from organically linked silica. *Journal of Materials Chemistry, 18*, 2150-2158.

Chang, C. H., Gopalan, R., & Lin, Y. S. (1994). A comparative study on thermal and hydrothermal stability of alumina, titania and zirconia membranes. *Journal of Membrane Science*, *91*, 27-45.

Chen, H., Hung, W. S., Lo, C. H., Huang, S. H., Cheng, M. L., Liu, G., Lee, K. R., Lai, J. Y., Sun, Y. M., Hu, C. C., Suzuki, R., Ohdaira, T., Oshima, N., & Jean, Y. C. (2007). Free-volume depth profile of polymeric membranes studied by positron annihilation spectroscopy: layer structure from interfacial polymerization. *Macromolecules*, *40*, 7542-7557.

Chng, M. L., Xiao, Y., Chung, T. S., Toriida, M., & Tamai, S. (2009). Enhanced propylene/propane separation by carbonaceous membrane derived from poly (aryl ether ketone)/2, 6-bis (4-azidobenzylidene)-4-methyl-cyclohexanone interpenetrating network. *Carbon*, *47*, 1857-1866.

Choi, J., Jeong, H. K., Snyder, M. A., Stoeger, J. A., Masel, R. I., & Tsapatsis, M. (2009). Grain boundary defect elimination in a zeolite membrane by rapid thermal processing. *Science*, *325*, 590-593.

Consolati, G., Mariani, M., Millini, R., & Quasso, F. (2009). Investigation on the porosity of zeolite NU-88 by means of positron annihilation lifetime spectroscopy. *Nuclear Instruments and Methods in Physics Research Section B: Beam Interactions with Materials and Atoms*, *267*, 2550-2553.

Cooper, C. A., & Lin, Y. S. (2002). Microstructural and gas separation properties of CVD modified mesoporous γ-alumina membranes. *Journal of Membrane Science*, *195*, 35-50.

Cui, L., Qiu, W., Paul, D. R., & Koros, W. J. (2011). Physical aging of 6FDA-based polyimide membranes monitored by gas permeability. *Polymer*, *52*, 3374-3380.

Dong, J., Lin, Y. S., Hu, M. Z. C., Peascoe, R. A., & Payzant, E. A. (2000). Template-removal-associated microstructural development of porous-ceramic-supported MFI zeolite membranes. *Microporous and Mesoporous Materials*, *34*, 241-253.

Dong, X., Huang, K., Liu, S., Ren, R., Jin, W., & Lin, Y. S. (2012). Synthesis of zeolitic imidazolate framework-78 molecular-sieve membrane: defect formation and elimination. *Journal of Materials Chemistry*, *22*, 19222-19227.

Dong, X., & Lin, Y. S. (2013). Synthesis of an organophilic ZIF-71 membrane for pervaporation solvent separation. *Chemical Communications*, *49*, 1196-1198.

Duke, M. C., Pas, S. J., Hill, A. J., Lin, Y. S., & da Costa, J. C. D. (2008). Exposing the molecular sieving architecture of amorphous silica using positron annihilation spectroscopy. *Advanced Functional Materials*, *18*, 3818-3826.

Eddaoudi, M., Kim, J., Rosi, N., Vodak, D., Wachter, J., O'Keeffe, M., & Yaghi, O. M. (2002). Systematic design of pore size and functionality in isoreticular MOFs and their application in methane storage. *Science, 295*, 469-472.

Eldridge, R. B. (1993). Olefin paraffin separation technology-A review. *Industrial & Engineering Chemistry Research, 32*, 2208-2212.

Faiz, R., Li, K. (2012) Polymeric membranes for light olefin/paraffin separation. *Desalination, 287*, 82-97.

Freeman, B. D. (1999). Basis of permeability/selectivity tradeoff relations in polymeric gas separation membranes. *Macromolecules, 32*, 375-380.

Fu, Y. J., Liao, K. S., Hu, C. C., Lee, K. R., & Lai, J. Y. (2011). Development and characterization of micropores in carbon molecular sieve membrane for gas separation. *Microporous and Mesoporous Materials, 143*, 78-86.

Fuertes, A. B. (2001). Effect of air oxidation on gas separation properties of adsorption-selective carbon membranes. *Carbon, 39*, 697-706.

Gascon, J., Kapteijn, F., Zornoza, B., Sebastian, V., Casado, C., & Coronas, J. (2012). Practical approach to zeolitic membranes and coatings: state of the art, opportunities, barriers, and future perspectives. *Chemistry of Materials, 24*, 2829-2844.

Geise, G. M., Doherty, C. M., Hill, A. J., Freeman, B. D., & Paul, D. R. (2014). Free volume characterization of sulfonated styrenic pentablock copolymers using positron annihilation lifetime spectroscopy. *Journal of Membrane Science, 453*, 425-434.

Geiszler, V. C., & Koros, W. J. (1996). Effects of polyimide pyrolysis conditions on carbon molecular sieve membrane properties. *Industrial & Engineering Chemistry Research, 35*, 2999-3003.

Giannakopoulos, I. G., & Nikolakis, V. (2005). Separation of propylene/propane mixtures using faujasite-type zeolite membranes. *Industrial & Engineering Chemistry Research, 44*, 226-230.

Gidley, D. W., Peng, H. G., & Vallery, R. S. (2006). Positron annihilation as a method to characterize porous materials. *Annual Review of Materials Research, 36*, 49-79.

Gouzinis, A., & Tsapatsis, M. (1998). On the preferred orientation and microstructural manipulation of molecular sieve films prepared by secondary growth. *Chemistry of Materials, 10*, 2497-2504.

Hara, N., Yoshimune, M., Negishi, H., Haraya, K., Hara, S., & Yamaguchi, T. (2014). Diffusive separation of propylene/propane with ZIF-8 membranes. *Journal of Membrane Science*, *450*, 215-223.

Hayashi, J. I., Mizuta, H., Yamamoto, M., Kusakabe, K., Morooka, S., & Suh, S. H. (1996). Separation of ethane/ethylene and propane/propylene systems with a carbonized BPDA-pp'ODA polyimide membrane. *Industrial & Engineering Chemistry Research*, *35*, 4176-4181.

He, X., & Hagg, M. B. (2011). Optimization of carbonization process for preparation of high performance hollow fiber carbon membranes. *Industrial & Engineering Chemistry Research*, *50*, 8065-8072.

Hedlund, J., Noack, M., Kölsch, P., Creaser, D., Caro, J., & Sterte, J. (1999). ZSM-5 membranes synthesized without organic templates using a seeding technique. *Journal of Membrane Science*, *159*, 263-273.

Hong, M., Falconer, J. L., & Noble, R. D. (2005). Modification of zeolite membranes for H_2 separation by catalytic cracking of methyldiethoxysilane. *Industrial & Engineering Chemistry Research*, *44*, 4035-4041.

Hong, Z., Zhang, C., Gu, X., Jin, W., & Xu, N. (2011). A simple method for healing nonzeolitic pores of MFI membranes by hydrolysis of silanes. *Journal of Membrane Science*, *366*, 427-435.

Hu, Y., Dong, X., Nan, J., Jin, W., Ren, X., Xu, N., & Lee, Y. M. (2010). Metal-organic framework membranes fabricated via reactive seeding. *Chemical Communications*, *47*, 737-739.

Huang, A., Dou, W., & Caro, J. (2010). Steam-stable zeolitic imidazolate framework ZIF-90 membrane with hydrogen selectivity through covalent functionalization. *Journal of the American Chemical Society*, *132*, 15562-15564.

Huang, S. H., Hung, W. S., Liaw, D. J., Li, C. L., Kao, S. T., Wang, D. M., De Guzman, M., Hu, C. C., Jean, Y. C., Lee, K. R., & Lai, J. Y. (2008). Investigation of multilayer pervaporation membrane by positron annihilation spectroscopy. *Macromolecules*, *41*, 6438-6443.

Huang, Y., & Paul, D. R. (2004). Physical aging of thin glassy polymer films monitored by gas permeability. *Polymer*, *45*, 8377-8393.

Iinitch, O. M., Semin, G. L., Chertova, M. V., Zamaraev, K. I. (1992). Novel polymeric membranes for separation of hydrocarbons. *Journal of Membrane Science*, *66*, 1-8.

Ito, A., & Hwang, S. T. (1989). Permeation of propane and propylene through cellulosic polymer membranes. *Journal of Applied Polymer Science*, *38*, 483-490.

Ito, K., Nakanishi, H., & Ujihira, Y. (1999). Extension of the equation for the annihilation lifetime of ortho-positronium at a cavity larger than 1 nm in radius. The *Journal of Physical Chemistry B*, *103*, 4555-4558.

Ismail, A. F., & David, L. I. B. (2001). A review on the latest development of carbon membranes for gas separation. *Journal of Membrane Science*, *193*, 1-18.

Jarvelin, H., & Fair, J. R. (1993). Adsorptive separation of propylene-propane mixtures. *Industrial & Engineering Chemistry Research*, *32*, 2201-2207.

Jean, Y. C., Mallon, P. E., & Schrader, D. M. (2003). Principles and applications of positron and positronium chemistry. World Scientific.

Jones, C. W., & Koros, W. J. (1994). Carbon molecular sieve gas separation membranes-II. Regeneration following organic exposure. *Carbon*, *32*, 1427-1432.

Jones, C. W. & Koros, W. J. (1995). Carbon composite membranes: A solution to adverse humidity, *Industrial & Engineering Chemistry Research*, *34*, 164-167.

Jones, C. W. & Koros, W. J. (1995). Characterization of ultramicroporous carbon membranes with humidified feeds, *Industrial & Engineering Chemistry Research*, *34*, 158-163.

Kanezashi, M., Kawano, M., Yoshioka, T., & Tsuru, T. (2011). Organic-inorganic hybrid silica membranes with controlled silica network size for propylene/propane separation. *Industrial & Engineering Chemistry Research*, *51*, 944-953.

Kanezashi, M., Miyauchi, S., Nagasawa, H., Yoshioka, T., & Tsuru, T. (2014). Gas permeation properties through Al-doped organosilica membranes with controlled network size. *Journal of Membrane Science*, *466*, 246-252.

Kanezashi, M., O'Brien, J., & Lin, Y. S. (2006). Template-free synthesis of MFI-type zeolite membranes: Permeation characteristics and thermal stability improvement of membrane structure. *Journal of Membrane Science*, *286*, 213-222.

Kanezashi, M., Shazwani, W. N., Yoshioka, T., & Tsuru, T. (2012). Separation of propylene/propane binary mixtures by bis (triethoxysilyl) methane (BTESM)-derived silica membranes fabricated at different calcination temperatures. *Journal of Membrane Science*, *415*, 478-485.

Kasik, A., Dong, X., & Lin, Y. S. (2015). Synthesis and stability of zeolitic imidazolate framework-68 membranes. *Microporous and Mesoporous Materials*, *204*, 99-105.

Kim, J. H., Koros, W. J., & Paul, D. R. (2006). Effects of CO_2 exposure and physical aging on the gas permeability of thin 6FDA-based polyimide membranes: Part 2. with crosslinking. *Journal of Membrane Science*, *282*, 32-43.

Kiyono, M., Williams, P. J., & Koros, W. J. (2010). Effect of pyrolysis atmosphere on separation performance of carbon molecular sieve membranes. *Journal of Membrane Science*, *359*, 2-10.

Kiyono, M., Williams, P. J., & Koros, W. J. (2010). Generalization of effect of oxygen exposure on formation and performance of carbon molecular sieve membranes. *Carbon*, *48*, 4442-4449.

Korelskiy, D., Ye, P., Zhou, H., Mouzon, J., & Hedlund, J. (2014). An experimental study of micropore defects in MFI membranes. *Microporous and Mesoporous Materials*, *186*, 194-200.

Kwon, H. T., & Jeong, H. K. (2013). In situ synthesis of thin zeolitic-imidazolate framework ZIF-8 membranes exhibiting exceptionally high propylene/propane separation. *Journal of the American Chemical Society*, *135*, 10763-10768.

Lagorsse, S., Magalhaes, F. D., & Mendes, A. (2008). Aging study of carbon molecular sieve membranes. *Journal of Membrane Science*, *310*, 494-502.

Lai, R., & Gavalas, G. R. (2000). ZSM-5 membrane synthesis with organic-free mixtures. *Microporous and Mesoporous Materials*, *38*, 239-245.

Lai, Z., Bonilla, G., Diaz, I., Nery, J. G., Sujaoti, K., Amat, M. A., Kokkoli, E., Terasaki, O., Thompson, R. W., Tsapatsis, M. & Vlachos, D. G. (2003). Microstructural optimization of a zeolite membrane for organic vapor separation. *Science*, *300*, 456-460.

Lai, Z., Tsapatsis, M., & Nicolich, J. P. (2004). Siliceous ZSM-5 membranes by secondary growth of b-oriented seed layers. *Advanced Functional Materials*, *14*, 716-729.

Li, H., Eddaoudi, M., O'Keeffe, M., & Yaghi, O. M. (1999). Design and synthesis of an exceptionally stable and highly porous metal-organic framework. *Nature*, *402*, 276-279.

Li, J. R., Ma, Y., McCarthy, M. C., Sculley, J., Yu, J., Jeong, H. K., Balbuena, P. B., & Zhou, H. C. (2011). Carbon dioxide capture-related gas adsorption and separation in metal-organic frameworks. *Coordination Chemistry Reviews*, *255*, 1791-1823.

Li, K., Olson, D. H., Seidel, J., Emge, T. J., Gong, H., Zeng, H., & Li, J. (2009). Zeolitic imidazolate frameworks for kinetic separation of propane and propene. *Journal of the American Chemical Society*, *131*, 10368-10369.

Li, S., Sun, J., Li, Z., Peng, H., Gidley, D., Ryan, E. T., & Yan, Y. (2004). Evaluation of pore structure in pure silica zeolite MFI low-k thin films using positronium annihilation lifetime spectroscopy. *The Journal of Physical Chemistry B*, *108*, 11689-11692.

Liao, K. S., Fu, Y. J., Hu, C. C., Chen, J. T., Lin, D. W., Lee, K. R., Tung, K. L., Jean, Y. C., & Lai, J. Y. (2012). Microstructure of carbon molecular sieve membranes and their application to separation of aqueous bioethanol. *Carbon*, *50*, 4220-4227.

Lin, Y. S., & Duke, M. C. (2013). Recent progress in polycrystalline zeolite membrane research. *Current Opinion in Chemical Engineering*, *2*, 209-216.

Lin, Y. S., Kumakiri, I., Nair, B. N., & Alsyouri, H. (2002). Microporous inorganic membranes. *Separation & Purification Reviews*, *31*, 229-379.

Liu, D., Ma, X., Xi, H., & Lin, Y. S. (2014). Gas transport properties and propylene/propane separation characteristics of ZIF-8 membranes. *Journal of Membrane Science*, *451*, 85-93.

Liu, X., Li, Y., Ban, Y., Peng, Y., Jin, H., Bux, H., Xu, L. Y., Caro, J., & Yang, W. (2013). Improvement of hydrothermal stability of zeolitic imidazolate frameworks. *Chemical Communications*, *49*, 9140-9142.

Lo, C. H., Liao, K. S., Hung, W. S., Guzman, M. D., Hu, C. C., Lee, K. R., & Lai, J. Y. (2011). Investigation on positron annihilation characteristics of CO2-exposed zeolite. *Microporous and Mesoporous Materials*, *141*, 140-145.

Ma, X., Lin, B. K., Wei, X., Kniep, J., & Lin, Y. S. (2013). Gamma-alumina supported carbon molecular sieve membrane for propylene/propane separation. *Industrial & Engineering Chemistry Research*, *52*, 4297-4305.

Masuda, T., Fukumoto, N., Kitamura, M., Mukai, S. R., Hashimoto, K., Tanaka, T., & Funabiki, T. (2001). Modification of pore size of MFI-type zeolite by catalytic cracking of silane and application to preparation of H2-separating zeolite membrane. *Microporous and Mesoporous Materials*, *48*, 239-245.

McLeary, E. E., Jansen, J. C., & Kapteijn, F. (2006). Zeolite based films, membranes and membrane reactors: Progress and prospects. *Microporous and Mesoporous Materials*, *90*, 198-220.

Menendez, I., & Fuertes, A. B. (2001). Aging of carbon membranes under different environments. *Carbon, 39*, 733-740.

Merkel, T. C., Lin, H. Q., Wei, X. T., Baker, R. (2010). Power plant post-combustion carbon dioxide capture: An opportunity for membranes. *Journal of Membrane Science, 359*, 126-139.

Motelica, A., Bruinsma, O. S. L., Kreiter, R., den Exter, M., Vente, J. F. (2012) Membrane retrofit option fhayashior paraffin/olefin separation-a technoeconomic evaluation. *Industrial & Engineering Chemistry Research, 51*, 6977-6986.

Noack, M., Mabande, G. T. P., Caro, J., Georgi, G., Schwieger, W., Kölsch, P., & Avhale, A. (2005). Influence of Si/Al ratio, pre-treatment and measurement conditions on permeation properties of MFI membranes on metallic and ceramic supports. *Microporous and Mesoporous Materials, 82*, 147-157.

O'Brien-Abraham, J., Kanezashi, M., & Lin, Y. S. (2007). A comparative study on permeation and mechanical properties of random and oriented MFI-type zeolite membranes. *Microporous and Mesoporous Materials, 105*, 140-148.

Ockwig, N. W., & Nenoff, T. M. (2007). Membranes for hydrogen separation. *Chemical Reviews, 107*, 4078-4110.

Okamoto, K. I., Kawamura, S., Yoshino, M., Kita, H., Hirayama, Y., Tanihara, N., & Kusuki, Y. (1999). Olefin/paraffin separation through carbonized membranes derived from an asymmetric polyimide hollow fiber membrane. *Industrial & Engineering Chemistry Research, 38*, 4424-4432.

Pan, M., & Lin, Y. S. (2001). Template-free secondary growth synthesis of MFI type zeolite membranes. *Microporous and Mesoporous Materials, 43*, 319-327.

Pan, Y., Li, T., Lestari, G., & Lai, Z. (2012). Effective separation of propylene/propane binary mixtures by ZIF-8 membranes. *Journal of Membrane Science, 390*, 93-98.

Park, K. S., Ni, Z., Côté, A. P., Choi, J. Y., Huang, R., Uribe-Romo, F. J., Chae, H. K., O'Keeffe, M., & Yaghi, O. M. (2006). Exceptional chemical and thermal stability of zeolitic imidazolate frameworks. *Proceedings of the National Academy of Sciences, 103*, 10186-10191.

Peng, Y., Li, Y., Ban, Y., Jin, H., Jiao, W., Liu, X., & Yang, W. (2014). Metal-organic framework nanosheets as building blocks for molecular sieving membranes. *Science, 346*, 1356-1359.

Pham, T. C. T., Kim, H. S., & Yoon, K. B. (2011). Growth of uniformly oriented silica MFI and BEA zeolite films on substrates. *Science, 334*, 1533-1538.

Qiu, S., Xue, M., & Zhu, G. (2014). Metal-organic framework membranes: from synthesis to separation application. *Chemical Society Reviews, 43*, 6116-6140.

Robeson, L. M. (2008). The upper bound revisited. *Journal of Membrane Science*, *320*, 390-400.

Rowe, B. W., Freeman, B. D., & Paul, D. R. (2009). Physical aging of ultrathin glassy polymer films tracked by gas permeability. *Polymer*, *50*, 5565-5575.

Rowe, B. W., Freeman, B. D., & Paul, D. R. (2010). Influence of previous history on physical aging in thin glassy polymer films as gas separation membranes. *Polymer*, *51*, 3784-3792.

Salleh, W. N. W., Ismail, A. F., Matsuura, T., & Abdullah, M. S. (2011). Precursor selection and process conditions in the preparation of carbon membrane for gas separation: A review. *Separation & Purification Reviews*, *40*, 261-311.

Sano, T., Hasegawa, M., Kawakami, Y., Kiyozumi, Y., Yanagishita, H., Kitamoto, D., & Mizukami, F. (1994). Potentials of silicalite membranes for the separation of alcohol/water mixtures. *Studies in Surface Science and Catalysis*, *84*, 1175-1182.

Saufi, S. M., & Ismail, A. F. (2004). Fabrication of carbon membranes for gas separation-a review. *Carbon*, *42*, 241-259.

Schultz, P. J., & Lynn, K. G. (1988). Interaction of positron beams with surfaces, thin films, and interfaces. *Reviews of Modern Physics*, *60*, 701.

Shao, L., Chung, T. S., & Pramoda, K. P. (2005). The evolution of physicochemical and transport properties of 6FDA-durene toward carbon membranes; from polymer, intermediate to carbon. *Microporous and Mesoporous Materials*, *84*, 59-68.

Shiflett, M. B., & Foley, H. C. (2000). On the preparation of supported nanoporous carbon membranes. *Journal of Membrane Science*, *179*, 275-282.

Sridhar, S., & Khan, A. A. (1999). Simulation studies for the separation of propylene and propane by ethylcellulose membrane. *Journal of Membrane Science*, *159*, 209-219.

Steel, K. M., & Koros, W. J. (2005). An investigation of the effects of pyrolysis parameters on gas separation properties of carbon materials. *Carbon*, *43*, 1843-1856.

Suda, H., & Haraya, K. (1997). Alkene/alkane permselectivities of a carbon molecular sieve membrane. *Chemical Communications*, *1*, 93-94.

Tanaka, K., Taguchi, A., Hao, J., Kita, H., & Okamoto, K. (1996). Permeation and separation properties of polyimide membranes to olefins and paraffins. *Journal of Membrane Science*, *121*, 197-207.

Tang, Z., Dong, J., & Nenoff, T. M. (2009). Internal surface modification of MFI-type zeolite membranes for high selectivity and high flux for hydrogen. *Langmuir*, *25*, 4848-4852.

Tao, S. J. (1972). Positronium annihilation in molecular substances. *The Journal of Chemical Physics*, *56*, 5499-5510.

Tavolaro, A., & Drioli, E. (1999). Zeolite membranes. *Advanced Materials*, *11*, 975-996.

Tin, P. S., Chung, T. S., & Hill, A. J. (2004). Advanced fabrication of carbon molecular sieve membranes by nonsolvent pretreatment of precursor polymers. *Industrial & Engineering Chemistry Research*, *43*, 6476-6483.

Tiscornia, I., Irusta, S., Téllez, C., Coronas, J., & Santamaría, J. (2008). Separation of propylene/propane mixtures by titanosilicate ETS-10 membranes prepared in one-step seeded hydrothermal synthesis. *Journal of Membrane Science*, *311*, 326-335.

Tseng, H. H., Shih, K., Shiu, P. T., & Wey, M. Y. (2012). Influence of support structure on the permeation behavior of polyetherimide-derived carbon molecular sieve composite membrane. *Journal of Membrane Science*, *405*, 250-260.

Wang, H., Chung, T. S., & Paul, D. R. (2014). Physical aging and plasticization of thick and thin films of the thermally rearranged ortho-functional polyimide 6FDA-HAB. *Journal of Membrane Science*, *458*, 27-35.

Wang, H., Chung, T. S., & Paul, D. R. (2014). Thickness dependent thermal rearrangement of an ortho-functional polyimide. *Journal of Membrane Science*, *450*, 308-312.

Wang, H., Dong, X., & Lin, Y. S. (2014). Highly stable bilayer MFI zeolite membranes for high temperature hydrogen separation. *Journal of Membrane Science*, *450*, 425-432.

Wang, H., & Lin, Y. S. (2012). Synthesis and modification of ZSM-5/silicalite bilayer membrane with improved hydrogen separation performance. *Journal of Membrane Science*, *396*, 128-137.

Wang, H., Liu, S., Chung, T. S., Chen, H., Jean, Y. C., & Pramoda, K. P. (2011). The evolution of poly (hydroxyamide amic acid) to poly (benzoxazole) via stepwise thermal cyclization: structural changes and gas transport properties. *Polymer*, *52*, 5127-5138.

Wang, H., & Lin, Y. S. (2012). Synthesis and modification of ZSM-5/silicalite bilayer membrane with improved hydrogen separation performance. *Journal of Membrane Science*, *396*, 128-137.

Wang, W., Dong, X., Nan, J., Jin, W., Hu, Z., Chen, Y., & Jiang, J. (2012). A homochiral metal–organic framework membrane for enantioselective separation. *Chemical Communications*, *48*, 7022-7024.

Wei, W., Xia, S., Liu, G., Gu, X., Jin, W., & Xu, N. (2010). Interfacial adhesion between polymer separation layer and ceramic support for composite membrane. *AIChE Journal*, *56*, 1584-1592.

Wegner, K., Dong, J., & Lin, Y. S. (1999). Polycrystalline MFI zeolite membranes: xylene pervaporation and its implication on membrane microstructure. *Journal of Membrane Science*, *158*, 17-27.

Wey, M. Y., Tseng, H. H., & Chiang, C. K. (2014) Improving the mechanical strength and gas separation performance of CMS membranes by simply sintering treatment of α-Al2O3 support, *Journal of Membrane Science*, *453*, 603-613.

Xomeritakis, G., & Tsapatsis, M. (1999). Permeation of aromatic isomer vapors through oriented MFI-type membranes made by secondary growth. *Chemistry of Materials*, *11*, 875-878.

Xu, L., Rungta, M., Brayden, M. K., Martinez, M. V., Stears, B. A., Barbay, G. A., & Koros, W. J. (2012). Olefins-selective asymmetric carbon molecular sieve hollow fiber membranes for hybrid membrane-distillation processes for olefin/paraffin separations. *Journal of Membrane Science*, *423*, 314-323.

Xu, L., Rungta, M., Hessler, J., Qiu, W., Brayden, M., Martinez, M., Barbay, G., & Koros, W. J. (2014). Physical aging in carbon molecular sieve membranes. *Carbon*, *80*, 155-166.

Xu, L., Rungta, M., & Koros, W. J. (2011). Matrimid (R) derived carbon molecular sieve hollow fiber membranes for ethylene/ethane separation. *Journal of Membrane Science*, *380*, 138-147.

Xu, X., Yang, W., Liu, J., & Lin, L. (2000). Synthesis of a high-permeance NaA zeolite membrane by microwave heating. *Advanced Materials*, *12*, 195-198.

Yaghi, O. M., O'Keeffe, M., Ockwig, N. W., Chae, H. K., Eddaoudi, M., & Kim, J. (2003). Reticular synthesis and the design of new materials. *Nature*, *423*, 705-714.

Yamamoto, M., Kusakabe, K., Hayashi, J. I., & Morooka, S. (1997). Carbon molecular sieve membrane formed by oxidative carbonization of a copolyimide film coated on a porous support tube. *Journal of Membrane Science, 133*, 195-205.

Yang, D. L., Martinez, R., Fayyaz-Najafi, B., Wright, R. (2010). Light hydrocarbon distillation using hollow fibers as structured packings. *Journal of Membrane Science, 362*, 86-96.

Yao, J., Dong, D., Li, D., He, L., Xu, G., & Wang, H. (2011). Contra-diffusion synthesis of ZIF-8 films on a polymer substrate. *Chemical Communications, 47*, 2559-2561.

Yao, J. F., & Wang, H. T. (2014). Zeolitic imidazolate framework composite membranes and thin films: synthesis and applications. *Chemical Society Reviews, 43*, 4470-4493.

Yoo, W. C., Stoeger, J. A., Lee, P. S., Tsapatsis, M., & Stein, A. (2010). High-performance randomly oriented zeolite membranes using brittle seeds and rapid thermal processing. *Angewandte Chemie International Edition, 49*, 8699-8703.

Yuan, W., Lin, Y. S., & Yang, W. (2004). Molecular sieving MFI-type zeolite membranes for pervaporation separation of xylene isomers. *Journal of the American Chemical Society, 126*, 4776-4777.

Zhao, Z., Ma, X., Kasik, A., Li, Z., & Lin, Y. S. (2012). Gas separation properties of metal organic framework (MOF-5) membranes. *Industrial & Engineering Chemistry Research, 52, 1102-1108.*

Zhao, Z., Ma, X., Li, Z., & Lin, Y. S. (2011). Synthesis, characterization and gas transport properties of MOF-5 membranes. *Journal of Membrane Science, 382*, 82-90.

Zhu, B., Doherty, C. M., Hu, X., Hill, A. J., Zou, L., Lin, Y. S., & Duke, M. (2013). Designing hierarchical porous features of ZSM-5 zeolites via Si/Al ratio and their dynamic behavior in seawater ion complexes. *Microporous and Mesoporous Materials, 173*, 78-85.

Zhu, B., Zou, L., Doherty, C. M., Hill, A. J., Lin, Y. S., Hu, X., Wang, H. T. & Duke, M. (2010). Investigation of the effects of ion and water interaction on structure and chemistry of silicalite MFI type zeolite for its potential use as a seawater desalination membrane. *Journal of Materials Chemistry, 20*, 4675-4683.

Zhu, W., Kapteijn, F., & Moulijn, J. A. (1999). Shape selectivity in the adsorption of propane/propene on the all-silica DD3R. *Chemical Communications, 24*, 2453-2454.

APPENDIX A

BASIC DEFINITIONS

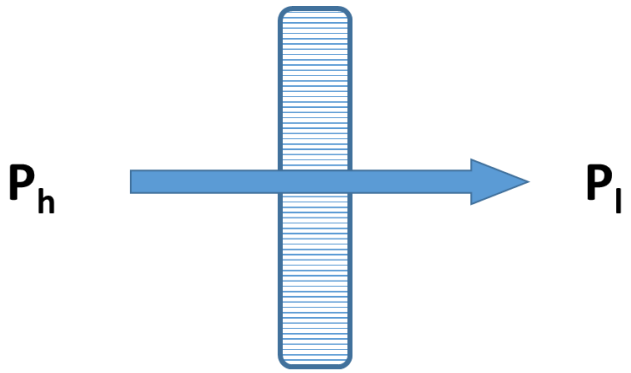

Permeation flow=Q_i (mol/s)

Membrane thickness = L

Permeation area = S

Permeation Flux: $J_i = \frac{Q_i}{S}$

Permeability: $f_i = \frac{LQ_i}{S(P_h - P_l)}$ SI unit: [mol/m·s·Pa] 1 Barrer = 3.35×10^{-15} mol/m·s·Pa

Permeance: $F_i = \frac{Q_i}{S(P_h - P_l)}$ SI unit: [mol/m^2·s·Pa] 1 GPU = 3.33×10^{-10} mol/m^2·s·Pa

Selectivity: $a_{ij} = \frac{F_i}{F_j}$

APPENDIX B

PREPARATION OF ALPHA-ALUMINA SUPPORTS

1. Mix A16 alumina powder (Almatis) and distilled water with a weight ratio of ~10:1, and place them in a mortar.
2. Carefully grind the powder and water mixtures using a pestle to destroy large agglomerates until homogeneous particles are obtained.
3. Measure 2.1 g homogeneous powders and add into the stainless steel mold (diameter = 22 mm), uniaxially press the powders under 150 MP for 2 minutes.
4. Place the pressed disk supports into a humidity oven (40 ℃, 60% RH) for 1 day.
5. After drying in the humidity oven for 1 day, sinter the disk supports using a programmable high temperature furnace following the programs shown in Table B.1.
6. After the sintering, polish one side of the support using SiC paper (#500, #800, #1200).
7. Dry the polished supports in a furnace at 200 ℃ for 12 hrs for future use.

Table B.1

Sintering programs of alpha-alumina supports

Step	Ramping Rate (℃/hr)	T_{set} (℃)	t_{hold} (hr)
1	60	600	0.1
2	96	1260	0.1
3	96	200	0.1
4	60	1150	30
5	60	50	End

APPENDIX C

PREPARATION OF GAMMA-ALUMINA SUPPORTS

C1. Preparation of 1M boehmite sol

1. Heat while stirring one liter of water to 90 ℃.
2. Add one mole aluminum-tri-sec-butoxide into the warm water while stirring
3. Keep stirring the solution at 90 ℃ for one hour.
4. Add 70 ml 1M HNO_3 solution into the solution prepared above.
5. Reflux at 90-100 ℃ for 10 hours.

C2. Preparation of a 30 g/L PVA solution

1. Mix 95 mL of distilled water and 5 mL of 1 M HNO_3 together in a beaker.
2. Add 3 g PVA (Fluka, WM=72000 g/mol) to the solution and keep stirring for 15 minutes.
3. Heat the solution up to 90 ℃ while keeping stirring.
4. Wait until the solution becomes clear, then cool down and filter the solution.

C3. Mix, dip-coating and calcination

1. Mix the 1M boehmite sol and 30 g/L PVA solution with a volume ratio of 20:13 into a glass vial.
2. Sonication treat the mixture for at least 10 minutes to get a well dispersed sol for dip-coating.
3. Dip-coat the polished side of the alpha-alumina support with the sol.
4. Dry the coated supports in a humidity oven (40 ℃, 60% RH) for 2 days, and then calcine the supports in a furnace at 550 ℃ for 3 hours with a heating/cooling rate of 0.5 ℃/min.

APPENDIX D

PREPARATION OF SILICALITE SEEDS LAYER

D1. Synthesis of silicalite seeds

1. Add 0.35 g NaOH to 25 mL TPAOH solution (1M) at room temperature. Stir the mixture until all the NaOH pellets are dissolved and a clear solution is obtained.
2. Heat the above solution up to 80 ℃.
3. Add 5 g fumed silica to the pre-heated solution while stirring.
4. Keep stirring the solution for at least 1 hour. The gel-like mixture will become very viscous.
5. Add balanced distilled water into the mixture to compensate the water evaporated during step 4.
6. Cool down the above solution and age at room temperature for 3 hours.
7. Transfer the above solution to an autoclave, and place the autoclave in an oven pre-heated at 120 ℃ for 12 hours. This step is the hydrothermal synthesis of the silicalite seeds. The synthesis temperature and time can be varied, depending on the requirement on the size of the seeds.
8. After the autoclave is cooled down, wash the silicalite seeds for at least 3 times using distilled water. Centrifugation and sonication are required during the washing step.
9. After the washing, store the seeds solution at room temperature.

D2. Coating of silicalite seeds layer

1. Prepare a seeds solution with the composition of 0.95-1.15 wt% silicalite/0.15 wt% HPC (MW 100,000)/ balance water.
2. Adjust the pH of the solution to be 3~4 using 1 M HNO_3.
3. Dip-coat the silicalite seeds on the polished side of alpha-alumina supports. The dip-coating time is controlled at ~10 s.

4. Dry the seeds coated supports in a humidity oven (40 ℃, 60% RH) for 2 days.
5. Calcine the seeded support in a furnace at 500 ℃ for 8 hours with a heating/cooling rate of 0.5 ℃/min.
6. The coating/drying/calcination will be repeated twice to ensure a defect-free seeds layer.

APPENDIX E

SYNTHESIS OF ZEOLITE MEMBRANE

1. Use the silicalite seeds coated supports prepared in Appendix C for the synthesis of all the four zeolite membranes with different microstructure.
2. Prepare the secondary growth solution with a molar composition of 1 KOH: 1 TPABr: 4.5 SiO_2: 16 C_2H_5O: 1000 H_2O. First add the KOH and TPABr to distilled water under stirring. Then add the TEOS to the solution after both KOH and TPABr are completely dissolved.
3. Stir the above solution at room temperature for 4 hours.
4. Place the seeded support in the Teflon autoclave. Use a home-made Teflon sample holder to vertically hold the seeded support.
5. Transfer the solution prepared in step 3 to the Teflon autoclave. Then put the autoclave to a pre-heated oven for hydrothermal secondary growth.
6. Follow the secondary growth conditions listed in Table 2.1 to synthesize the three zeolite membranes by templated methods.
7. Dry the three templated synthesized membranes at room temperature overnight, and then calcine the membranes at 550 ℃ in air for 8 h with a ramping rate of 0.5 ℃/min to remove the templates.
8. Prepare a synthesis solution with a molar composition of 5 g SiO_2: 60 g H_2O: 1.15 g NaOH: 0.65 g $Al_2(SO_4)_3 \cdot 18H_2O$ for the synthesis of template-free membrane.
9. Dissolve a certain amount of NaOH and $Al_2(SO_4)_3 \cdot 18H_2O$ in distilled water
10. Heat the above solution up to 80 ℃, and add fumed silica the solution while vigorously stirring.
11. Keep stirring the solution at 80 ◦C for about 2 h, then cool down the solution and age the synthesis solution for 1 day.

12. Transfer the solution into a Teflon-lined stainless steel autoclave in which the silicalite seeded support is held vertically by Teflon holders.
13. Place the autoclave in an oven and conduct the secondary growth following the condition listed in Table 2.1.
14. After synthesis, dry the template free synthesized membrane at 200 ℃ for 8 hours.

APPENDIX F

SYNTHESIS OF CARBON MEMBRANE

1. Dissolve the 6FDA-based polyimide polymer precursors in acetone to prepare polymer solution with different concentrations. This step is a slow process. The solution is usually heated and then treated in sonication machine to accelerate the dissolving of polymers.
2. The prepared polyimide solution needs to be sealed in a glass vial to prevent the evaporation of acetone.
3. Prepare a polymer film on both alpha- and gamma-alumina support by dip-coating the supports with the polymer precursor solutions. The dip-coating time is carefully controlled. The concentration of polymer solution is varied to obtain polymer films with different thicknesses.
4. Dry the supported polymer films at room temperature for 3 hours, then at 100 ℃ for 12 hours, and finally annealed at 140 ℃ for 5 hours. All these drying steps are conducted in lab air environment.
5. Place the supported polymer membranes on a ceramic crucible, and then put the crucible into the tubular high temperature furnace.
6. Carefully seal the tubular furnace to ensure no leakage.
7. Before pyrolysis, the copper catalyst inside the fixed bed reactor were first activated by reduction of the copper oxides to metallic copper using a reducing 2% H_2/Ar mixture at a flow rate of 100 mL/min at 175 ℃ for 24 h.
8. During pyrolysis, set the temperature of the fixed bed reactor at around 150 ℃. Feed ultra high purity Ar gas to the furnace with a flow rate of 100 mL/min. Keep purging the tubular furnace using UHP Ar for at least 4 hours to remove all the other gas impurities.

9. Start the furnace with different programs to conduct the pyrolysis.
10. After the pyrolysis, store the membranes in the tubular furnace filled with UHP Ar gas before gas permeation and separation measurements.

APPENDIX G

X-RAY DIFFRACTION AND SCANNING ELECTRON MICROSCOPY

G.1 X-ray Diffraction

1. X-ray diffraction (XRD) (Bruker AXS-D8, Cu Kα radiation) is used to characterize the crystal structure, especially the orientation of MFI zeolite membranes prepared at different conditions.
2. Put the disk membrane in the sample pan, place sample pan onto the sample holder of XRD machine.
3. Set 2θ in the range of 5-40 °, and a scan rate of 5 °/min.

G.2 Scanning electron microscopy

1. Use scanning electron microscopy (SEM, Phillips, FEI XL-30) to check the morphology of gamma-alumina support, carbon and zeolite membranes.
2. Use pliers to crack the disk membrane sample, and use compressed air to blow away the debris on sample.
3. Use conducting adhesive tape to stick samples onto sample pan. Coat the sample surface with Au for 4 minutes.
4. Place the samples into the SEM machine, and choose voltage 20 kV and spot size 3 for the measurement.

APPENDIX H

PAS MEASUREMENTS

The PAS were conducted in National University of Singapore using a setup shown in Figure H.1. The procedures for the measurements were described in Chapter 2.

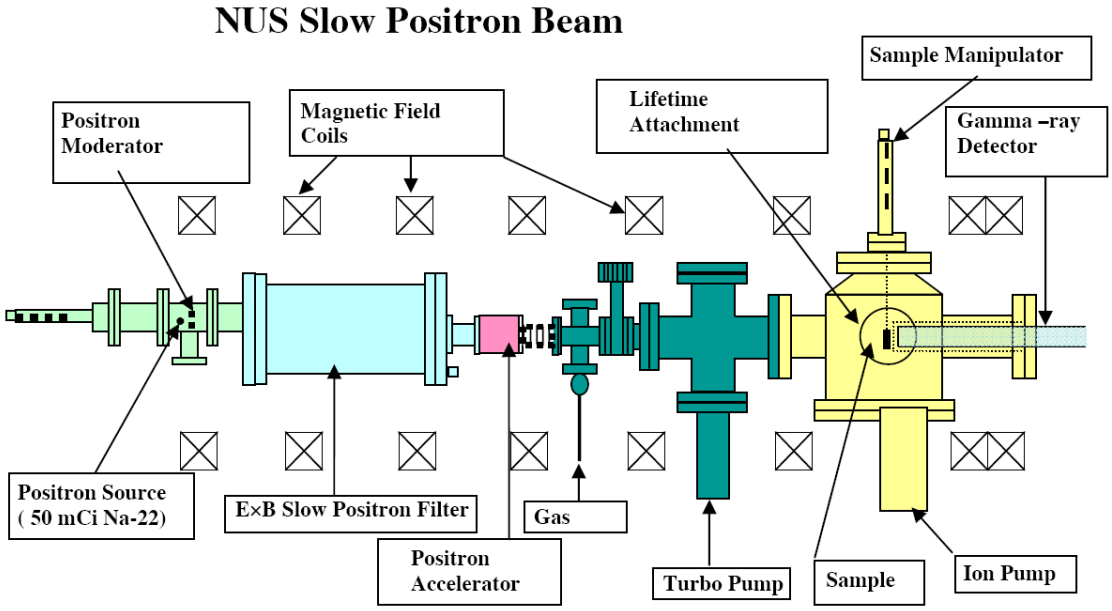

Figure H.1 A schematic diagram of variable mono-energy (0-30 keV) slow positron beam at National University of Singapore

The semi-empirical equation 2.1 was used to calculate the pore radius. 1.656 Å was used for ΔR in this work. This equation was reported to be valid for o-Ps lifetime smaller than ~20 ns or pore radius smaller than 1 nm, but not very accurate when the lifetime is more than around 20 ns (Ito et al., 1999). The definition of 20 ns is just a rough estimation from the plot shown in Figure H.2. The only lifetime larger than 20 ns in our work is about 22 ns, which is τ_4 of the TC membrane. Since the boundary at 20 ns is not sharp and 22 ns is pretty close to 20 ns as compared to the entire scale, the model is still reliable enough to calculate the pore size.

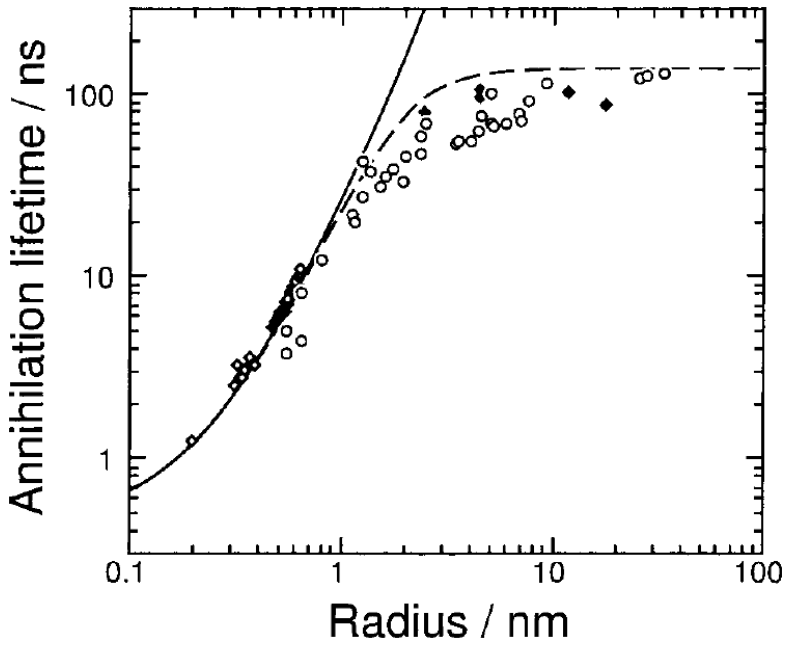

Figure H.2 Annihilation lifetimes of o-Ps measured in various porous materials as a function of average pore radius. The solid line is a correlation curve between o-Ps lifetime and a pore radius calculated from equation 2.1

Figure H.3 schematically shows the definitions of S, W and R parameters in DBES measurements. S parameter is defined as the ratio of integrated counts from central region (area A of Figure H.3) to total counts. W parameter is a ratio of integrated counts between energy 508.0 and 509.4 keV and between energy 512.6 and 514.0 keV (area B of Figure H.3) to total counts. R parameter defined as the ratio of 3γ annihilation (the total count from the valley region between 364.2 and 496.2 keV) to 2γ annihilation (the total count from the 511 keV peak region). The S parameters is sensitive to the microstructural changes and is usually used to detect the free volume profile in polymer membranes. The R parameter provides information about large pores (nm to μm).

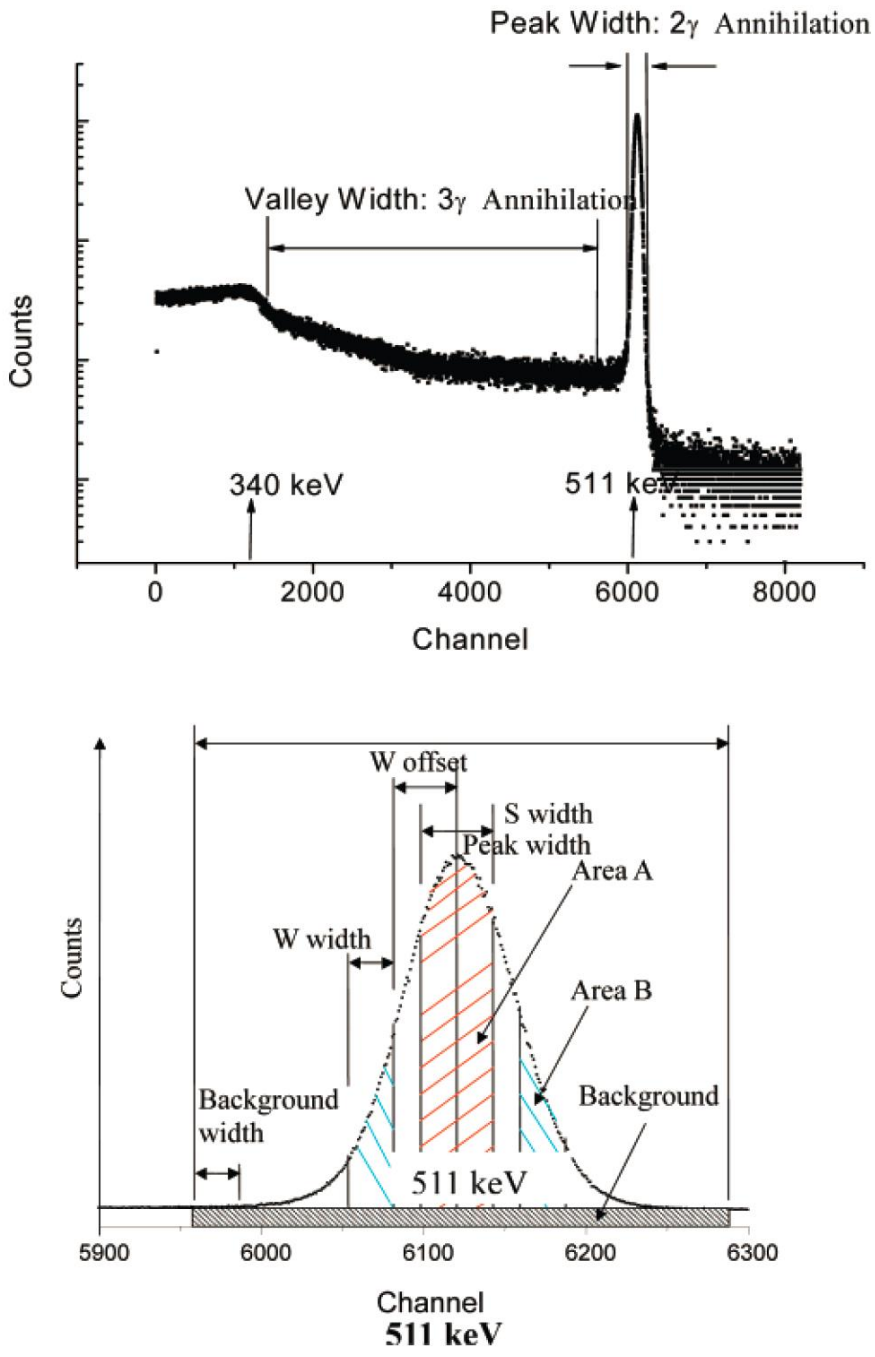

Figure H.3 Doppler broadening energy spectrum (DBES, top) and definitions of S, W, and R parameters from DBES (Chen et al., 2007)

APPENDIX I

SINGLE COMPONENT PERVAPORATION TEST

1. The zeolite membranes used for the pervaporation test are first dried at 200 ℃ to remove any adsorbed water or other species inside the framework.
2. Place and seal the zeolite membrane in a stainless steel pervaporation cell with the membrane side facing to the feed side, as shown in Figure I.1.
3. Feed the tank with either xylene isomer. The zeolite membrane layer is directly contacted with the liquid feed.
4. The temperature of the feed side can be controlled by a heating jacket. Room temperature was used in this work.
5. Weigh the weight of the dry and empty glass cold trap, W_1. And then connect the cold trap to the downstream side of the setup.
6. With the feed solution filled, the downstream side of the pervaporation setup is evacuated using a vacuum pump for at least 1 hour to reach an equilibrium state before collecting sample.
7. Use a dewar filled with liquid nitrogen to immerse the cold trap, and start to collect the permeated liquid sample. Make sure the liquid nitrogen level is maintained half way up the cold trap during the whole run.
8. After collecting the sample for a certain time (t), release the vacuum, and weigh the weight of the cold trap with the condensed liquid inside, W_2.
9. Use the following equation to calculate the flux.

$$J = \frac{W_2 - W_1}{At} \qquad \text{(I.1)}$$

where A is the membrane area in the unit of m^2. Flux is in the unit of $kg/m^2 \cdot hr$.

10. Take the membrane out from the cell after the test of one component. Place the membrane in a vacuum oven at 120 ℃ for 24 hours to activate the membrane.
11. Put the membrane back to the pervaporation cell and feed the tank with the second component, and run the test again.
12. The ideal selectivity is defined as the ratio of the flux for each component.

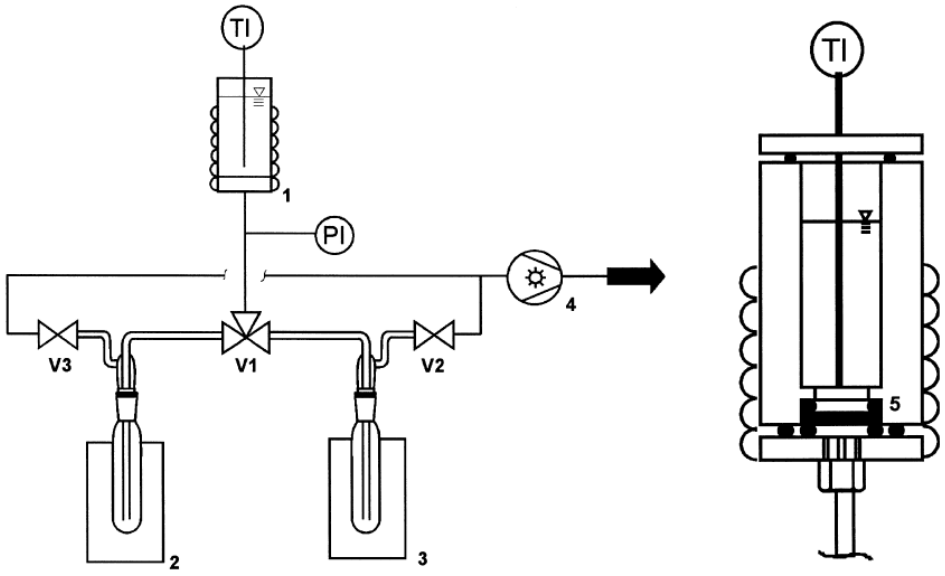

Figure I.1 Schematic of the pervaporation setup, 1: membrane cell with feed tank; 2,3: liquid nitrogen cold trap; 4: vacuum pump; 5:membrane (Wegner et al., 1999)

APPENDIX J

PROPYLENE/PROPANE MIXTURE SEPARATION MEASUREMENTS

J.1 Mixture gas separation measurements

1. The mixed gas separation performances of membranes were measured using a cross-flow setup shown in Figure J.1.
2. Load the membrane into a stainless steel permeation cell. Use Viton o-rings to seal the membrane.
3. Feed the propylene/propane mixture gas to the membrane side. Use mass flow controllers to control the flow rate of each gas, so as to control the feed composition. The total flow rate of feed gas is controlled at 50 mL/min.
4. On the retentate line, use a needle valve to control the feed pressure, and read the pressure value from a digital pressure sensor.
5. Use nitrogen gas with a flow rate of 50 mL/min as sweeping gas. Use bubble flow meter to measure the actual total flow rate on the permeate line.
6. Use gas chromatography (GC) (SRI Instruments, SRI 8610C) equipped with a flame ionization detector (FID) to measure the propylene/propane gas composition on the feed and permeate side.

J.2 Gas chromatography (GC) measurements

1. The GC used for measuring propylene/propane composition has a flame ionization detector (FID) and a 6 feet long silica gel column (OD: 1/8 inch).
2. He gas with a flow rate of 20 mL/min is used as carrier gas. The column temperature and detector temperature is 130 ℃.
3. The GC calibration curves for propylene and propane gases are shown in Figure J.2 and J.3. The GC constants for propylene and propane are 832 and 866, respectively. A typical chromatogram of propylene and propane gases were shown in Figure J.4.

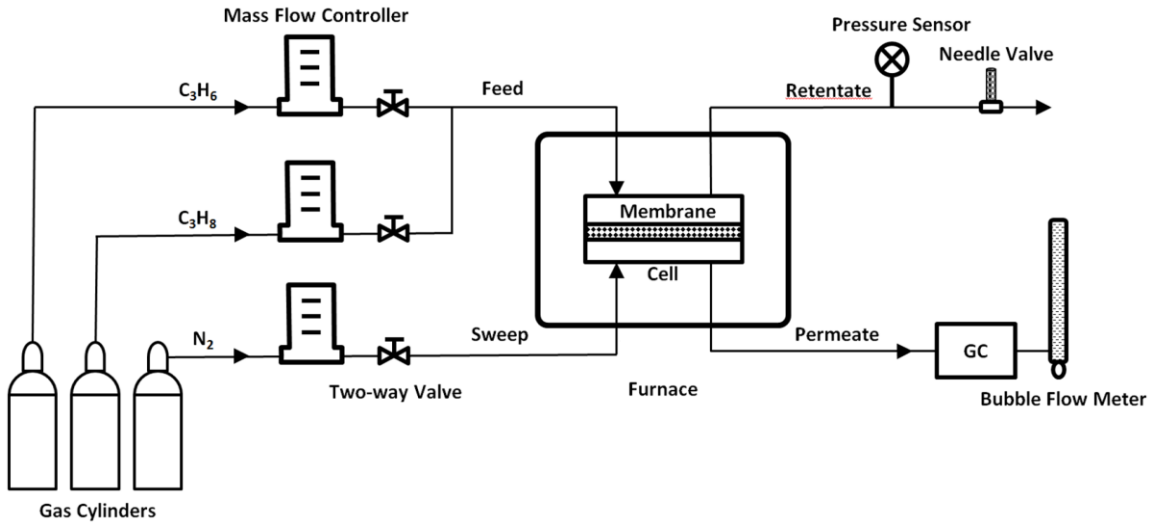

Figure J.1 Cross-flow setup for the measurements of C_3H_6/C_3H_8 mixture gas separation properties

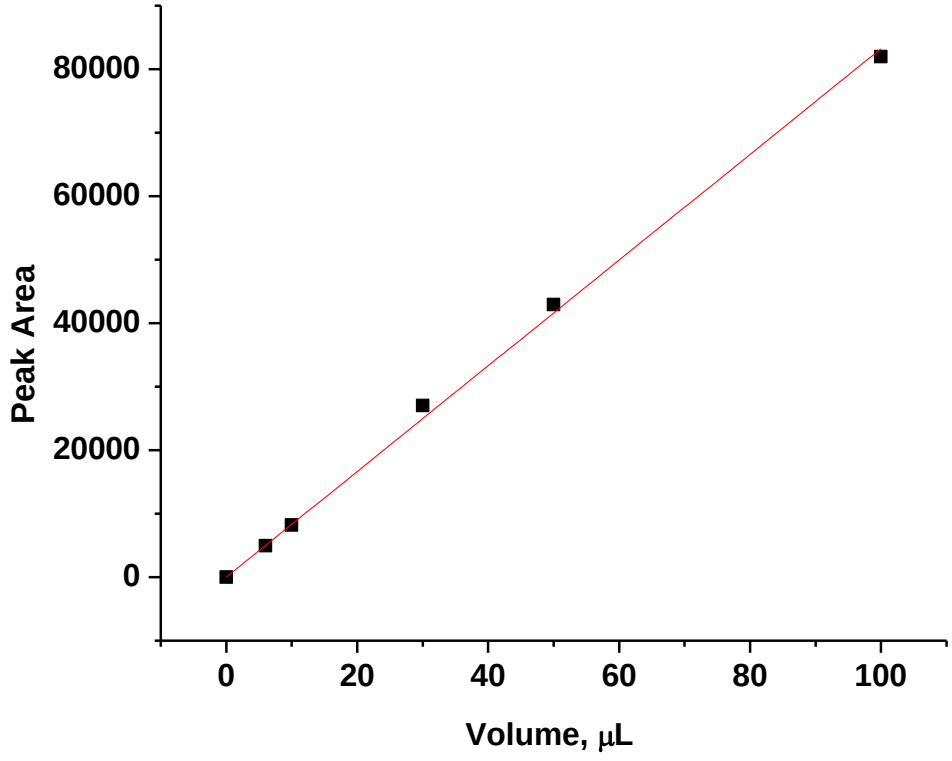

Figure J.2 GC calibration curve of propylene gas

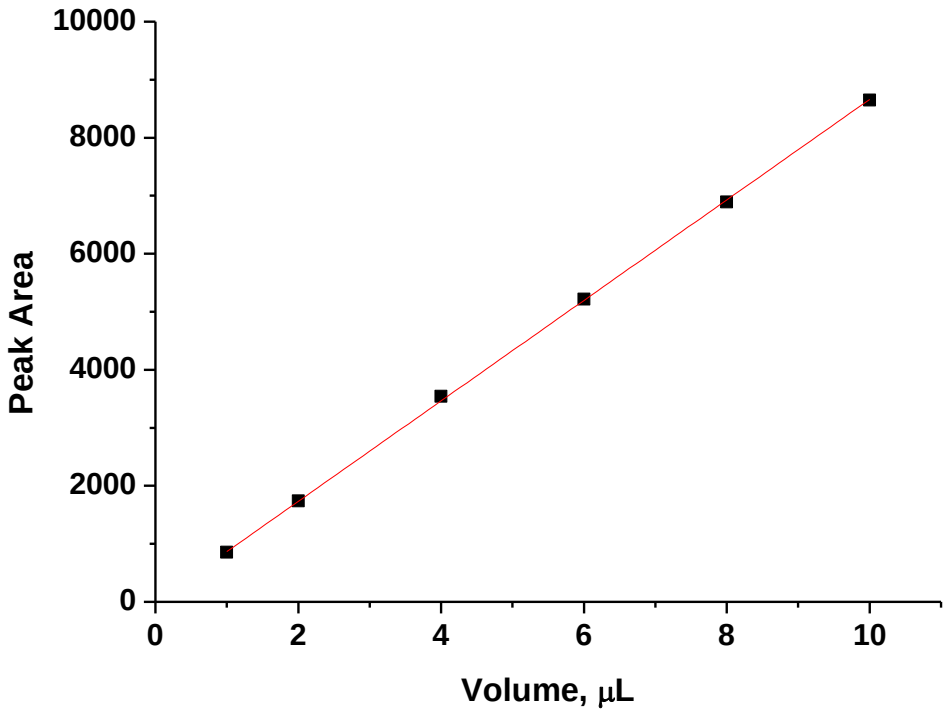

Figure J.3 GC calibration curve of propane gas

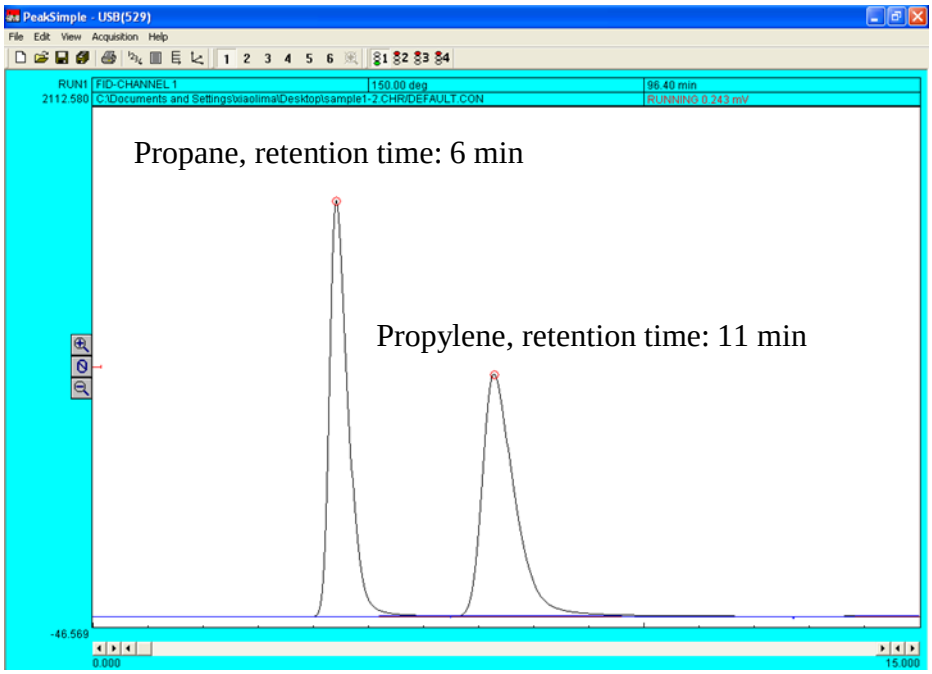

Figure J.4 A typical chromatogram of propylene and propane gases